The effects of 2-hydroxypropyl-β-cyclodextrin on hematopoiesis and the white adipose tissue

in the context of metaflammation and atherosclerosis

Doctoral thesis

to obtain a doctorate (PhD)

from the Faculty of Medicine

of the University of Bonn

Christabel Mennicken
from Berlin, Germany
2026

Written with authorization of

the Faculty of Medicine of the University of Bonn

First reviewer: Prof. Dr. Eicke Latz

Second reviewer: Prof. Dr. Karsten Hiller

Day of oral examination: 24.02.2026

From the Institute of Innate Immunity

Table of contents

List of abbreviations

27-OHC	27-hydroxycholesterol
Abca1	ATP binding cassette subfamily A member 1
ACK	Ammonium chloride potassium
APOE	Apolipoprotein E
ASCVD	Atherosclerotic cardiovascular diseases
AT	Adipose tissue
ATAC	Assay for Transposase-Accessible Chromatin
ATM	Adipose tissue macrophage
BW	Body weight
CCL	C-C motif chemokine ligand
CCR	C-C chemokine receptor
CD	Control diet
cDNA	Complementary deoxyribonucleic acid
CHIP	Clonal haematopoiesis of indeterminate potential
CMP	Common myeloid progenitors
CXCL	C-X-C motif chemokine ligand
DE	Differential expression
ER	Endoplasmatic reticulum
FACS	Fluorescent-activated cell sorting
FDR	False discovery rate
FGF21	Fibroblast growth factor 21
GMP	Granulocyte-monocyte progenitors
gWAT	Gonadal white adipose tissue
HP5	2-hydroxypropyl-β-cyclodextrin Cavitron^{TM} W7 HP5
HP7	2-hydroxypropyl-β-cyclodextrin Cavitron^{TM} W7 HP7
HPβCD	2-hydroxypropyl-β-cyclodextrin
HSC	Hematopoietic stem cells
HSPC	Hematopoieitic stem and progenitor cells
i.p.	intraperitoneal
IL	Interleukin

LAL	Lysosomal acid lipase
LDL	Low-density lipoprotein
LDL-C	LDL-cholesterol
Ldlr	Low-density lipoprotein receptor
LPS	Lipopolysaccharide
LXR	Liver-X-receptor
MEP	Megakaryocyte-erythrocyte progenitors
MSC	Mesenchymal stromal cells
NCD	Noncommunicable disease
NLRP3	Nucleotide-binding domain leucine-rich repeat containing (NLR) family, pyrin domain containing 3
NPC	Niemann-Pick type C disease
oxLDL	Oxidized LDL
PCA	Principal component analysis
PCSK9	Proprotein convertase subtilisin/kexin type 9
PDGFcc	Platelet-derived growth factor cc
PPARγ	Peroxisome proliferator-activated receptor-γ
PRR	Pattern recognition receptors
RNA	Ribonucleic acid
RT	Room temperature
s.c.	Subcutaneous
SC	Standard chow diet
SFA	Saturated fatty acids
SREBP-2	Sterol regulatory element-binding protein 2
SVF	Stromal vascular fraction
TET2	Ten-eleven translocation methylcytosine dioxygenase 2
TI	Trained immunity
Tim4	T cell immunoglobulin mucin protein 4
TNFα	Tumor necrosis factor α
Veh	Vehicle
WAT	White adipose tissue
WD	Western-type diet

1. Introduction

1.1 Western diet affects the innate immune system

1.1.1 Metaflammation and the adipose tissue

Obesity is increasing worldwide, and it is an important risk factor for chronic inflammatory noncommunicable diseases (NCDs) like cardiovascular disease, cancer and type 2 diabetes (Hildebrand and Pfeifer, 2025). The link between obesity and NCDs is excess nutrient availability, which leads to a low-grade chronic inflammation, termed "metaflammation" (Hotamisligil, 2017) (**Fig. 1**). Obesity induces chronic inflammation in metabolically active tissues such as the white adipose tissue (WAT) (Kawai et al., 2021), liver (Koyama and Brenner, 2017), skeletal muscle (Wu and Ballantyne, 2017), brain (Jais and Brüning, 2017) and pancreatic islets (Yong et al., 2021). Metaflammation studies center around the WAT as it is both an energy-storage as well as an endocrine organ. Adipokines, secreted from the adipose tissue (AT), encompass adipocyte-specific molecules, such as leptin and adiponectin, as well as cytokines, such as interleukin (IL)-6 and tumor necrosis factor α (TNFα) (Tilg et al., 2025). Adipokines can be considered key regulators of metabolic inflammation as they enable the communication between different tissues and organs via specific receptor expression on the target organ. Other metabolic organs also communicate by releasing signaling mediators, called hepatokines (liver), enterokines (gut) or myokines (muscle) (Dos Santos et al., 2021; Tilg et al., 2025). A prototypic hepatokine is fibroblast growth factor 21 (FGF21), which is also an important adipokine (Flippo and Potthoff, 2021; Tilg et al., 2025). It affects various metabolic processes, e.g., enhances insulin sensitivity and regulates energy homeostasis (J. Xu et al., 2009 a; J. Xu et al., 2009 b), and has anti-inflammatory effects, e.g., mitigating lupus nephritis progression (Zou et al., 2024).

Immune cells in the AT adopt pro-inflammatory phenotypes during obesity, leading to systemic complications such as insulin resistance, hyperglycemia, and dyslipidemia that increase cardiometabolic risk (Schleh et al., 2023). In obese AT, regulatory T cells (Tregs) are decreased (Feuerer et al., 2009), while CD8+ cytotoxic T cells are increased compared to helper CD4+ T cells (Kiran et al., 2021; Nishimura et al., 2009).

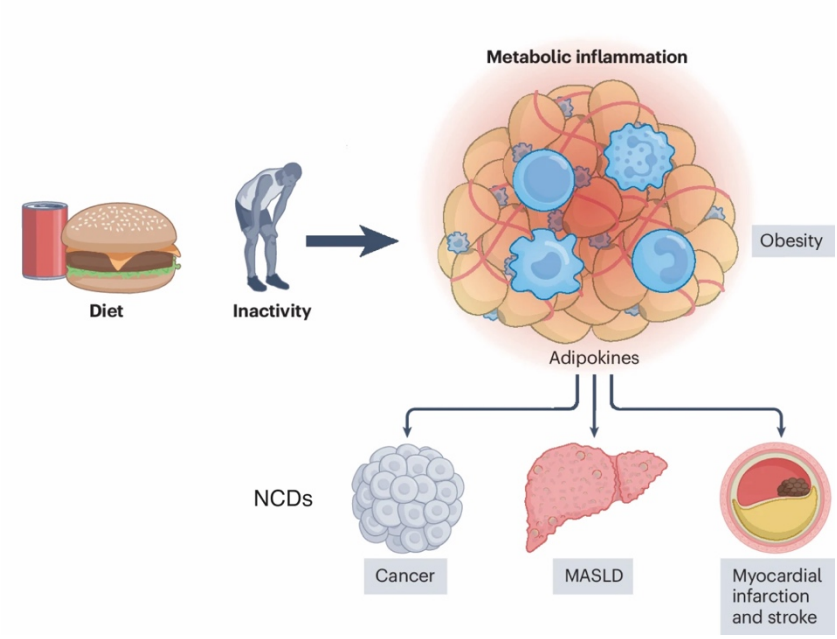

Fig. 1: Metaflammation: link between lifestyle adaptations and NCDs. Nutrient excess leads to obesity and metabolic inflammation. Adipokines mediate the development of NCDs, such as MI and stroke. Further details in text. Adapted from Tilg et al. (2025); MASLD = Metabolic dysfunction-associated steatotic liver disease

Among CD4+ T cells, pro-inflammatory Th1/Th17 cells are increased as opposed to anti-inflammatory Th2 cells (Nishimura et al., 2009; Strissel et al., 2010), promoting the infiltration of macrophages (Nishimura et al., 2009).

Macrophages are the most abundant immune cells in AT, increasing from about 10 % of all immune cells in the lean state to over 40 % in obesity (Lumeng et al., 2007; Weisberg et al., 2003a). They are highly plastic and adapt to local cues to maintain tissue homeostasis through functions such as tissue repair, debris clearance through phagocytosis, and metabolic regulation (Coats et al., 2017). In the AT specifically, macrophages help buffer lipids, present antigens, and coordinate communication within and between organs (Schleh et al., 2023). Different macrophage populations exist in the AT, identifiable by different surface marker expression. Pro-inflammatory macrophages express the classical marker CD11c which was found in mice during obesity, but not in the lean state (Lumeng et al., 2007). Another pro-inflammatory marker, relevant for antigen presentation, is histocompatibility complex class II (MHC II) (Gautier et al., 2012), whereas anti-inflammatory murine macrophage markers are CD206, CD163, and T cell immunoglobulin mucin protein 4 (Tim4) (Félix et al., 2021). However, the classical division into pro- and anti-inflammatory macrophages is not sufficient to describe adipose tissue macrophages (ATM) as surface marker expression patterns differ from activated macrophages as described *in vitro* (Kratz et al., 2014). In obese AT, ATM increase glycolysis and oxidative phosphorylation which are potentially driven by increased levels of inflammatory lipids, hypoxia, insulin, and leptin signaling and are therefore termed

metabolically activated macrophages (Coats et al., 2017; Kratz et al., 2014). Proteomic analysis of human ATM revealed a distinct set of metabolically activated macrophage marker expression including adenosine triphosphate (ATP) binding cassette subfamily A member 1 (ABCA1), scavenger receptor CD36, and perilipin 2 (PLIN2), which are involved in lipid metabolism (Kratz et al., 2014).

The interplay of macrophages and adipocytes has been demonstrated by recent work of Cox et al. (2021), showing that tissue-resident macrophages control the lipid storage and expansion of white adipocytes in the visceral (around abdominal organs) and subcutaneous (underneath the skin) fat via the platelet-derived growth factor cc (PDGFcc) which they release upon diet-intake. Blockade of PDGFcc lead to reduced fat storage and increased energy expenditure, especially via thermogenesis in brown adipose tissue. Notably, these effects were independent of the effects mediated by C-C chemokine receptor (CCR)2+ monocyte-derived macrophages, i.e. insulin resistance and liver steatosis. CCR2+ monocytes infiltrate the obese AT and are associated with a pro-inflammatory AT profile (Weisberg et al., 2006). The described interplay shows the importance of ATM on AT homeostasis and remodeling.

WAT expands through hyperplasia, the formation of new adipocytes, or hypertrophy, the enlargement of existing adipocytes by storage of fat (Haczeyni et al., 2018). When hypertrophic growth predominates, it promotes tissue hypoxia, fibrosis, and inflammation, contributing to the development of metabolically unhealthy obesity characterized by insulin resistance and systemic metabolic dysfunction (Ghaben and Scherer, 2019). Acute loss of insulin signaling in mice results in lipodystrophy, marked by enhanced lipolysis and adipocyte apoptosis, leading to increased blood glucose levels, insulin resistance and hepatic steatosis. Notably, these metabolic disturbances are transient; within 10–30 days, AT regenerates through increased preadipocyte proliferation and differentiation, restoring adipose mass and metabolic homeostasis (Sakaguchi et al., 2017).

Committed preadipocytes develop from multipotent, mesenchymal precursor cells, which can develop into myoblasts, chondroblasts, or osteoblasts (Cawthorn et al., 2012). Committed preadipocytes retain a fibroblast-like morphology once they enter a growth

arrest. Upon an adipogenic stimulus, preadipocytes re-enter the cell cycle and generate daughter cells for the differentiation into mature adipocytes by upregulation of the master regulator of adipogenesis peroxisome proliferator-activated receptor-γ (PPARγ), as well as the transcription co-activators CCAAT/enhancer-binding protein α and β (C/EBPα and C/EBPβ) (Ghaben and Scherer, 2019). *In vivo*, insulin is the only known physiological stimulus, *in vitro*, the differentiation factors insulin, the glucocorticoid dexamethasone, and the cyclic adenosine monophosphate (cAMP)-elevating drug IBMX induce adipogenesis in the murine pre-adipose cell line 3T3-L1 (Cave and Crowther, 2019) and in murine primary stromal vascular fraction (SVF) (Rodeheffer et al., 2008).

1.1.2 Trained innate immunity induced by Western Diet

The bone marrow niche is a dynamic microenvironment that maintains hematopoietic stem cells (HSC), supports their self-renewal and differentiation, and regulates the release of blood cells into the circulation (Mendelson and Frenette, 2014; Morrison and Scadden, 2014). It comprises diverse cell types, including endothelial and mesenchymal stromal cells (MSC), adipocytes, osteoblasts, and immune cells, all of which adapt to physiological changes such as infection, inflammation, aging, or metabolic stress (Ambrosi et al., 2017; Burberry et al., 2014; Woods and Guezguez, 2021). Endothelial and stromal cells are important for HSC maintenance and mobilization, by producing C-X-C motif chemokine ligand (CXCL)12 to control HSC retention (Greenbaum et al., 2013; Sugiyama et al., 2006).

Under inflammatory stress or infection, emergency myelopoiesis occurs - a shift in hematopoiesis toward rapid myeloid cell production (Chavakis et al., 2019; Swann et al., 2024). Increased levels of granulocyte-monocyte progenitors (GMP) are observed which give rise to circulating monocytes that may infiltrate tissues to combat microbial infections (Weiskopf et al., 2016). Cytokines, growth factors, and pathogen-associated signals (e.g. lipopolysaccharide (LPS)) stimulate this process (Demel et al., 2022; Manz and Boettcher, 2014). Acute exposure of the pro-inflammatory cytokine IL-1β promotes early myeloid differentiation, addressing the need for increased levels of myeloid cells, however chronic IL-1 exposure leads to HSC exhaustion and impaired regeneration (Pietras et al., 2016). Similarly, transient interferon-α (IFNα) signaling activates quiescent HSC, whereas

prolonged stimulation reduces their self-renewal (Essers et al., 2009). Beyond hematopoietic cells, stromal components actively shape emergency hematopoiesis: MSC secrete C-C motif chemokine ligand (CCL)2 upon LPS stimulation, promoting myeloid differentiation via CCR2 (Yamazaki et al., 2024), while endothelial cells increase vascular permeability to facilitate vascular leakage and hence egress of immune cells into the circulation (Prendergast et al., 2017; Vandoorne et al., 2018).

Trained immunity (TI) describes a metabolic and epigenetic remodeling of innate immune memory leading to enhanced myelopoiesis and cytokine responsiveness upon secondary encounter of a stimulus (**Fig. 2**) (Johansson et al., 2023; Netea et al., 2020; Ochando et al., 2023). TI can be divided into central TI, the reprogramming of stem cells in the bone marrow, and peripheral TI, the reprogramming in circulating and tissue-resident cells (H. Y. Kim and Lee, 2025). TI is induced by both infection-related triggers such as β-glucan (Mitroulis et al., 2018) and Bacillus-Calmette-Guérin (BCG) vaccination (Kaufmann et al., 2018; Kleinnijenhuis et al., 2014; Sun et al., 2024), and endogenous metabolic triggers such as oxidized low-density lipoprotein (oxLDL) (Bekkering et al., 2014; Keating et al., 2020) and mevalonate (Bekkering et al., 2018). Metabolic and epigenetic mechanisms involve increased glycolysis and oxidative phosphorylation, along with elevated levels of TCA cycle-derived metabolites (α-ketoglutarate, fumarate, succinate) that regulate histone modification enzymes like ten-eleven translocation (TET) methylcytosine dioxygenases (Arts et al., 2016; Bhargavi and Subbian, 2024; Ferreira et al., 2024).

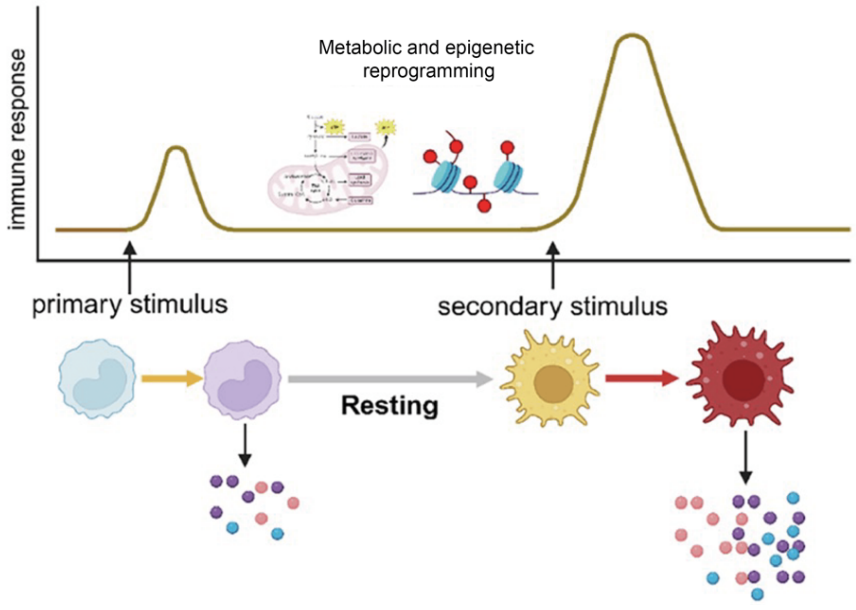

Fig. 2: Basic mechanism of trained immunity. A primary stimulus induces metabolic and epigenetic changes that lead to a heightened cytokine response upon a secondary stimulus. Detailed description in text. Adapted from H. Y. Kim and Lee (2025).

TI can be beneficial - enhancing protection against infections and tumors - but may also become maladaptive, sustaining chronic inflammation and increased risk for disease progression (Bekkering et al., 2021; Bhargavi and Subbian, 2024; Ochando et al., 2023; Schlüter et al., 2025). Previously encountered inflammatory diseases such as myocardial infarct, heart failure, ischemic stroke, and periodontitis, induce maladaptive TI which have been shown to exacerbate atherosclerosis (Dong et al., 2024), cardiac dysfunction (Nakayama et al., 2024; Simats et al., 2024), arthritis (Li et al., 2022), and cancer (Koelwyn et al., 2020), respectively. Notably, most of these studies have been conducted in mice and further research is needed to confirm these findings in humans.

Due to globally increased hygiene conditions and medication to treat infectious disease, and simultaneous increases in availability of processed foods, rich in fat and sugars, maladaptive TI - through metabolic imbalances and chronic inflammation (metaflammation) - is on the rise. Christ et al. (2018), demonstrated that Western-type diet (WD) feeding of low-density lipoprotein (LDL) receptor knockout mice (*Ldlr*$^{-/-}$) mice leads to TI in the bone marrow. WD consumption triggered systemic inflammation, enhanced myelopoiesis, and epigenetic and transcriptional reprogramming of GMP**;** effects that persisted even after returning to a normal diet. Additionally, weight cycling (losing and regaining weight) showed acceleration of atherosclerosis progression (Scolaro et al., 2025) and alternating high fat and chow diet feeding has been shown to increase the risk for atherosclerosis by neutrophil reprogramming (Lavillegrand et al., 2024).

Hyperlipidemia and dietary fatty acids have been linked to maladaptive TI, with the AT playing a role in sustaining inflammatory memory. Mice switched from a high-fat to a chow diet retain elevated adipose inflammation, insulin resistance, and glucose intolerance, indicating long-term immune imprinting (Blaszczak et al., 2020). Saturated fatty acids (SFAs), abundant in Western and ketogenic diets, have also been investigated**.** Seufert et al. (2022), showed that ketogenic diet feeding increased myelopoiesis in the bone marrow and amplified systemic inflammation after LPS challenge. Similarly, palmitic acid, a key SFA, enhances macrophage inflammation *in vitro* and increases mortality *in vivo* following secondary LPS stimulation, implicating it in immunometabolic dysfunction. Pre-incubation with the appetite-regulating adipokine and hormone leptin promotes innate immune training by augmenting TNFα production upon re-stimulation with LPS or R848

in human primary monocytes (Gomez et al., 2024). Together, these findings indicate that lipid excess - particularly through saturated fatty acids and AT-derived signals - can drive maladaptive TI, perpetuating inflammation and metabolic disease.

A key driver of maladaptive TI is signaling via IL-1β which is downstream of nucleotide-binding domain leucine-rich repeat containing (NLR) family, pyrin domain containing 3 (NLRP3) inflammasome activation and which is secreted mainly by myeloid cells. Blocking the NLRP3-IL-1β signaling axis was shown to limit maladaptive TI (Christ et al., 2018; Li et al., 2022; Simats et al., 2024).

Thus, while the ability of the bone marrow to “train” HSC provides a mechanism for rapid immune readiness, its dysregulation under chronic metabolic or inflammatory stress contributes to persistent myeloid activation and the pathogenesis of NCDs (**Fig. 3**).

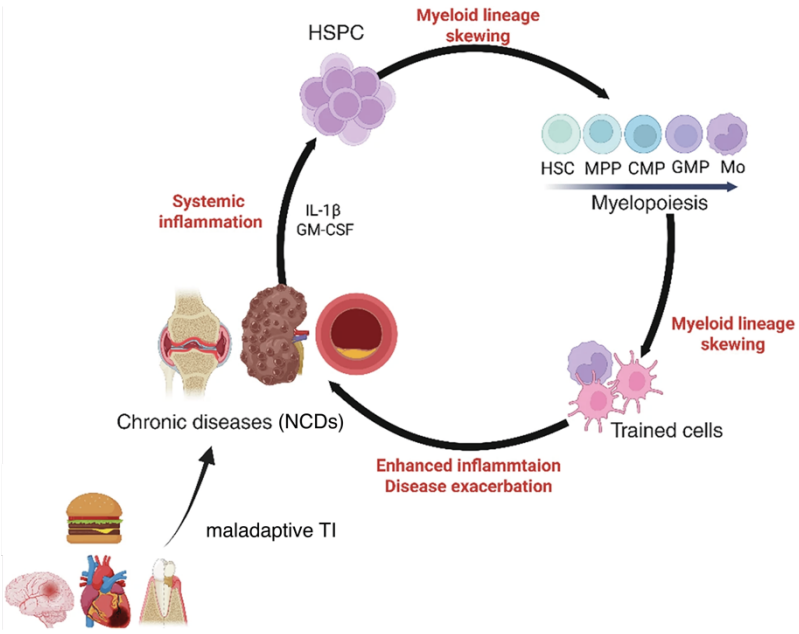

Fig. 3: The connection between TI and chronic inflammatory diseases. NCDs sustain an inflammatory loop by secretion of cytokines, which leads to a myeloid skewing in the bone marrow. Trained cells in the periphery enhance inflammation and disease exacerbation. Lifestyle factors, such as dietary habits, and co-morbidities amplify the inflammatory loop via (maladaptive) TI. Adapted from H. Y. Kim and Lee (2025)

1.2. Atherosclerosis

Atherosclerotic cardiovascular diseases (ASCVD) have become a global health burden and remain the leading cause of death worldwide. In 2021, ischemic heart disease alone accounted for 13% of all deaths (WHO). Atherosclerosis, the underlying pathology, is a dyslipidemic and chronic inflammatory condition, characterized by the formation of atherosclerotic plaques within the artery walls, ultimately leading to impaired blood flow

(Libby, 2021). These plaques can restrict oxygen and nutrient delivery to tissues and organs, and their rupture obstruct blood flow in critical arteries, resulting in life-threatening events such as myocardial infarct and stroke.

1.2.1 The role of monocytes and macrophages in disease pathogenesis

Atherosclerosis begins when the endothelial barrier of arteries becomes compromised, allowing LDL-cholesterol (LDL-C) to infiltrate the subendothelial space through interactions with LDL receptors (Ldlr) on endothelial cells (Tabas et al., 2007). In response, vascular cells release chemokines and express adhesion molecules which recruit monocytes into the intima. Non-classical Ly6C^{low} monocytes are more efficient at lipid uptake within the circulation, a feature that promotes their patrolling activity and contributes to atheroprotection (Marcovecchio et al., 2017; Quintar et al., 2017), whereas classical Ly6C^{high} monocytes display a greater tendency to infiltrate the arterial wall (I. Hilgendorf et al., 2015). Monocyte recruitment to the subendothelial space is crucial for atherosclerosis induction and is coordinated via CCR2 (Boring et al., 1998; Saederup et al., 2008), CCR5 and CX3 motif chemokine receptor 1 (CX3CR1) (Tacke et al., 2007). Monocytes migrate beneath the endothelium and differentiate into macrophages which internalize oxLDL via scavenger receptors, e.g., CD36 (Park, 2014). Continuous oxLDL uptake leads to cytosolic cholesterol ester lipid droplet accumulation and the formation of lipid-laden “foam cells”, a hallmark of atherosclerosis (Hansson and Libby, 2006). Macrophages in the atheromatous plaque display a high heterogeneity and different ontogenies, and may have specialized functions in inflammation, lipid handling, and homeostasis (von Ehr et al., 2022).

Beyond lipid accumulation, oxLDL acts as a danger-associated molecular pattern (DAMP) that triggers sterile inflammation through pattern recognition receptors (PRRs). Specifically, it signals via Toll-like receptor (TLR) 4 and TLR6 heterodimers, which is regulated by the CD36 scavenger receptor (Stewart et al., 2010). The downstream signaling cascade of this heterotrimeric complex activates MyD88-dependent nuclear factor-κB (NF-κB), a key transcription factor that drives inflammatory priming and expression of proinflammatory genes. Among the many genes regulated by this pathway, NLR family pyrin domain containing 3 (NLRP3) – a member of the NOD-like receptor

(NLR) subfamily of pattern-recognition receptors (PRR) – has become major focus of inflammatory research and is implicated in a wide range of disease conditions. NLRP3 forms a multimeric protein complex, involving the adapter protein apoptosis-associated speck-like protein containing a CARD (ASC) and the effector zymogen caspase-1, termed NLRP3 inflammasome. Following transactivation, caspase-1 becomes cleaved and activated, and processes other effector molecules including pro-IL-1b into its active form. The NLRP3 inflammasome is a central mediator of inflammation, and its activation is a tightly regulated process (Latz et al., 2013).

Notably, cholesterol crystals – hallmark of atherosclerotic plaque - are potent activators of NLRP3, linking dysregulated lipid metabolism directly to inflammatory signaling (Duewell, Kono, Rayner, Sirois, Bauernfeind, et al., 2010). High cholesterol crystal-containing oxLDL can provide both signals within the NLRP3 activation cascade: it activates TLR4–NF-κB signaling to induce inflammasome and pro-IL-1b/-IL-18 priming, and increased oxLDL uptake can lead to intracellular cholesterol crystal deposition, which causes lysosomal damage and NLRP3 activation (Duewell et al., 2010; Sheedy et al., 2013). As result, NLRP3 activation triggers the cleavage of pro-IL-1β and pro-IL-18 into their active cytokine forms and subsequent pyroptosis, a pro-inflammatory cell death pathway (Ding et al., 2016). These processes drive leukocyte recruitment, inflammation, and plaque instability, forming the immunometabolic foundation of atherosclerosis progression. Furthermore, oxLDL, cholesterol crystals and IL-1β are important triggers of maladaptive TI and preventing the accumulation of these factors may contribute to reduced systemic low-grade inflammation induced by myeloid cells.

1.2.2 Risk factors

The American Heart Association publishes annual updates on the latest statistics concerning heart disease, stroke, and cardiovascular risk factors. These reports encompass both “core health behaviors” - such as smoking, physical activity, nutrition, sleep, and obesity - and “health factors,” including cholesterol levels, blood pressure, glucose regulation, and metabolic syndrome, all of which contribute to overall cardiovascular health (Martin et al., 2025).

An emerging risk factor is clonal hematopoiesis of indeterminate potential (CHIP), a condition characterized by an age-related clonal expansion of leukemogenic mutations in HSC, increasing the risk especially for cancer (Genovese et al., 2014; Jaiswal et al., 2014) and cardiovascular diseases (Jaiswal and Ebert, 2019; Tall and Fuster, 2022). Aging skews HSC differentiation toward myeloid-biased lineages (Dykstra et al., 2011; Pang et al., 2011), which potentiates the risk of developing CHIP and consequently adverse cardiovascular risk (Díez-Díez et al., 2024; Gumuser et al., 2023). Among CHIP mutations, loss-of-function mutations of Tet methylcytosine dioxygenase 2 (*Tet2)* promote vascular inflammation through NLRP3 inflammasome-mediated IL-1β production, and atherosclerosis progression in mice (Fuster et al., 2017). Hematopoietic aging, marked by the loss of regenerative capacity, shows increased IL-1β production, which fosters the development of inflammatory MSC and steady state engagement of emergency myelopoiesis in the bone marrow (Mitchell et al., 2023). Both aging and high fat diet lead to the accumulation of adipocytes in the bone marrow which impairs both hematopoietic and bone regeneration (Ambrosi et al., 2017). These findings demonstrate how closely the bone marrow niche and atherosclerosis are tied together and point out the importance of investigating how atherosclerosis can be treated on bone marrow level.

1.2.3 Current treatment

The major strategy for preventing atherosclerosis are cholesterol-lowering therapies. Significant and sustained reductions in LDL-C are achieved through pharmacological interventions targeting different aspects of cholesterol metabolism, including cholesterol biosynthesis (e.g., statins, bempedoic acid), intestinal cholesterol absorption (ezetimibe), and hepatic LDL particle clearance via proprotein convertase subtilisin/kexin type 9 (PCSK9) inhibition (Visseren et al., 2021). The contribution and chronification of inflammatory responses to disease pathogenesis and progression are widely accepted, and clinical trials have been conducted to study the effect of anti-inflammatory treatments. The CANTOS trial (Canakinumab Anti-inflammatory Thrombosis Outcomes Study) unequivocally demonstrated the validity of the inflammation hypothesis by showing that selective inhibition the NLRP3 inflammasome substrate IL-1β significantly lowered the risk of recurrent cardiovascular events, independently of lipid levels (Ridker et al., 2017). However, canakinumab (monoclonal antibody targeting L-1β)-treated patients had a

higher risk of death from infection, as compared to the placebo group. This underscores the importance of balancing the antiinflammtory effects in favor of mitigating CVD risk, and the proinflammtory effects to clear infections. In addition, large-scale randomized clinical trials have demonstrated that low-dose colchicine effectively reduces recurrent major cardiovascular events (Nidorf et al., 2020; Tardif et al., 2019). This benefit is attributed to its inhibition of tubulin polymerization and alteration of leukocyte responsiveness (Cronstein et al., 1996; Dalbeth et al., 2014; Leung et al., 2015). Based on this evidence, the Food and Drug Administration (FDA) approved the first anti-inflammatory therapy for ASCVD in 2023 (Libby and Soehnlein, 2025). In contrast, clinical trials using other anti-inflammatory treatments, such as low-dose methotrexate, did not show benefits (Ridker et al., 2019). Emerging evidence suggests that the cardiovascular benefits of incretin mimetic therapies may partly result from their anti-inflammatory effects, which appear at least partly independent of weight loss, as reduced inflammation was seen even in conditions without weight loss (Drucker, 2016). In the SELECT trial (Semaglutide Effects on Cardiovascular Outcomes in People with Overweight or Obesity), semaglutide treatment in obese, non-diabetic individuals reduced the inflammatory marker high-sensitivity C-reactive protein (hsCRP) levels to a degree comparable to IL-1β inhibition in the CANTOS study (Lincoff et al., 2023).

1.2.4 Mouse models of atherosclerosis

Investigating specific aspects of atherosclerosis pathogenesis requires suitable animal models, as this multifactorial disease involves numerous interacting processes that cannot be easily isolated or studied in humans. Although mouse models do not fully replicate human physiology, they offer several key advantages: they allow genetic manipulation, straight forward to handle, reproduce fast, and develop disease in a reasonable amount of time (Emini Veseli et al., 2017a). Among murine models, the decision of which one to use strongly depends on the research question, for example, whether early or advanced plaque stages are of interest, whether the focus lies on disease development under chow diet, lipid metabolism, immune response and inflammation, or plaque instability. Correspondingly, different mouse models allow detailed investigation of spontaneous lesion formation, diabetes-associated atherosclerosis, lipoprotein metabolism, reverse cholesterol transport (RCT), immune regulation and inflammation, or fibrosis and plaque

rupture (Oppi et al., 2019). The two most commonly used mouse lines are *Apoe*$^{-/-}$ (Plump et al., 1992; S. H. Zhang et al., 1992) and *Ldlr*$^{-/-}$ (Ishibashi et al., 1993) mice. More recently, the PCSK9-AAV model, which uses an adenoviral vector for the induction of hypercholesterolemia and atherosclerosis, has gained popularity due to the flexibility of genetic background and animal species that can be used (Gisterå et al., 2022).

Apolipoprotein E (ApoE) is a glycoprotein primarily synthesized in the liver and the brain and it is present on specific lipoproteins. It serves as a ligand for receptor-mediated uptake and clearance of chylomicron and very low-density lipoproteins (VLDL) remnants from the circulation. Several mouse models expressing human *APOE* isoforms (APOE ε2, APOE ε3, APOE ε4) demonstrate clear isoform-specific effects on lipid handling and disease risk. APOE ε4-expressing mice show a lower astrocytic cholesterol efflux (Gong et al., 2002), and exhibit more severe neural and metabolic phenotypes than APOE ε3 mice (Raber et al., 1998). In humans, there is conserved proinflammatory immune signature of APOE ε4 carriers leading to an increased susceptibility for neurodegenerative diseases (Shvetcov et al., 2025). In the absence ApoE, these particles accumulate in the bloodstream, leading to elevated cholesterol levels. *Apoe*$^{-/-}$ mice spontaneously develop atherosclerotic plaques as early as of 3 months of age even when fed a standard chow diet, and plaque development is further accelerated when the animals are fed a high fat and high cholesterol containing diet, a so called western-type diet (Western Diet; WD) (Plump et al., 1992). ApoE is also expressed on the surface of hematopoietic stem and progenitor cells (HSPC), and *Apoe* deficiency induces the HSPC proliferation, leading to monocytosis and neutrophilia and finally monocyte accumulation within atherosclerotic lesions (Murphy et al., 2011). Mechanistically, ApoE has been suggested to influence cholesterol efflux by modulating ATP-binding cassette (ABC) transporters ABCA1 and ABCG1. Compared to *Ldlr*$^{-/-}$ mice, *Apoe*$^{-/-}$ exhibit markedly higher cholesterol levels (hypercholesterolemia) and a stronger inflammatory phenotype, reflected by pronounced leukocytosis.

1.3 Cyclodextrins

Cyclodextrins are cyclic oligosaccharides consisting of a macrocyclic ring of five or more α-D-glucopyranose units linked by α-(1,4) glycosidic bonds (**Fig. 4a**). They are produced from starch by enzymatic digestion (Schmid, 1989). Their distinctive toroidal structure -

with a hydrophilic exterior and hydrophobic inner cavity - enables the formation of inclusion complexes with a wide range of lipophilic molecules. This host-guest interaction can modify the solubility, stability, and bioavailability of encapsulated compounds, making cyclodextrins valuable tools in pharmaceutical formulation and drug delivery. The three naturally occurring cyclodextrins - α-, β-, and γ-cyclodextrin - differ primarily in cavity size and aqueous solubility, allowing for tailored applications (Loftsson and Brewster, 2010). For example, α-cyclodextrin is effective in binding phospholipids, whereas β-cyclodextrin is more effective in binding cholesterol (Del Valle, 2004; Ohtani et al., 1989). The most common cyclodextrin complex type consists of one 'guest' molecule per cyclodextrin (1:1 ratio) which stands in a dynamic equilibrium with free molecules in solution (Challa et al., 2005) (**Fig. 4c**).

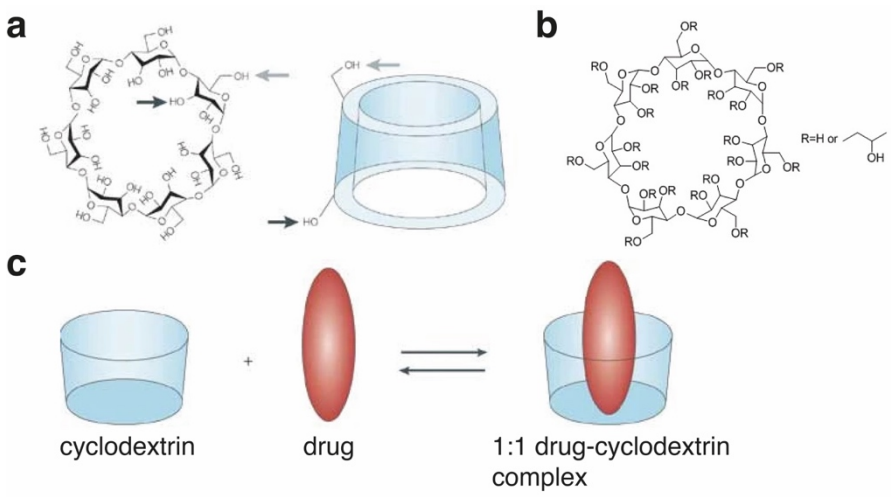

Fig. 4: Schematic representation of β-cyclodextrin. A) Ring structure and truncated cone shape b) Hydroxyl groups are substituted with hydroxypropyl groups in HPβCD. c) Cyclodextrins form inclusion complexes with lipophilic drugs. Further explanation in text. Adapted from Davis and Brewster (2004)

Although cyclodextrins possess a predominantly hydrophilic outer surface, they exhibit relatively low aqueous solubility, ranging from 2 % (w/w) for β-cyclodextrin to 26 % for γ-cyclodextrin (Davis and Brewster, 2004). To overcome this limitation, numerous chemically modified derivatives have been developed in which hydroxyl groups are randomly substituted with other functional moieties, greatly enhancing solubility (**Fig. 4b**). The most common modifications include methylation, hydroxypropylation, and sulfobutylation. Chemically modified derivatives, such as 2-hydroxypropyl-β-cyclodextrin (HPβCD) and sulfobutylether-β-cyclodextrin (SBEβCD), are particularly relevant in parenteral formulations, where they increase drug safety and tolerability (Challa et al., 2005). HPβCD has shown therapeutic promise as an active drug in cholesterol-related

disorders such as Niemann-Pick type C (NPC) disease (B. Liu et al., 2009, 2010; Matencio et al., 2020) and atherosclerosis (H. Wang et al., 2019; Zimmer et al., 2016), by promoting cholesterol solubilization, transport, and efflux. Ongoing research into novel cyclodextrin derivatives continues to expand their potential as versatile platforms for both novel therapeutic and diagnostic applications (Neaz et al., 2024).

1.3.1 2-hydroxypropyl-β-cyclodextrin (HPβCD)

HPβCD exhibits a markedly improved aqueous solubility of approximately 60% (w/w), compared to only 2% (w/w) or 16.6 mM of the parental β-cyclodextrin (Davis and Brewster, 2004). An inherent limitation of β-cyclodextrin are nephrotoxic effects at highly dosed s.c. administration, as urinary excretion is the main elimination route. Due to the relatively poor water solubility of β-cyclodextrin, it causes renal tubular damage (Karl-Heinz Frömming and József Szejtli, 1994; Perrin et al., 1978). Studies on the toxicity and pharmacokinetics of HPβCD demonstrated that nephrotoxic effects are markedly reduced, compared to the parental β-cyclodextrin, and its toxic effects are minimal in model animals (rats, mice, and dogs), particularly following oral administration, where fecal excretion represents the primary elimination route (Gould and Scott, 2005). Intravenous administration of HPβCD caused histopathological alterations in the lungs, liver, and kidneys, which were reversible.

Human studies have similarly shown good tolerability without signs of nephrotoxicity. In a clinical investigation of intravenously administered itraconazole/HPβCD inclusion complexes, HPβCD exhibited a small volume of distribution (VD ≈ 0.2 L/kg) and a short half-life ($t_{1/2}$ ≈ 1.7 h), indicating very low tissue penetration and plasma protein binding (Zhou et al., 1998). Following parenteral administration, HPβCD is not metabolized and mainly eliminated in the urine, with total plasma clearance following glomerular filtration rate. Consequently, renal impairment can prolong its elimination half-life. However, in individuals with normal kidney function, approximately 90 % of the administered HPβCD is excreted within 6 hours, and 99 % within 12 hours (Loftsson and Brewster, 2010).

1.3.2 Therapeutic potential of HPβCD in atherosclerosis treatment

Atherosclerosis is marked by excessive cholesterol accumulation, making it a compelling target for therapeutic interventions with HPβCDs. Owing to their high cholesterol-binding

affinity (Ganjali Koli and Fogolari, 2023), which enables cholesterol mobilization from foamy macrophages (Atger et al., 1997; S. M. Liu et al., 2003), and the encouraging outcomes observed in NPC treatment (B. Liu et al., 2009, 2010), HPβCD has been proposed a promising candidate for atherosclerosis therapy. Notably, work by Zimmer et al. (2016), demonstrated that HPβCD exerts atheroprotective effects *in vivo*, further supporting its potential to modulate cholesterol homeostasis and attenuate disease progression. In *Apoe*$^{-/-}$ mouse models of atherosclerosis, s.c. administration of HPβCD led to the reduction of plaque burden in both a prophylactic and therapeutic setting. The study showed that HPβCD led to a significant reduction of cholesterol crystals within atherosclerotic lesions. Mechanistically, in vitro data show that HPβCD increased cholesterol crystal dissolution and cellular cholesterol efflux from both cholesterol crystal-loaded and normocholesterolemic macrophages.

mRNA profiling of murine bone marrow-derived macrophages and *ex vivo* cultured human atherosclerotic plaques showed that HPβCD induced cellular reprogramming of macrophages and increased the production of cholesterol-derived oxysterol metabolites such as 27-hydroxycholesterol (27-OHC). Oxysterols are modifiers of sterol regulatory element-binding protein 2 (SREBP-2) (Griffiths and Wang, 2020), a transcription factor involved in cholesterol synthesis, and are potent activator of liver-X-receptors (LXR). Liver X receptors LXRα and LXRβ are oxysterol-activated nuclear receptors that coordinate cholesterol efflux, lipid metabolism, and inflammatory gene regulation, with LXRα being highly expressed in liver and adipose tissue**,** while LXRβ is ubiquitously expressed and maintains systemic cholesterol homeostasis (Repa et al., 2000; Tontonoz and Mangelsdorf, 2003). LXRs induce the reverse cholesterol transport, the excretion of cholesterol from cells via ABCA1/ABCG1 transporters, and promotes anti-inflammatory effects (B. Wang and Tontonoz, 2018). Notably, the observed atheroprotective activity of HPβCD was independent of ABCA1 and ABCG1, which is in alignment with previous findings showing that LXR agonists reduced atherosclerosis in the absence of ABCA1/G1 (Kappus et al., 2014). In contrast, studies in rabbits sugggest that the atheroprotective effects of HPβCD are mediated through enhanced cholesterol efflux via ABCA1 and ABCG1, increased levels of high-density lipoprotein (HDL)-cholesterol and a reduction in triglycerides (H. Wang et al., 2019), all of which are positively linked to reduced

atherosclerosis risk (Groenen et al., 2021). Notably, in these studies HPβCD was administered orally rather than subcutaneously, which implies distinct bioavailability and may explain differences in the underlying mechanisms.

1.4 Research aims

HPβCD ameliorates atherosclerosis in mice through several proposed mechanisms, including enhanced cholesterol crystal solubilization, stimulation of macrophage cholesterol metabolism and efflux, and anti-inflammatory effects mediated by LXR-dependent suppression of inflammatory gene expression. What remains unclear, however, is whether HPβCD acts exclusively on macrophages within atherosclerotic plaques or whether it also affects HSPC in the bone marrow and circulating immune cells. This question is particularly relevant because WD not only drives plaque formation but also induces trained myelopoiesis in the bone marrow, thereby contributing directly to atherogenesis. Thus, preventing or reversing WD-induced TI could represent an additional mechanism by which HPβCD reduces atherosclerosis.

Moreover, WD profoundly alters metabolic tissues, including inducing WAT hypertrophy and inflammation, which exert systemic effects and increase cardiovascular risk. Determining whether HPβCD modulates this immunometabolic axis - through reduced secretion of proinflammatory mediators or changes in adipose-tissue immune composition - may reveal previously unrecognized atheroprotective pathways and deepen our understanding of HPβCD as a therapeutic candidate.

In this thesis, I pursued two central objectives.

1. To determine whether HPβCD modulates WD–induced TI in bone marrow HSPC**,** which generate primed myeloid cells that enter the circulation and may infiltrate atherosclerotic lesions.
2. To assess whether HPβCD influences the WAT **-** the primary site of metaflammation and a key driver of systemic low-grade chronic inflammation.

2. Material and methods

2.1 Material

2.1.1 Consumables

Table 1: List of consumables

Product	Company
Pipette Tips RT L TS 1000 µL FL 768A/8	Mettler Toledo
Pipette Tips RT L TS 200 µL FL 960A/10	Mettler Toledo
Pipette Tips RT L TS 20 µL FL 768A/8	Mettler Toledo
Microlance™ 3 needle, 23 G x 1'', 0.6 x 25 mm	BD Biosciences
Microlance™ 3 needle, 26 G x 1/2", 0.45 x 13 mm	BD Biosciences
100 Sterican® needle, 27 G x 3/4'', 0.40 x 20 mm	B. Braun
Omnifix®-F Luer-Lock Solo syringe, 1 mL	B. Braun
Tissue culture plates (96-well), sterile, flat bottom, with lid	Greiner Bio-One
Tissue culture plates (96-well), sterile, U-shaped bottom, with lid	Greiner Bio-One
Microscopy plates (96-well), sterile, flat bottom, black wall, clear bottom, with lid	Revvity, Inc.
MicroWellTM Plates, 96 well, Nunc-ImmunoTM (ELISA plate)	ThermoFisher
Tissue culture plates (24-well)	Greiner Bio-One
Cell culture dish, PS, 60/15 mm	Greiner Bio-One
MicroAmp Optical 384-Well Reaction Plate (qPCR plate)	Applied Biosystems™, ThermoFisher
Microplate, 384 Well, PS, F-Boden (HTRF plate)	Greiner Bio-One
15 and 50 mL centrifuge tubes	Greiner Bio-One
8-well RealTime PCR-Gef./tubes, PP, clear	BRAND
Easystrainer 70 and 100 µm, sterile	Corning
Whatman® filter FP 30/0.2 CA-S, 0.2 µm, 7 bar max.	Merck
0.5, 1.5, and 2.0 mL Eppendorf safe-lock tube	Eppendorf

5 mL Polystyrene flow cytometry tubes	Sarstedt
LS-Columns	Miltenyi Biotec
Microscope slides ISO 8037/1	epredia

2.1.2 Cell culture and biochemistry

Table 2: List of cell culture materials

Product	Company
Fetal calf serum (FCS)	GibcoTM
Fatty acid-free bovine serum albumin (BSA) (Albumin-H2)	PanReac Applichem
Penicillin-Streptomycin (Pen/Strep) (10,000 U/ml)	GibcoTM
Dulbecco's Phosphate-buffered saline (PBS)	GibcoTM
RPMI 1640 Medium	GibcoTM
DMEM/F-12 (1:1) + GlutaMAXTM-I	GibcoTM
DMEM, high glucose, HEPES, no phenol red	GibcoTM
Lipopolysaccharide (LPS)-EB Ultrapure	InvivoGen
Pam3CysK4	InvivoGen
R848 (Resiquimod)	InvivoGen
CpG ODN 1668	InvivoGen
DMXAA (5,6-dimethylxanthenone-4-acetic acid, Vadimezan)	InvivoGen
TrypLE Express	GibcoTM
Biotin	Sigma
D-PA	Sigma
IBMX (3,7-Dihydro-1-methyl-3-(2-methylpropyl)-1*H*-purine-2,6-dione)	Sigma-Aldrich
Dexamethasone	Sigma-Aldrich
Insulin solution human	Sigma-Aldrich
Rosiglitazone	Sigma-Aldrich
Norepinephrine	Sigma-Aldrich
Formaldehyde Solution (PFA) 16 % (w/v) Methanol-free	ThermoFisher
Formalin, formaldehyde, 10 % buffered solution	EMS

Table 3: List of buffers

Buffer	Components
WAT buffer	PBS containing 0.5 % BSA
Blocking buffer ELISA	PBS containing 1 % BSA
MACS/FACS buffer	PBS containing 2 % FCS and 2 mM EDTA
PBS/EDTA buffer	PBS containing 2 mM EDTA
Red blood cell lysis buffer (RBC)	ddH2O containing 150 mM NH_4Cl, 10 mM $KHCO_3$, 0.1 mM Na_2EDTA, pH 7.2–7.4, sterile filtrated

2.1.3 Commercial reagents and kits

Table 4: List of commercial reagents and kits

Product	Company
Mouse IL-6 DuoSet ELISA	R&D Systems, Bio-Techne
Mouse TNFα DuoSet ELISA	R&D Systems, Bio-Techne
Mouse FGF-21 DuoSet ELISA	R&D Systems, Bio-Techne
HTRFTM Mouse IL-6	Cisbio, revvity
HTRFTM Mouse TNFα	Cisbio, revvity
Mouse 12-plex cytokine panel	Ayoxxa Biosystems GmbH
Mouse 11-plex chemokine panel	Ayoxxa Biosystems GmbH
Olink Target 48 Mouse Cytokine panel	Olink
Mouse Luminex Discovery Assay (customized 19 plex panel)	R&D Systems, Bio-Techne
MILLIPLEX MAP Mouse Adipokine Magnetic Bead Panel-Multiplex	Millipore, Merck
MILLIPLEX MAP Mouse Adiponectin Magnetic Bead- Single Plex	Millipore, Merck
Adipose Tissue Progenitor Isolation Kit, mouse	Miltenyi Biotec
UltraPureTM 0.5 M EDTA, pH 8.0	Invitrogen
7-AAD Viability Staining Solution	BioLegend
TheraPEAK® ACK Lysing Buffer (1x)	Lonza

Precision Count BeadsTM	BioLegend
FcR Blocking Reagent, mouse	Miltenyi Biotec
MACS® Cell Storage Solution	Miltenyi Biotec
BeadBug™ prefilled tubes, 2.0 mL capacity	Merck
QIAzol Lysis Reagent	QIAGEN
miRNeasy RNA isolation kit	QIAGEN
SuperScript™ III Reverse Transcriptase 10,000 U (200 U/µL)	ThermoFisher
primaQUANT 2x qPCR CYBR-Green Master Mix, no ROX, blue	Steinbrenner Laborsysteme GmbH
primaQUANT CYBR ADVANCED 2x qPCR SYBRGreen Master Mix with ROX, blue	Steinbrenner Laborsysteme GmbH
Pierce™ BCA Protein Assay Kit	ThermoFisher
NP-40 10 %	Sigma/Roche
Tween-20	Sigma/Roche
Digitonin	Promega
1 M Tris-HCl	ThermoFisher
1 M MgCl2	Sigma
Illumina Tagment DNA Enzyme and Buffer (TDE1)	Illumina
MinElute Reaction Cleanup Kit	QIAGEN
IDT® for Illumina® DNA/RNA UD Indexes Set A, Tagmentation (96 Indexes, 96 Samples)	Illumina
NEBNext High-Fidelity 2X PCR Master Mix	NEB
D1000 ScreenTape Assay	Agilent
AMPure XP Beads for DNA Cleanup	Beckman Coulter
ChemiBLOCKER	Millipore, Merck
Nonidet® P40 (Substitute) BioChemica (Triton-X 100)	PanReac AppliChem
Aqua-Poly/Mount Mounting Medium	Polyscience
Tissue-Tek® O.C.T.™ Compound	Sakura
mPIC proteinase inhibitor cocktail	Sigma
Free Glycerol Reagent	Sigma-Aldrich

Glycerol Standard Solution	Sigma-Aldrich
12-230 kDa Separation Module	ProteinSimple, part of Bio-Techne
EZ Standard Pack 1 12-230 kDA	ProteinSimple, part of Bio-Techne
Luminol-S	ProteinSimple, part of Bio-Techne
Peroxide	ProteinSimple, part of Bio-Techne
Streptavidin HRP	ProteinSimple, part of Bio-Techne
ATGL (30A4) Rabbit mAb #2439	Cell Signaling Technology
Anti-Rabbit Secondary Antibody	ProteinSimple, part of Bio-Techne

2.1.4 Animal experiments

Table 5: List of reagents for animal experiments

Product	Company
2-hydroxypropyl-β-cyclodextrin, Cavitron™ W7 HP5 Pharma cyclodextrin	Ashland
2-hydroxypropyl-β-cyclodextrin, Cavitron™ W7 HP7 Pharma cyclodextrin	Ashland
NaCl 0.9 % Isotonische Kochsalzlösung	Fresenius Kabi
Dulbecco's Phosphate-buffered saline (PBS)	Gibco™, ThermoFisher
Heparin-Natrium Braun 25.000 IE/ 5 ml Injektions-/Infusionslösung	B. Braun
Ketamin	serumwerk bernburg
Xylazin	serumwerk bernburg

2.1.5 Antibodies

Table 6: List of antibodies and dyes for flow cytometry/FACS

Ab reactivity	Fluoro-chrome	Clone	Dilution	Company	Catalog Number
LIVE/DEADTM Fixable Near-IR			1:2000	ThermoFisher	L34976A
Ter-119	APC-Cy7	TER-119	1:50	BioLegend	116223
Ly6G	APC	1A8	1:200	BioLegend	127614
Ly6C	APC	HK1.4	1:400	BioLegend	128016
CD11b	APC	M1/70	1:200	BioLegend	101212
CD5	AF647	53-7.3	1:200	BioLegend	100613

CD34	AF647	RAM34	1:400	BD	560230
CD117 (c-Kit)	FITC	2B8	1:200	BD	561680
CD16 (FcγRIII)/ CD32 (FcγRII)	BV650	2.4G2	1:200	BD	740457
Sca-1 (Ly6A/E)	PE	D7	1:150	BD	562059
CD45R (B220)	FITC	RA3-6B2	1:400	ThermoFisher	11-0452-82
CD19	FITC	1D3	1:400	ThermoFisher	11-0193-82
CD3e	FITC	500A2	1:400	ThermoFisher	11-0033-82
CD4	FITC	RM4-5	1:400	ThermoFisher	11-0042-82
CD8b	FITC	H35-17.2	1:400	ThermoFisher	11-0083-82
TER-119	FITC	TER-119	1:400	ThermoFisher	11-5921-82
CD2	FITC	RM2-5	1:400	ThermoFisher	11-0021-82
LY6G	FITC	1A8	1:400	BioLegend	127605
CD11b	FITC	M1/70	1:400	ThermoFisher	11-0112-82
CD117 (c-Kit)	APC-eFluor780	ACK2	1:400	ThermoFisher	47-1172-82
Sca-1 (Ly6A/E)	Pacific Blue	D7	1:400	BioLegend	108120
CD16 (FcγRIII)/ CD32 (FcγRII)	PE	93	1:200	BioLegend	101307
CD34	AF647	HM34	1:200	BioLegend	128606
CD45	PE-Cy7	30-F11	1:200	BD	552848
CD11b	BV510	M1/70	1:200	Biolegend	101245
Ly6C	APC	HK1.4	1:200	Biolegend	128016
Ly6G	BV421	1A8	1:200	Biolegend	127628
CD115 (CSF-1R)	PE	AFS98	1:200	Biolegend	135505
CD3e	FITC	500A2	1:200	ThermoFisher	11-0033-82
CD19	APC-Cy7	6D5	1:200	BioLegend	115530
7AAD			1:50	BioLegend	420403
CD335 (NKp46)	PE	29A1.4	1:400	BioLegend	137604
CD3	PE	17A2	1:400	BioLegend	100206
CD19	PE	1D3/CD19	1:400	BioLegend	152408
Ly-6G	PE	1A8	1:400	BioLegend	127608
CD170 (Siglec-F)	PE	S17007L	1:400	BioLegend	155506
CD45	APC-Cy7	30-F11	1:400	BioLegend	103116
CD11b	PE-Cy7	M1/70	1:400	BioLegend	101216
F4/80	BV421	BM8	1:400	BioLegend	123131
TIM4	AF647	F31-5G3	1:400	BioLegend	129907
CD11c	BV605	N418	1:400	BioLegend	117333
CD3e, CD11b, CD45R, Ly-76, Ly6G/Ly6C	V450	500A2, M1/70, RA3-6B2, TER-119, RB6-8C5	1:400	BD Biosciences	561301

Sca-1 (Ly6A/E)	BV786	D7	1:400	BD Biosciences	563991
CD117 (c-Kit)	FITC	2B8	1:400	BD Biosciences	561680
CD135 (FLT3)	PE-Cy5	A2F10	1:400	BioLegend	135312
CD48 (BLAST-1)	PerCP-Cy5.5	HM48-1	1:400	BioLegend	103422
CD150 (SLAM)	PE	W19132B	1:400	BioLegend	162606
CD16 (FcγRIII)/ CD32 (FcγRII)	BV711	93	1:400	BioLegend	101337
CD127 (IL7R-α)	BV650	A7R34	1:400	ThermoFisher	25-1271-82
CD34	PE/DazzleTM 594	SA376A4	1:200	BioLegend	152209
CD41 (ITGA2B)	APC	MWReg30	1:200	BioLegend	133913
CD61 (ITGB3)	BV480	2C9.G2	1:200	BD Biosciences	746665

2.1.6 Fluorescent staining for microscopy

Table 7: List of antibodies and dyes used for fluorescent staining

Antibody or dye	Manufacturer	Catalog number
Ki-67	Invitrogen	14-5698-82
Alexa Fluor® 647 AffiniPure® Donkey Anti-Rat IgG (H+L)	Dianova	712-605-153
DAPI	Invitrogen	D1306
LD540	Prof. Christoph Thiele, LIMES, University of Bonn	NA

2.1.7 qPCR primers

Table 8: List of qPCR primer sequences

Gene	Forward primer sequence	Reverse primer sequence
Hprt	TGAAGTACTCATTATAGTCAAGGGCA	CTGGTGAAAAGGACCTCTCG
Pnpla2	TGTGGCCTCATTCCTCCTACC	GCAGATGTCACTCTCGCCTG
Lipe	CAGAAGGCACTAGGCGTGATG	GCTTGCGTCCACTTAGTTCCA

2.1.8 Instruments

Table 9: List of instruments

Instrument	Company
ID7000 Spectral Analyser 5L	Sony Biotechnology
BD FACSAriaTM Fusion Flow Cytometer	BD Biosciences
Attune NxT Flow Cytometer	ThermoFisher
BD FACS Canto™ II	BD
LuminexTM FLEXMAP 3DTM Instrument System	ThermoFisher
LUNARIS Reader 96	Ayoxxa Biosystems
Evos FL Microscope	Life technologies
ZEISS Stemi 508	Zeiss
ZEISS Celldiscoverer 7	Zeiss
ZEISS Axio Scan.Z1	Zeiss
Leica Stellaris 8	Leica
QuantStudio 6 Flex Real-Time-PCR System	ThermoFisher
Wes™	ProteinSimple, part of Bio-Techne
NanoDrop One Microvolume Spectrophotometer	ThermoScientific
peqSTAR 2x Gradient Thermocycler	Peqlab, VWR
VI-CELL BLU	Beckmann Coulter
Homogeniser Bead Mill MAX	VWR
SpectraMax i3x, Multi-Mode Microplate Reader	Molecular Devices
4200 TapeStation System	Agilent

2.1.9 Software

Table 10: List of software

Software	Developer
GraphPad Prism v. 10.6.1	GraphPad Software LCC
RStudio for MacOS v. 2024.04.2+764	Posit PBC
FlowJo for MacOS v.10.10.0	FlowJo, LCC (BD)
Adobe Illustrator 27.8	Adobe
Microsoft® Excel for Mac v.16.78	Microsoft Corporation
Microsoft® Word for Mac v.16.78	Microsoft Corporation
Mendeley Reference Manager v. 2.138.0	Elsevier Ltd.

Fiji (based on ImageJ2 v. 2.16.0/1.54p)	Fiji Community
Zen Blue 3.1	Zeiss
BioRender.com	BioRender

2.2 Mice

2.2.1 Husbandry

All animal experiments were performed in accordance with the German law of animal protection and local institutional animal care committees (Landesamt für Natur, Umwelt und Verbraucherschutz, LANUV) and with the permission of the state North Rhine-Westphalia (81-02.04.2019.A111, 81-02.04.2023.A004). Mice were kept under specific pathogen-free conditions in individually ventilated cages in the mouse facilities of the University Hospital Bonn, the Haus für Experimentelle Therapie (HET), and the Immunological Facility of Experimental Therapy (iFET). The enclosures for laboratory rodents in both the HET and the iFET had a standardized air temperature of 22 °C, 50 - 60 % humidity and up to 15 air changes per hour. The animals were housed in polysulfone cages under standard conditions with a 12-hour light/dark cycle and they were provided with complete feed and fresh water *ad libitum*. Purchased mice were acclimatized for at least one week before the diet was changed to an experimental diet. Either standard chow diet (SC) (Cat. No. V1534-300, Sniff Spezialdiäten GmbH), WD containing 21% fat, 19.5% Casein, 1.25% Cholesterin (Cat. No. 88137, Ssniff) or the matched purified control diet (CD) to 88137 were given, depending on the experimental condition. Mice were euthanized under deep anesthesia induced by ketamine and xylazine, followed by a terminal blood collection via cardiac puncture. In the experiments involving *Ldlr*$^{-/-}$ and *Apoe*$^{-/-}$ mice, animals were perfused with PBS to allow subsequent brain analysis by collaboration partners.

2.2.2 Mouse lines

2.2.2.1 B6J wildtype

The C57BL/6J mice (JAX stock #000664) is the inbred to which *Ldlr*$^{-/-}$ and *Apoe*$^{-/-}$ lines were backcrossed. B6J wildtype (WT) mice were either purchased from Charles River or bred inhouse.

2.2.2.2 *Ldlr*$^{-/-}$

The B6.129S7-*Ldlrtm1Her/J* mutant strain (JAX stock #002207, common name *Ldlr*$^{-/-}$) was purchased from Charles River. The insertion of a neomycin-resistance cassette into the gene encoding for the low-density lipoprotein receptor (*Ldlr*) is predicted to encode a truncated protein that will not bind LDL (Ishibashi et al., 1993). This leads to elevated serum cholesterol levels (200-400 mg/dL), which can reach very high levels (>2,000 mg/dL) when fed a high fat diet (Ishibashi et al., 1994).

2.2.2.3 *Apoe*$^{-/-}$

The B6.129P2-*Apoetm1Unc*/J mutant strain (JAX stock #002052, common name *Apoe*$^{-/-}$) was purchased from Charles River. *Apoe*$^{-/-}$ mice have a mutant *Apoe* gene, inactivated by insertion of a neomycin-resistance gene that disrupts the *Apoe* gene (Piedrahita et al., 1992). Mice that are homozygous for the mutant gene have no APOE in the plasma, but markedly elevated total plasma cholesterol. *Apoe*$^{-/-}$ mice have baseline hypercholesterolemia of approximately 600-700 mg/dL at eight weeks of age and develop fatty streaks in the proximal aorta at three months of age.

2.2.3 Mouse models

2.2.3.1 *Ldlr*$^{-/-}$ diet induction model

Female, nine-week-old *Ldlr*$^{-/-}$ mice were fed a WD or CD for four weeks. HPβCD (Cavitron^{TM} W7 HP7) or PBS as vehicle (Veh) control were administered as single doses via oral gavage (500 mg/kg/day) or subcutaneous (s.c.) injection (2g/kg/day) on the last two days before euthanasia. The mice were housed in the HET.

2.2.3.2 WT diet induction model

Male, eight-week-old WT mice were fed a WD for six weeks. During the last three weeks HPβCD (Cavitron^{TM} W7 HP5) or PBS was administered s.c. twice per week (2g/kg/day). The mice were housed in the iFET.

2.2.3.3 *Apoe*$^{-/-}$ atherosclerosis model

Female and male, eight-week-old *Apoe*$^{-/-}$ mice were used for atherosclerosis experiments and were housed in the HET facility. The studies were designed and conducted by the

group of Prof. Sebastian Zimmer (Heart Centre, University Hospital Bonn) who kindly shared access to samples and data. During the prevention (prophylactic) model, mice were fed a WD for eight weeks and were concomitantly treated with HPβCD (Cavitron™ W7 HP5 or W7 HP7) or sodium chloride (NaCl) as Veh control. An additional dietary control group was fed with SC and did not undergo any injections, allowing for organ retrieval under untreated conditions. The study included 10 male and 5 female mice per treatment group, and 5 mice of each sex for the chow-fed control group. In the regression (therapeutic) model, mice were first fed a WD for eight weeks to induce atherosclerosis, followed by a four-week chow diet phase during which HPβCD or NaCl was administered. HPβCD and NaCl were administered via intraperitoneal (i.p.) injection (2g/kg/day) twice a week in both models.

2.3 Methods

2.3.1 Preparation of HPβCD

HPβCD was prepared by dissolving it in PBS or NaCl as indicated. For cell culture experiments, a stock solution of 200 mM HPβCD was prepared and filtrated using a 0.2 µm filter unit attached to a sterile syringe. It was stored at 4°C and used for up to two weeks. Prior to use, the solution was vortexed to ensure homogeneity.
Several forms of HPβCD exist and two of them were used in the following work, which are Cavitron™ W7 HP5, Ashland (referred to as “HPβCD-HP5” or “HP5”) and Cavitron™ W7 HP7, Ashland (referred to as “HPβCD-HP7” or “HP7”), manufactured by Wacker Chemie.

2.3.2 Isolation of primary cells

2.3.2.1 Bone marrow

To isolate bone marrow cells, legs were dissected into femora and tibiae, and muscle and connective tissue were carefully removed. Bones were disinfected with 70 % ethanol prior to cutting open both ends. For Fluorescent-activated cell sorting (FACS) of GMP, front legs were dissected in addition to the hind legs. Bone marrow was flushed with 20 mL PBS/EDTA buffer using a 27 G needle attached to a 20 mL syringe. For flow cytometry and cell culture experiments, bones were placed in a 0.5 mL microcentrifuge tube with a hole at the bottom, which was positioned inside a 1.5 mL tube pre-filled with 100 µL of sterile FACS buffer. The bone marrow was centrifuged at 2,500 x g for 1 min, and the

supernatant was collected in PCR strips. These samples were centrifuged again at 350 x g for 5 min at 4°C. The cell-free supernatant was transferred into fresh PCR strips and stored at -20°C for IL-1β ELISA. The cell pellet remaining in the 1.5 mL tube was resuspended in 1 mL RBC lysis buffer and incubated on ice for 15 min. The cell suspension was then passed through a 70 µm cell strainer into a 50 mL Falcon tube, and the reaction was stopped by adding 10 mL PBS/EDTA buffer. Cells were centrifuged at 340 x g for 5 min at 4°C, the supernatant was aspirated, and the pellet was resuspended in 1 mL FACS buffer. Finally, cell numbers were determined using an automated cell counter.

2.3.2.2 Blood

Blood was drawn by cardiac puncture from the left arterial ventricle using a 23 G needle coated with EDTA and transferred into a 1.5 mL tube containing 10 µL of 0.5 M EDTA. For serum collection, no anticoagulant was used and the samples were kept at room temperature (RT) for approximately 30 min to allow complete coagulation, and were then centrifuged at 1,000 x g for 15 min at 4°C. The resulting serum was immediately snap frozen in liquid nitrogen. For plasma collection, blood was centrifuged at 800 x g for 10 min at 4°C or 7,500 rpm for 8 min at 4°C, and the plasma layer was collected and snap frozen. In experiments involving atherosclerotic plaque analysis, blood was drawn from the inferior vena cava using a heparinized 26 G needle. For isolation of circulating immune cells, red blood cells were lysed by adding 1 mL RBC buffer. After 15 min incubation at RT, samples were centrifuged at 350 x g for 5 min at 4°C. The lysis step was repeated once, and the remaining cells were resuspended in 1 mL FACS buffer. 500 µL of the cell suspension were used for flow cytometry analysis.

2.3.2.3 Stromal vascular fraction

Gonadal white adipose tissue (gWAT) was surgically removed from mice and processed for stromal vascular fraction (SVF) isolation. The gWAT was transferred into 2 mL tubes containing 1 mL of ice-cold WAT buffer and was minced into small pieces (approx. 2 mm). The minced tissue was transferred into a 50 mL Falcon tube and the 2 mL tube was rinsed with 2 mL of WAT buffer which was added to the 50 mL Falcon tube. An freshly prepared enzyme solution (Table 11) was added 1:1 and tissues were digested for 30 min at 37°C

with agitation (180-190 rpm). For cell culture experiments, the following steps were done under sterile conditions. The digestion was quenched by adding WAT buffer and the dissociated cells were passed through a 100 µm cell strainer and centrifuged at 500 × g for 10 min at 4°C. The resulting supernatant containing mature adipocytes was aspirated, and the pellet, consisting of the SVF, was resuspended in Ammonium-chloride-potassium lysis buffer (ACK) lysis buffer for 2 min at RT. The reaction was stopped by adding WAT buffer and another round of centrifugation at 500 × g for 7 min at 4°C. Isolated cells were then further subjected to antibody staining for flow cytometry.

Table 11: Enzyme solution for SVF isolation.

Total volume (per tissue)	WAT buffer	Collagenase II (200 mg/mL in PBS)	CaCl2 (1 M)	DNAse (15,000 U/mL)
3 mL	3 mL	30 µL	15 µL	15 µL

2.3.3 Flow cytometry

Bone marrow cells, circulating immune cells and ATM were analyzed by flow cytometry. If the analysis was done on the next day, cells were stored in MACS Cell Storage Solution overnight. Isolated cells were stained in a 96-well flat bottom plate. For staining circulating cells and ATM, FcR blocking reagent was added (1:100). If LIVE/DEAD™ Fixable Near-IR was used, cells were incubated in 100 µL of the diluted dye (1:1,000 in PBS) for 20 min at RT protected from light. After a washing step with PBS, cells were stained with antibody staining solution for 30 min at 4°C in the dark, then 60 µL FACS buffer was added and the plate was centrifuged at 350 x g for 5 min at 4°C. The supernatant was decanted and the pellets were resuspended in 100 µL FACS buffer. For measurements at the Attune NxT Flow cytometer cells remained in the 96-well plate, for other cytometers the cells were transferred into 5 mL polystyrene tubes and the volume was adjusted equally with FACS buffer. When 7-AAD was used as Live/Dead stain, it was added shortly before measurement (1:50). Counting beads were added as a last step (1:15-1:8). Samples were analyzed on the Attune NxT Flow Cytometer, BD FACS Canto™ II, ID7000 Spectral Analyser 5L and BD FACSAriaTM Fusion Flow Cytometer. Cell counts per µL were calculated with the following formula:

$$\frac{\text{cells}}{\mu\text{L}} = \frac{\#\text{cells} * \text{cell volume [µL]}}{\#\text{beads} * \text{bead volume [µL]}} * 1{,}000\ \frac{\text{beads}}{\mu\text{L}}$$

2.3.4 Sorting of cells

2.3.4.1 Fluorescent-activated cell sorting (FACS)

GMP were sorted from mixed bone marrow cell populations by FACS with the BD FACSAriaTM Fusion Flow Cytometer. Cells were stained as described above and sorted into 1.5 mL tubes containing either 700 µL ice-cold phenol/guanidine-based QIAzol Lysis Reagent, if the downstream analysis was RNA-seq, or 250 µL FACS buffer, if the downstream analysis was Assay for Transposase-Accessible Chromatin (ATAC)-seq.

2.3.4.2 Magnetic-activated cell sorting

Adipocyte-precursor cells were isolated from SVF cells using Magnetic-activated cell sorting (MACS) according to the manufacturer's instructions (Miltenyi Biotec). SVF cells were incubated with the non-adipocyte progenitor depletion cocktail of the Adipose Tissue Progenitor Isolation Kit (1:10) which contains anti-CD31, anti-CD45 and anti-TER119 antibodies conjugated to magnetic beads. Samples were run through LS columns followed by three washes with MACS buffer. Unlabeled cells were collected, centrifuged at 500 x g for 7 min at 4°C and resuspended in growth medium for culturing (referred to as SVF Lin- cells).

2.3.5 *Ex vivo* stimulation of bone marrow cells

96-well cell culture plates were pre-filled with 50 µL of stimuli (4x) in RPMI1640 supplemented with L-Glut, 10 % FCS and 1 % Pen/Strep beforehand and thawed on the day of the experiment. Bone marrow cell suspensions were prepared as described above and were added to the prepared plates in 150 µL of medium (200,000 cells/well). Cells were stimulated with the following ligands overnight: Pam3CysK4 (TLR2; 0.1, 10, or 100 ng/mL;), LPS (TLR4; 1, 10, or 100 ng/mL), R848 (TLR7/8; 10 or 100 ng/mL, or 10 µg/mL), CpG (TLR9; 1 or 5 µM) and DMXAA (murine STING agonist; 50 µg/mL). On the following day, plates were centrifuged at 350 x g for 5 min at 4°C to promote attachment of the cells to the plate bottom. Subsequently, supernatants were collected and stored at -20°C for cytokine measurement by ELISA or HTRF.

2.3.6 *In vitro* adipogenesis

The media used were either published (K. I. Hilgendorf et al., 2019) or established by the lab of Prof. Dagmar Wachten (Institute of innate Immunity, University of Bonn). SVF Lin$^-$ cells were pre-seeded in 6 cm cell culture dishes with 5 mL growth medium and incubated at 37°C and 5 % CO2. The next day, cells were washed three times with growth medium and fresh medium was added for further incubation. The medium was exchanged two days later and cells were seeded one day after, before reaching total confluency estimated using the Evos FL. Cells were harvested with trypsin, counted using an automated cell counter and were seeded into a black 96-well microscopy plate with 20,000 cells/well in 300 µL of medium. On the following day, adipogenesis was induced (day 0) using the minimal or full induction cocktail, and with or without of HPβCD-HP5 or HP7. The undifferentiated control cells received growth medium. The induction medium was replaced by maintenance medium on day 3. On day 6, the old medium was exchanged and stored at -20°C for FGF-21 ELISA. On day 8 post induction, the medium was removed, cells were fixed with 4 % paraformaldehyde (PFA) for 10 min and subsequently washed with PBS. For studying the kinetics of the proliferation marker Ki-67, cells were fixed on day 0, 3, 6, and 8, in order to compare the development of Ki-67 expression over time. Fluorescence images of adipogenesis assays were acquired automatically using a ZEISS Celldiscoverer 7 microscope. Image analysis was performed in Fiji (ImageJ) and AdipoQ (Sieckmann et al., 2022) with customized parameters to identify adipocytes and lipid droplets. Representative images are shown as maximum projections around the sharpest focal plane, generated with the ImageJ plugin *ExtractSharpestPlane_JNH* (Hansen et al., 2021; https://doi.org/10.5281/zenodo.5646492).

Table 12: Media for the adipogenesis assay

Medium	Components
Growth medium	DMEM/F-12 (1:1) (1x) + GlutamaxTM-I + 10 % FCS + 1 % Pen/Strep + 0.1 % Biotin (33 µM) + 0.1 % D-Pantothenic acid (17 µM)

Full induction cocktail	Growth medium + 5 µg/mL insulin + 1 µM Dexamethasone + 100 µM 3-isobutyl-1-methylxanthine (IBMX) + 1 µM rosiglitazone
Minimal induction cocktail	Growth medium + 0.4 µg/mL insulin + 0.1 µM Dexamethasone + 20 µM 3-isobutyl-1-methylxanthine (IBMX)
Maintenance medium	Growth medium + 1 µg/mL insulin

2.3.7 Explant culture

Male, four days old (P4) pups were euthanized by decapitation using scissors. The precursor tissue of the gWAT was collected by isolation of the testis. Using the ZEISS Stemi 508 and fine scissors and forceps, the testis was removed from the epididymis and the precursor adipose tissue. The remaining tissue was cultured in 150 µL RPMI medium with 10 % FCS, 1 % Pen/Strep, with or without HPβCD-HP5 and HP7 in a 96-well tissue culture plate at 37°C and 5°C CO_2. On the following day, 250 µL medium were added and three days later the complete medium was exchanged with fresh 500 µL medium. On day five after explant isolation, the tissues were fixed with 4 % PFA for 30-40 min at RT and subsequently washed with PBS. Confocal imaging was done using z-stacks and images were analyzed in Fiji (ImageJ) and AdipoQ (Sieckmann et al., 2022) with customized parameters to identify lipid droplets.

2.3.8 Fluorescent staining

Differentiated and fixed adipocytes were blocked with CT (0.5 % Triton X-100, 5 % ChemiBLOCKER in PBS) for 30 min at RT. Cells were stained with the primary antibody against the proliferation marker Ki-67 (1:500) for 60 min, followed by the secondary antibody (anti-rat AF647, 1:150) and DAPI (1:10,000) for 30 min. Lastly, lipid droplets were

stained with LD540 (1:2000-1:10,000, depending on batch) for 15 min. Cells were stored in PBS at 4°C until they were imaged with the ZEISS Celldiscoverer 7.
Fixed gWAT explants were blocked with CT for 15 min at RT, washed with PBS and stained with LD540 (1:2000) and DAPI (1:10,000) in PBS for 30-45 min at RT. Tissues were washed three times with PBS and mounted on a slide using PolyA Mount. The slides were dried overnight protected from light and then stored at 4°C until imaging at the confocal microscope Leica Stellaris 8.

2.3.9 Lipids

2.3.9.1 Lipolysis assay

The *ex vivo* lipolysis assay was adapted from the protocol by Roy et al., 2022. The gWAT from male and female WT mice was excised and cut into equally weighed pieces of approximately 15 mg. Tissue fragments were first placed in ice-cold PBS and then transferred to a 24-well plate containing 200 µL of lipolysis assay medium (high glucose DMEM supplemented with 2% fatty acid-free BSA) and the indicated concentrations of HPβCD. Norepinephrine (NE, 1 µM) served as a positive control. Tissues were minced into small pieces (approx. 2 mm) and incubated for 2 h at 37°C and 5 % CO2. Following incubation, 40 µL of the medium was transferred in duplicates to a 96-well plate, and 60 µL of free glycerol reagent was added. A free glycerol standard solution was included as a positive control and for quantification. After 5 min incubation at 37°C, absorbance was measured at 540 nm using a SpectraMax Microplate Reader. Glycerol concentrations were calculated in Microsoft Excel and normalized to tissue weight and the untreated control condition.

2.3.9.2 Cholesterol

Sterols and oxysterols in plasma were quantified using gas chromatography (GC) coupled with either flame ionization detection (FID) for cholesterol or mass spectrometry in selected ion monitoring mode (GC–MS–SIM) for non-cholesterol sterols and oxysterols, following established protocols (Šošić-Jurjević et al., 2019). The work was conducted by the laboratory of Prof. Dr. Dr. rer. nat. Dieter Lütjohann (Institute of Clinical Chemistry and Clinical Pharmacology, University Hospital Bonn).

Sterols were converted into O-trimethylsilylated (TMSi) and oxysterols into di-O-trimethylsilylated derivatives to enhance volatility and chromatographic separation. Chromatographic separation was performed on a DB-XLB column (30 m × 0.25 mm i.d., 0.25 µm film; J&W Scientific Alltech, USA). GC–FID analyses were conducted on an Agilent HP 6890 Series system, and GC–MS analyses on an Agilent HP 6890N coupled to an HP 5975B quadrupole mass detector, both equipped with automated injectors and samplers. Each plasma sample was spiked with internal standards: 5α-cholestane (50 µg), epicoprostanol (1 µg), and deuterated oxysterols: [$^2H_4$]24(R,S)-hydroxycholesterol (50 ng), [$^2H_6$]7α-hydroxycholesterol (100 ng), and [$^2H_5$]27-hydroxycholesterol (100 ng). Samples were saponified with 1 M ethanolic NaOH at 60 °C for 1 h, and lipids were extracted three times with cyclohexane. The extracts were evaporated under nitrogen at 60 °C and redissolved in n-decane (80 µL). Aliquots were derivatized using a trimethylsilylating reagent (chlorotrimethylsilane: hexamethyldisilazane:pyridine = 9:3:1) for 1 h at 70 °C. Automated splitless injections (2 µL) were performed using helium (1 mL/min) for GC–MS–SIM and hydrogen (1 mL/min) for GC–FID. The GC oven was held at 150 °C for 3 min, increased to 290 °C at 20 °C/min, and held for 34 min. Sterol and oxysterol concentrations were determined from peak area ratios relative to internal standards using calibration curves from authentic reference compounds. Compound identities were confirmed by full-scan mass spectra and characteristic fragment ions, ensuring accurate and specific quantification of plasma sterols and oxysterols.

2.3.9.3 Lipidomics

Lipid extraction from gWAT and plasma were performed by Dr. Jelena Zurkovic in the lab of Prof. Christoph Thiele (Life and Medical Sciences Institute (LIMES), University of Bonn). All solvents were HPLC grade or LC-MS grade. Lipid extraction from murine plasma and adipose tissue was performed using a $CHCl_3$/MeOH (1:5) extraction. For plasma samples, 2 µL of plasma were mixed with 500 µL of extraction mix containing class-specific internal standards. For adipose tissue, up to 10 mg of tissue (precisely weighed) were processed using the same extraction solvent with proportional amounts of internal standards. Samples were sonicated (10 s for serum, 15 min for tissue) and centrifuged at 20,000 × g for 2 min. The supernatant was combined with 200 µL $CHCl_3$ and 800 µL 1 % acetic acid, briefly vortexed, and centrifuged again at 20,000 × g for 2 min. The upper aqueous phase

was discarded, and the lower organic phase was collected and evaporated in a speed vacuum concentrator (45 °C, 10 min). Dried lipids were reconstituted in spray buffer (2-propanol/MeOH/H_2O, 8:5:1, 10 mM ammonium acetate) and sonicated for 5 min prior to analysis. Samples were analyzed by shotgun lipidomics using a Thermo Q Exactive Plus mass spectrometer equipped with a HESI II ion source. Spectra were acquired in positive ion mode, and raw files were converted to *.mzML* format for analysis with LipidXplorer using custom mfql files. Lipid species were identified and quantified based on internal standard intensities. Data was analyzed in Microsoft Excel.

2.3.10 Gene expression analysis

2.3.10.1 RNA isolation

Ribonucleic acid (RNA) was extracted using the QIAzol Lysis Reagent and the miRNeasy RNA isolation kit. Bone marrow cells were lysed and isolated according to the manufacturer's protocol. For gWAT, pre-filled BeadBugTM tubes were filled with 700 µL QIAzol and the tissue was added and homogenized using the Bead Mill MAX. Samples were centrifuged at 10,000 x g for 10 min at 4°C and the supernatant was transferred into a clean RNase-free 1.5 mL tube. Centrifugation and supernatant transfer were repeated approximately 4-5 times until the supernatant was clear of fat. Then the column-based RNA isolation was performed.

2.3.10.2 cDNA synthesis

RNA was converted to complementary deoxyribonucleic acid (cDNA) by reverse transcription. The final reaction was set up to a volume of 20 µL containing RNA (approx. 100-500 ng), 0.5 µM Oligo(dT)18 primer, 5 mM DTT, 0.5 mM dNTPs and 20 U SuperScript III reverse transcriptase with associated first-strand buffer. The cDNA synthesis was conducted by first diluting the RNA with ribonuclease (RNAse)-free water and adding Oligo(dT)18 primer. Samples were heated up in a thermocycler to 65°C for 5 min, the program was paused, and samples were cooled down on ice for at least one minute. The mastermix containing DTT, dNTPs, the reverse transcriptase and the according buffer was added. The reverse transcription was performed at 50°C for 50 min and the reaction was inactivated at 85°C for 5 min. The cDNA was stored at -20°C until usage.

2.3.10.3 qPCR

The quantitative polymerase chain reaction (qPCR) was set up in a 384-well plate and a final volume of 10 µL containing cDNA, 0.4 µM gene-specific primer pairs (Table 8), RNAse-free water and primaQUANT 2x qPCR CYBR-Green Master Mix, no ROX, blue (alternatively ADVANCED with ROX). The amplification was performed using the QuantStudio 6 Flex and the following temperature cycles: 95°C 10 min; 40x [95°C, 15 sec; 60°C, 1 min]. The target gene expression relative to the housekeeping gene hypoxanthin-guanin-phosphoribosyltransferase *(Hprt)* was calculated using the ΔΔCT method.

2.3.10.4 Bulk RNA-sequencing and analysis

RNA-sequencing (seq) was performed at the Next generation sequencing (NGS) Core facility of the University of Bonn. RNA integrity was determined using the High Sensitivity RNA Screen tape assay with a 4200 TapeStation system (Agilent). RNA libraries were prepared using the QuantSeq 3′ mRNA Library Prep Kit (Lexogen). Sequencing was carried out on an Illumina NovaSeq 6000 platform in single-end mode with a read length of 1 × 100 bp, yielding an average coverage of approximately 15 million raw reads per sample.

Data analysis was performed by Lena Standke and Dr. Jamie Gearing from the Latz lab, Institute of Innate Immunity, Bonn and DRFZ, Berlin, using R (R Core Team, 2023). Read alignment of adapter-trimmed FASTQ files was performed with default settings. Stranded gene counts were then obtained using the featureCounts function and the Ensembl *Mus musculus* GRCm39 GTF annotation file (v107).

Differential gene expression analyses were performed using using the edgeR (Robinson et al., 2009) and limma (Ritchie et al., 2015) packages. A DGEList object was created from the featureCounts output analysis and Ensembl gene IDs were annotated using the biomaRt package (Durinck et al., 2005, 2009). A design matrix was constructed with samples grouped according to their combination of diet (WD or CD), treatment (HP7 or Veh) and application route (oral or sc). One outlier sample (WD_Veh_oral_5) was excluded from further processing. Lowly expressed genes were removed using the filterByExpr function with a minimum count of 20 and normalisation factors were calculated using the TMM method (Robinson and Oshlack, 2010).

The edgeR cpm function was used to calculate $\log_2$ counts per million (CPM) normalised expression values. Principal component analysis (PCA) plots were created using the plotMDS function with a common gene selection of the top 50 most variable genes. Counts were transformed using the voom method (Law et al., 2014) and a linear model was fit using the edgeR voomLmFit function. Groups were compared using the contrasts.fit function and moderated *t*-statistics were calculated using eBayes (Phipson et al., 2016). Differentially expressed gene were defined as those with a false discovery rate (FDR)-adjusted *p* -value < 0.05. Venn diagrams showing the overlap of significantly up- and down-revaluated between different comparisons were made with help of the limma vennDiagram function.

The eBayes moderated *t*-statistics for comparisons of interest were used with the limma barcodeplot function to display monocytic signature (*Cd34*, *Csf1r*, *Cfp*, *Ly86*) and granulocytic signature (*S100a8*, *S100a9*, *Ets1*, *Pglyrp1*, *Cd63*, *Ceacam1*) gene sets (Christ et al., 2018) and an LXR target gene set (Zimmer et al., 2016).

For comparison with other cell types, gene counts and sample annotation were obtained from the Haemopedia mouse RNA-seq data set (Choi et al., 2019). The edgeR cpm function was used to calculate $\log_2$CPM expression values. Genes were restricted to the 11,950 common genes between the RNA-seq data set and the Haemopedia data. Haemopedia data were then filtered to only bone marrow progenitor cells and the top 1,000 most variable genes across these samples were selected. Average $\log_2$CPM values for the RNA-seq data were calculated using the aveLogCPM function. Pearson correlations were then calculated between each Haemopedia progenitor sample and the average RNA-seq data based on these 1,000 genes.

2.3.11 ATAC-sequencing and analysis

For ATAC-seq 50,000 flow sorted GMP were processed following the published protocol by Buenrostro et al., 2013, with modifications by the Kaestner lab, University of Pennsylvania and adjustments made by the S. Schmidt/Latz group. Briefly, cells were washed with cold PBS, centrifuged at 350 x g for 5 min, resuspended in lysis buffer and after 3 min incubation on ice were rinsed with wash buffer. After centrifugation at 500 x g for 10 min at 4°C, the supernatant was discarded and the pellet containing the nuclei was resuspended with the transposition reaction mix using the Illumina Tagment DNA Enzyme

and Buffer (TDE1) kit. Samples were incubated at 37°C for 30 min on a thermomixer at 1,000 rpm and DNA was isolated using the MinElute Reaction Cleanup Kit. ATAC-seq libraries were generated by PCR amplification and using the IDT® for Illumina® DNA/RNA UD Indexes Set A, Tagmentation kit. PCR products were purified using double-sided bead purification with AMPure XP beads and library quality was assessed using Agilent D1000 ScreenTape Assays for TapeStation. Libraries were sequenced on an Illumina NovaSeq 6000 platform using an S1 flow cell at the NGS Core facility, University of Bonn. The sequencing was carried out in paired-end mode with a read length of 2 × 50 bp (100 cycles in total) and each sample achieved an average coverage of approximately 40 million reads.

Table 13: Buffers for ATAC-seq cell preparation

Buffer	Components
Resuspension Buffer	Nuclease-free H2O + 10 mM Tris-HCl, pH 7.5 + 10 mM NaCl + 3 mM MgCl2
Lysis Buffer	Resuspension Buffer + 0.1 % v/v NP-40 + 0.1 % v/v Tween-20 + 0.1 % v/v Digitonin
Wash Buffer	Resuspension Buffer + 0.1 % Tween-20

ATAC-seq analysis was done by Svetozar Nesic, PhD, Bioinformatics Core facility, University of Bonn. The data was processed using the nf-core/atacseq pipeline (v1.2.2) implemented in Nextflow (v22.04.5) with the Docker profile. Fastq reads were trimmed and aligned to the *Mus musculus* reference genome (GRCm38) using the Burrows-Wheeler Aligner (BWA). Genome annotation files (FASTA, GTF, and BED) were obtained from Ensembl, and blacklisted regions (GRCm38-blacklist.bed) were excluded from downstream analysis. Duplicate reads and mitochondrial fragments were removed prior to peak calling. Peaks were called with MACS2 (broad peaks, cutoff = 0.1) using an

effective genome size of 1.87 × 109 bp. Read counting and differential chromatin accessibility analysis were performed using DESeq2 to identify differentially open chromatin regions (DORs) between experimental groups. The Bioconductor package csaw (Lun A, Smyth G., 2024) was used to determine differentially open regions using a sliding window analysis. Statistical significance was determined based on the FDR and absolute $\log_2$ fold change ($|\log_2 FC|$). Regions with FDR < 0.05 and $|\log_2 FC| > 1$ were considered significantly differentially accessible. Regions with FDR > 0.05 and $|\log_2 FC| < 1$ were classified as non-significant, while those with FDR > 0.05 but $|\log_2 FC| > 1$ were highlighted as showing large, yet statistically non-significant, changes.

2.3.12 Histology

2.3.12.1 Atherosclerotic plaque

Preparation of atherosclerotic plaques was performed by members of the Zimmer laboratory (Heart Center, University hospital Bonn). Hearts and aortas were rinsed with NaCl and embedded in Tissue-Tek® O.C.T.™. Cryosections of 8 µm thickness were prepared from the aortic root area of the heart and subsequently stained with hematoxylin and eosin (HE). Images were acquired using a ZEISS Axio Observer 7 microscope, and image analysis was carried out with ZEN 3.19 (ZEN lite).

2.3.12.2 Adipocyte morphology in gWAT

Excised gWAT samples were fixed in formalin for 30 min at RT, then washed and stored in PBS. Paraffin embedding, sectioning, and HE-staining were performed at the Histology Platform of the University Hospital Bonn. Sections were imaged using a Zeiss Axio Scan. Z1 microscope of the Microscopy Core Facility of the University of Bonn. Image analysis was conducted in Fiji (Image J) and AdipoQ (Sieckmann et al., 2022) with customized preferences to identify and analyze adipocyte morphology.

2.3.13 Protein Biochemistry

2.3.13.1 Preparation of protein lysates

For gWAT protein lysates, pre-filled BeadBugTM tubes were filled with 1 mL protein lysis buffer (in mM: 10 Tris/HCl pH 7.6, 140 NaCl, 1 EDTA, 1 % (v/v) TritonX-100, 1:500

mPIC) and the tissue was added and homogenized using the Bead Mill MAX. Samples were centrifuged at 10,000 x g for 10 min at 4°C and the supernatant was transferred into a clean RNase-free 1.5 mL tube. Centrifugation and supernatant transfer were repeated approximately 3-5 times until the supernatant was clear of fat. Protein concentrations were determined using the Pierce™ BCA Protein Assay Kit following the manufacturer's instructions, with minor modifications. The assay volumes were reduced from 200 µL to 190 µL of BCA reagent mix and from 25 µL to 10 µL of sample or standard. Bovine serum albumin (BSA) standards were prepared in protein lysis buffer, and absorbance was measured using a SpectraMax Microplate Reader.

2.3.13.2 Simple Western protein analysis (Wes^{TM})

Protein separation and detection was performed using the Wes^{TM} system and its corresponding separation module following the manufacturer's protocol. Protein quantification was based on the area under curve (AUC), calculated in the Compass software. For the regression model, 5 µg of protein were used and for the prevention model 1 µg (females) or 1.5 µg (males) were loaded. Samples were diluted in ddH2O prior to analysis.

2.3.13.3 Measurement of cytokine secretion and analysis

Enzyme-linked immunosorbent assays (ELISA), homogeneous time-resolved fluorescence assays (HTRF), and multiplex assays (Ayoxxa, Olink, and Luminex Discovery Assay) were performed according to the manufacturer's instructions. For ELISA, assay volumes of capture and detection antibody, as well as sample volume were reduced by half. For HTRF, assay volumes were reduced by a fourth from 16 µL to 12 µL of sample volume and from 4 µL to 3 µL antibody mix. Absorbance or emission were measured with a SpectraMax Microplate Reader. The Ayoxxa panels were read on the LUNARIS™ Reader 96, and Olink measurements were carried out using the Olink Signature Q100 at the Max Delbrück Center, Berlin, Germany. For bead-based assays from Millipore or R&D Systems, samples were analyzed on a Luminex™ FLEXMAP 3D™ instrument. Missing values for adiponectin of females in the regression model are due to limited capacity of sample number on the plate and dropouts of two samples with low bead counts.

Data analysis of ELISA and HTRF were done in Microsoft Excel. Cytokine data from Ayoxxa were analyzed in R by Kai Zimmer (guest scientist in S. Schmidt lab, Institute of Clinical Chemistry and Clinical Pharmacology, Bonn) and Titus Schlüter (Netea lab, Radboud University, Nijmegen). Data from the Olink Target 48 Mouse Cytokine panel were pre-processed by Matthias Ziehm (MDC & BIH Proteomics Platform, Max Max Delbrück Center, Berlin) and analyzed by Dr. Jamie Gearing (Latz lab, DRFZ, Berlin) in R using the limma package (Ritchie et al., 2015). A design matrix was created based on diet (WD or CD) and treatment (HP5 or Veh), including plate as a batch effect. One sample (WD-HP5, mouse 10) was excluded due to QC warnings, and two cytokines (IL-31, CXCL12) were removed for being below quantification limits in > 50% of the samples, resulting in 41 out of 43 total analytes for analysis. DE was assessed with lmFit**,** contrasts.fit, and eBayes (Phipson et al., 2016) (including a mean–variance trend). Proteins with an adjusted $p < 0.05$ were considered significantly differentially expressed. For Luminex assays, the median fluorescence intensity of the beads was recorded and quantified using Flexmap 3D software with five-parameter logistic (5-PL) weighted analysis. Data analysis and visualization was performed in RStudio. Samples with low bead counts for all measured protein were excluded, as were proteins with more than 50 % missing data or low bead numbers (< 30). Missing values are shown in grey.

2.3.14 Statistics

Statistical analysis was performed using GraphPad Prism. Data were analyzed by one-way or two-way analysis of variance (ANOVA), followed by appropriate post hoc tests with correction for multiple comparisons. Dunnett's test was applied when comparing each treatment group to a designated control, while Tukey's multiple comparison test was used for pairwise comparisons among all groups. Statistical significance was determined at an alpha level of 0.05 (95% confidence interval). Significance levels are indicated as follows: * $p < 0.05$, ** $p < 0.01$, *** $p < 0.001$ and **** $p < 0.0001$.

3. Results

3.1 Effects of Cavitron™ W7 HP7 (HPβCD-HP7) on inflammation and hematopoiesis in the *Ldlr*$^{-/-}$ model

To examine how HPβCD influences the effects of WD on the immune system, we conducted an experiment adapted from the TI model published by Christ et al. (2018). Female *Ldlr*$^{-/-}$ mice received a WD or matched CD for 4 weeks, and HPβCD (Cavitron™ W7 HP7, here: HPβCD-HP7) was administered orally or via s.c. injection on two consecutive days preceding euthanasia and subsequent tissue collection (**Fig. 5a**).

3.1.1. Effects of WD and HPβCD-HP7 on the bone marrow and systemic cytokines

In the oral treatment group, WD induced significantly increased weight, which was lower in the HPβCD-HP7 treatment group. Within the s.c. group, WD had no effect on BW, whereas HPβCD**-**HP7 co-administration significantly increased it (**Fig. 5b-c**).

Cytokine and chemokine profiling were performed to assess systemic inflammatory responses. The cytokine assay revealed no elevation among the eight detectable cytokines (**Fig. 5d**). Four cytokines (IL-1β, TNFα, IL-4 and IL-17A) were below the detection limit. In contrast, the chemokine assay showed markedly increased levels of CCL3, CCL22, CCL5 and CCL19 under WD conditions, which were attenuated by additional HPβCD-HP7 treatment. These findings indicate that WD feeding primarily induces a chemokine-driven inflammatory response that is mitigated by HPβCD-HP7 (**Fig. 5e).** Other chemokines like CCL11, CXCL10, CCL4, CCL2 and CXCL1 were higher in the WD group, and there was no difference compared to the mice that were additionally treated with HPβCD.

To examine myelopoiesis, a hallmark of WD-induced effects, we assessed GMP using flow cytometry (**Fig. 5f, Fig. S1**). WD feeding led to an increase in GMP compared to CD, which was reduced following HPβCD-HP7 treatment (**Fig. 5g**). This was significant in the oral condition, but not in the s.c. group. In the latter, frequencies were generally lower in than in the oral group.

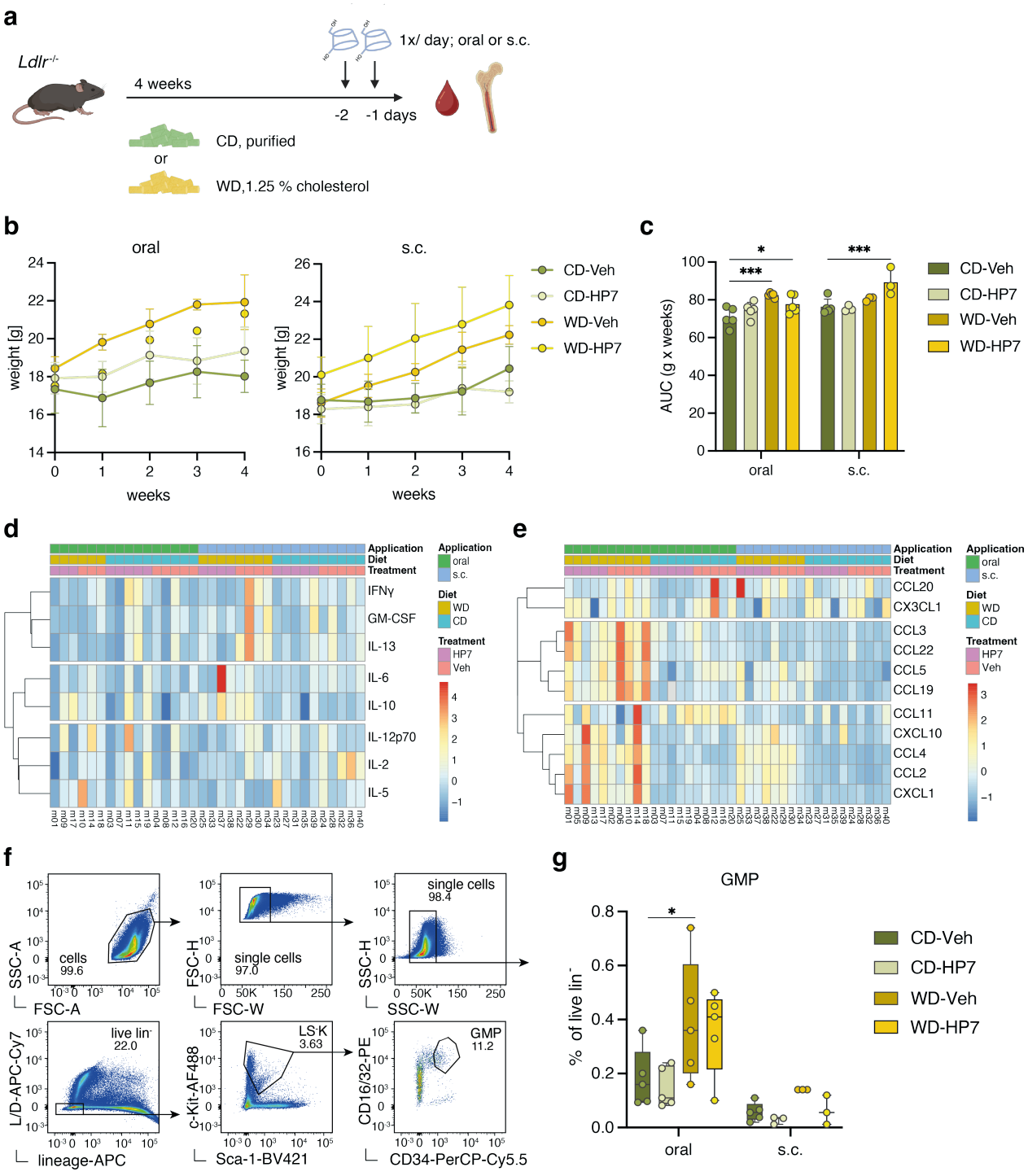

Fig. 5: Systemic effects of short-term HPβCD-HP7 administration in *Ldlr*$^{-/-}$ mice on WD. a) Study design: female *Ldlr*$^{-/-}$ mice received a WD for four weeks and were treated with HPβCD-HP7 (HP7; 2 g/kg BW) or PBS (Veh) orally or via s.c. injection on two consecutive days prior to euthanasia. Blood and bone marrow were collected for downstream analysis. b) BW development over time in oral vs s.c. treatment groups. c) Quantified weight change expressed as AUC. (d, e) Heat maps of serum cytokines (d) and chemokines (e) stratified by application route, diet, and treatment. (f) Flow cytometry gating strategy for bone marrow analysis. (g) Frequency of GMP in the bone marrow.

Statistical analysis was performed by two-way ANOVA and Dunnett's multiple comparisons post hoc test; displayed *p*-values are adjusted for multiple testing. *n* = 3-5 mice per group.

3.1.2 Transcriptomic response of GMP to WD feeding and HPβCD-HP7 treatment

GMP were sorted for RNA- and ATAC-sequencing. To confirm GMP enrichment we used the transcriptomic data to compare the gene expression profiles of the sorted cells with known hematopoietic progenitor subsets using the Haemopedia database (**Fig. 6a**). The analysis supports that the identified gene sets are predominantly associated with GMP, rather than with other progenitor subsets such as common lymphoid progenitors (CLP) or megakaryocyte–erythrocyte progenitors (MEP). After data normalization, unsupervised clustering of the top 50 differentially expressed genes was performed to identify the main drivers of variation within the dataset (**Fig. 6b**). The principal components PC1 and PC2 had values of 14 % and 9 %, indicating that overall, there was a rather small difference between the samples. As indicated by different coloring of conditions, neither diet nor treatment appeared as significant driver of clustering, whereas the route of administration (oral vs s.c.) showed the strongest impact (**Fig. S2**). Differential expression (DE) analysis revealed fewer than ten DE genes in the WD vs. CD and HP7 vs. Veh comparisons (**Fig. 6c**). The WD-Veh vs. CD-Veh comparison in the oral group showed the highest number of DE genes. Here, six genes were downregulated (*mt-Nd4*, *C1qc*, *mt-Nd2*, *Casp2*, *Smg1*, *Bcl9*) and three genes were upregulated (*Hmox1*, *Apoc1*, *Psap*) (**Fig. 6d**). Increased *Apoc1* mRNA expression stood out with the highest fold change (FC) indicating changes related to increased lipid and cholesterol uptake, which is expected during WD feeding. In the comparison WD-HP7 vs WD-Veh, up to four genes were significantly altered. One of them, *mt-Atp6*, was downregulated in the s.c. group and upregulated in the oral group. Further, *Hmox1* and *C1q1* were influenced by both WD and HPβCD-HP7 (**Fig. 6c**). Heme oxygenase (*Hmox1*) is an inducible enzyme that becomes activated upon oxidative stress, such as reactive oxygen species and free heme, but also by hypoxia or lipid accumulation and acts as a cellular stress-response protein (Vijayan et al., 2018).

Following an unbiased approach, we further investigated whether we could observe the gene signature enrichments that have been described for GMP in Christ et al. (2018).

a

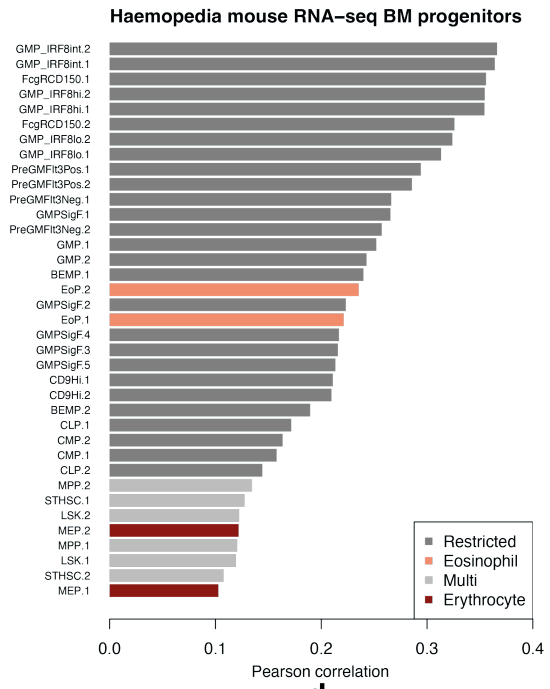

b

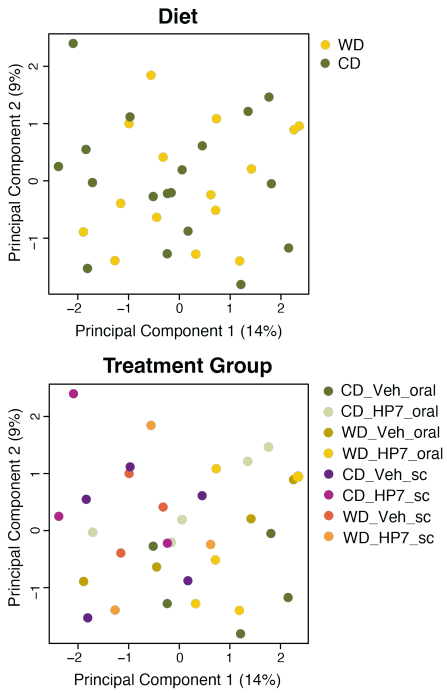

c

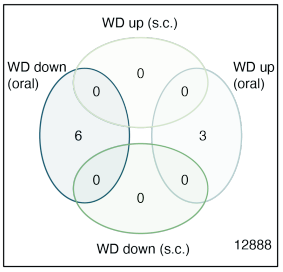

WD-Veh oral v CD-Veh oral
vs.
WD-Veh sc v CD-Veh sc

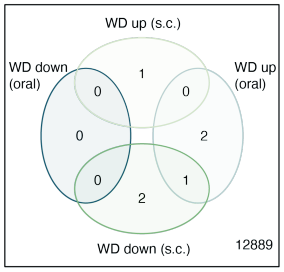

WD-HP7 oral v WD-Veh oral
vs.
WD-HP7 sc v WD-Veh sc

d

WD-Veh oral vs CD-Veh oral

Gene name	AveExpr	logFC	adj.P.Val	UP_KW_Biological Process
Hmox1 (heme oxygenase 1)	11.729	0.653	2.97E-38	Apoptosis
mt-Nd4 (NADH dehydrogenase 4, mitochondria)	12.777	-0.461	1.13E-17	Electron transport, Respiratory chain, Transport
C1qc (complement component 1, q subcomponent, C chain)	11.944	-0.090	7.87E-17	Complement pathway, Immunity, Innate immunity
mt-Nd2 (NADH dehydrogenase 2, mitochondria)	12.382	-0.950	9.79E-16	Electron transport, Respiratory chain, Transport
Casp2 (caspase 2)	0.454	-8.711	2.67E-02	Apoptosis
Apoc1 (apolipoprotein C-1)	8.144	2.292	3.05E-02	Lipid transport, Transport
Smg1 (nonsense mediated mRNA decay associated PI3K related kinase)	0.708	-9.107	3.05E-02	DNA damage, DNA repair, Nonsense-mediated mRNA decay
Psap (prosaposin)	11.419	0.610	3.05E-02	NA
Bcl9 (B cell CLL/lymphoma 9)	2.160	-8.400	3.05E-02	Wnt signaling pathway

WD-HP7 oral vs WD-Veh oral

Gene name	AveExpr	logFC	adj.P.Val	UP_KW_Biological Process
Hmox1	11.729	0.457	1.07E-07	Apoptosis
mt-Atp6 (ATP synthase 6, mitochondria)	12.255	0.386	2.36E-02	ATP synthesis, Hydrogen ion transport, Ion transport, Transport
mt-Nd4 (NADH dehydrogenase 4, mitochondria)	12.777	0.328	2.84E-02	Electron transport, Respiratory chain, Transport

WD-HP7 sc vs WD-Veh sc

Gene name	AveExpr	logFC	adj.P.Val	UP_KW_Biological Process
mt-Atp6 (ATP synthase 6, mitochondria)	12.255	-0.580	1.29E-09	ATP synthesis, Hydrogen ion transport, Ion transport, Transport
Ftl1 (ferritin light polypeptide 1)	12.424	-0.558	2.04E-05	Iron storage
C1qc (complement component 1, q subcomponent, C chain)	11.944	-0.532	1.30E-03	Complement pathway, Immunity, Innate immunity
Ifitm3 (interferon induced transmembrane protein 3)	8.463	1.868	6.83E-03	Antiviral defense, Immunity, Innate immunity

e

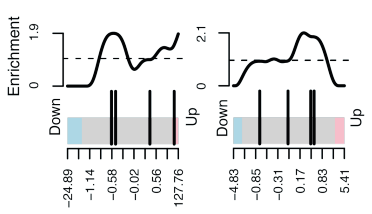

WD-Veh oral vs CD-Veh oral | WD-Veh sc vs CD-Veh sc

f

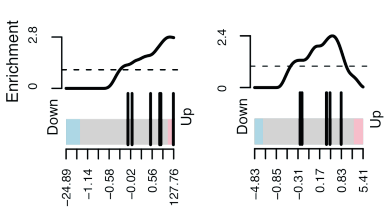

WD-Veh oral vs CD-Veh oral | WD-Veh sc vs CD-Veh sc

g

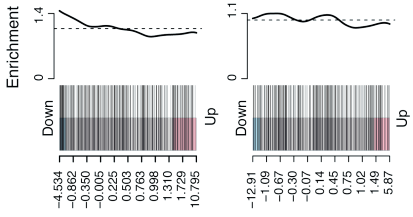

WD-HP7 oral vs WD-Veh oral | WD-HP7 sc vs WD-Veh sc

Fig. 6: Transcriptomic profiling of GMP after WD feeding and HPβCD-HP7 (HP7) treatment. GMP were FACS-sorted from bone marrow and subjected to RNA-seq analysis. a) Comparison of gene expression profiles with hematopoietic progenitor subsets using the Haemopedia database. b) Unsupervised clustering of the top 50 differentially expressed genes and principal component analysis (PCA1, PCA2), colored by diet or treatment group. c) Venn diagram of DE genes from the indicated comparisons. d) List of DE genes with annotated biological processes (Uniprot keywords, UP_KW). Red shading indicates positive average expression (AveExpr) or $\log_2$-transformed FC (logFC); blue shading indicates a low AveExpr or negative logFC. (e-g) Barcode plots showing the enrichment of (e) monocytic, (f) granulocytic and (g) LXR target genes signatures.

The monocytic signature (*Cd34*, *Csf1r*, *Cfp*, and *Ly86*) was not enriched in the WD groups compared to the CD group (**Fig. 6e**). Granulocytic signature genes (*S100a8* and *S100a9*, *Ets1*, *Pglyrp1*, *Cd63*, and *Ceacam1*) were slightly upregulated in the oral group and unchanged in the s.c. group (**Fig. 6f**). In addition to WD effects, we examined whether HPβCD-HP7 induces the liver-X-receptor (LXR) target genes, as reported by Zimmer et al. (2016). No enrichment was observed in HPβCD-HP7-treated GMP compared to Veh, with LXR targets (**Fig. S3**) being distributed among both up- and downregulated genes (**Fig. 6g**).

3.1.2 Chromatin accessibility profiling of GMP in response to WD feeding and HPβCD-HP7 treatment

Epigenetic changes are a hallmark of TI and have previously been described as an effect of WD by Christ et al. (2018). To investigate this, open chromatin regions of sorted GMP were analyzed by ATAC-seq. Among the relevant comparisons, only the WD vs. CD comparison in the oral group showed significant changes in chromatin accessibility after FDR correction (**Fig. 7a**). Eleven of the seventeen regions with an FDR < 0.05 and a $|\log_2 FC| > 1$ were unannotated. Two regions corresponded to computationally predicted genes (Gm44939 and Gm11175), and four overlapped with protein-coding loci (*Jund*, *Iqcn*, *Akap12* and *Coq2*), suggesting potential regulation on transcription factor level and within oxidative phosphorylation pathways. These loci were unaffected in the corresponding s.c. group (**Fig. 7a**). Analysis of HPβCD-HP7 compared to Veh during WD feeding displayed no regions that matched the significance criteria.

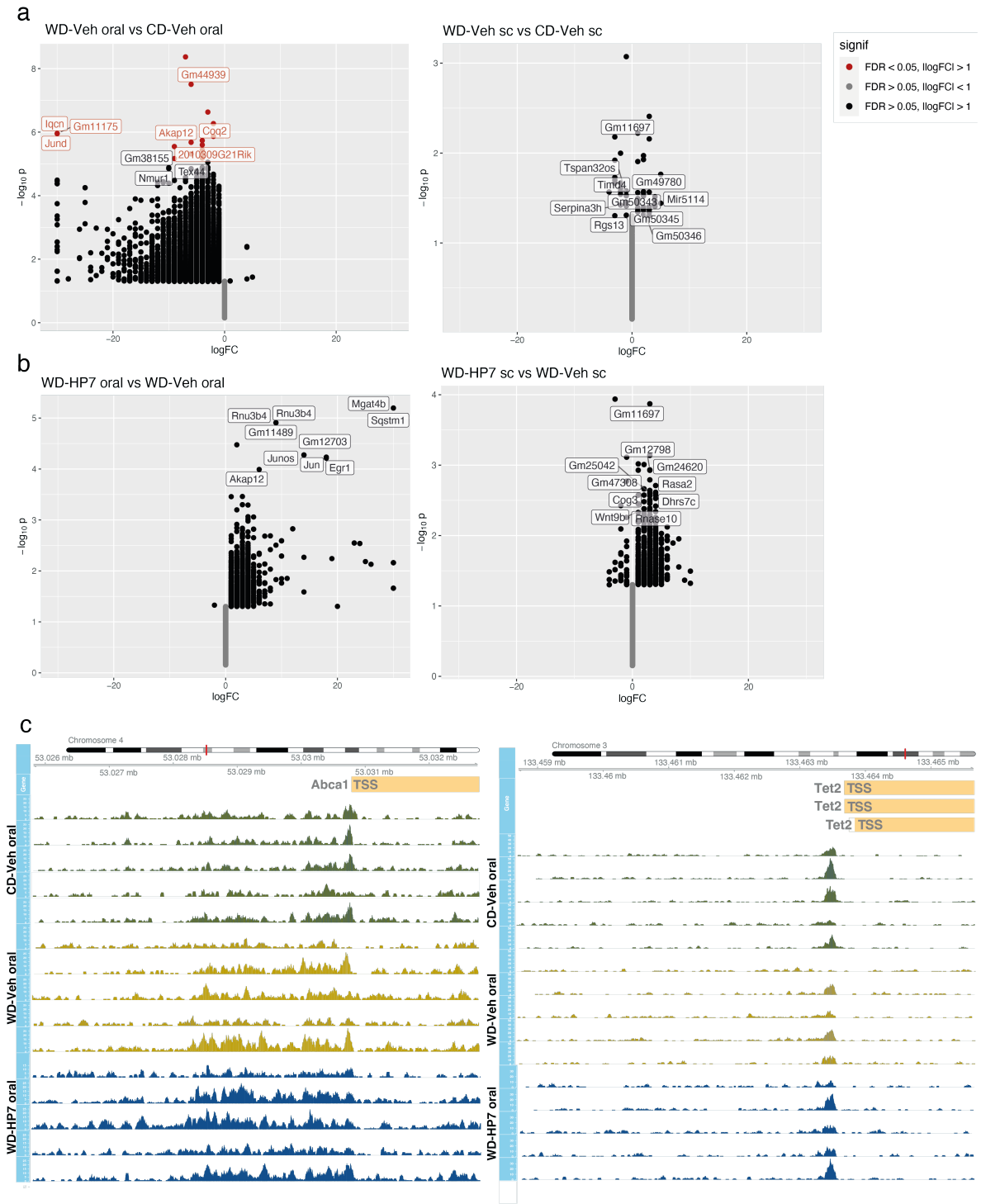

Fig. 7: Chromatin accessibility profiling of GMP after WD feeding and HPβCD-HP7 treatment. (a,b) Volcano plots showing differentially open chromatin regions (DOR) identified by ATAC-seq in GMP comparing (a) WD-fed vs CD-fed *Ldlr*$^{-/-}$ mice and (b) HPβCD-HP7 (HP7)-treated vs Veh-treated mice. (c) Chromatin accessibility tracks at the transcription start sites (TSS) of *Abca1* and *Tet2* (oral treatment groups). Statistical significance was determined using FDR correction and $\log_2$FC thresholds, as indicated.

Nevertheless, a few regions showed a |log2FC| > 1; for example, *Jun* and *Akap12* that showed enhanced chromatin accessibility upon HPβCD-HP7 treatment (**Fig. 7b**). This trend contrasts with the effect of WD, which appeared to reduce the chromatin accessibility, as compared to CD. In the s.c. group, five annotated gene regions were induced by HPβCD-HP7 - none of which overlapped with those from the oral group (**Fig. 7b**) - indicating differential effects dependent on the route of treatment administration.

Similar to the transcriptome analysis, a targeted approach of selected genes of interest followed the initial unbiased approach. Christ et al. (2018) reported that WD increased chromatin accessibility at the *Abca1* and *Tet2* loci. In our analysis, neither diet, nor HPβCD treatment affected accessibility of these gene regions (**Fig. 7c**).

Together, the results of multiplex cytokine and chemokine profiling, FACS analysis of bone marrow-resident GMP, and subsequent RNA and ATAC-seq analyses revealed only minimal effects of WD compared to CD across all levels examined. The same holds true for HPβCD-HP7 effects compared to the Veh group.

3.2 Modulation of inflammation and hematopoiesis by Cavitron™ W7 HP5 (HPβCD-HP5) in WD-fed WT mice

Previous experiments in *Ldlr*$^{-/-}$ mice provided no compelling evidence for an effect of either the diet or the HPβCD treatment. Consequently, we adapted the experimental design to account for potential cofounding factors. Because mouse facilities differ in their microbiological environments, which can influence the gut microbiome and thereby diet-related outcomes, the study was relocated within the university hospital campus from the HET to the iFET. In addition, the WD feeding period was extended from four to six weeks, and male WT mice were used instead of female *Ldlr*$^{-/-}$ mice. Finally, the treatment compound Cavitron™ W7 HP7 (HPβCD-HP7) was exchanged for Cavitron™ W7 HP5 (HPβCD-HP5), an analogue with a lower degree of hydroxyl substitutions used in the previous publication by Zimmer et al. (2016). Two independent experiments were conducted. Due to limitations in animal numbers, the group receiving the CD and HPβCD was omitted from the follow-up experiment. Male WT mice were fed either a WD or matched CD for six weeks, and HPβCD-HP5 was administered s.c. twice weekly (similar to Zimmer et al. (2016), beginning in the third week of the study (**Fig. 8a**). BW changes

over time were calculated as the area under the curve (AUC) using the trapezoidal rule (**Fig. S3**) and indicated minor batch effects between experiments. For better intra-experimental comparison, values were normalized to the CD/Veh group (**Fig. 8b**). Both WD groups showed significant weight gain relative to the CD group, with HPβCD-HP5 treatment resulting in an even greater increase compared to the Veh group.

3.2.1 Effects of HPβCD-HP5 on immune cells in the bone marrow and circulation

Hematopoiesis in the bone marrow was analyzed by flow cytometry, including HSC and oligopotent cell populations other than GMP (**Fig. 8c**). Results show that there was significant increase in HSC populations (both cell counts and frequencies) with WD and HPβCD-HP5 compared to control groups (**Fig. 8d**). In contrast, HPβCD-HP5 alone did not induce this effect in CD-fed mice. Other analyzed cell populations remained unaffected by both WD and HPβCD-HP5 treatment.

To assess circulating immune cells egressing from the bone marrow, an additional flow cytometric analysis was performed (**Fig. 8e**). The CD-Veh group was excluded from the analysis due to an insufficient number of data points resulting from handling issues in the initial experiment. There were no changes in the frequencies of both lymphoid and myeloid cell populations (**Fig. 8f**).

To further address WD-induced immune cell priming, bone marrow cells were stimulated overnight with various TLR ligands and the stimulator of interferon genes (STING) ligand 5,6-dimethylxanthenone-4-acetic acid (DMXAA). TNFα and IL-6 served as biomarker readout for TLR- or DMXAA-induced cytokine response (**Fig. 9**). WD alone led to no or minor increases in cytokine levels. The strongest effect was observed upon CpG stimulation (**Fig. 9a**). HPβCD-HP5 partially enhanced the WD effect, resulting in higher TNFα levels following LPS or R848 stimulation, and slightly increased levels of IL-6 following CpG stimulation. DMXAA induced neither TNFα nor IL-6. To capture a broader dynamic range of the potential innate immune training effects, different concentrations of the stimuli were applied (**Fig. 9b**).

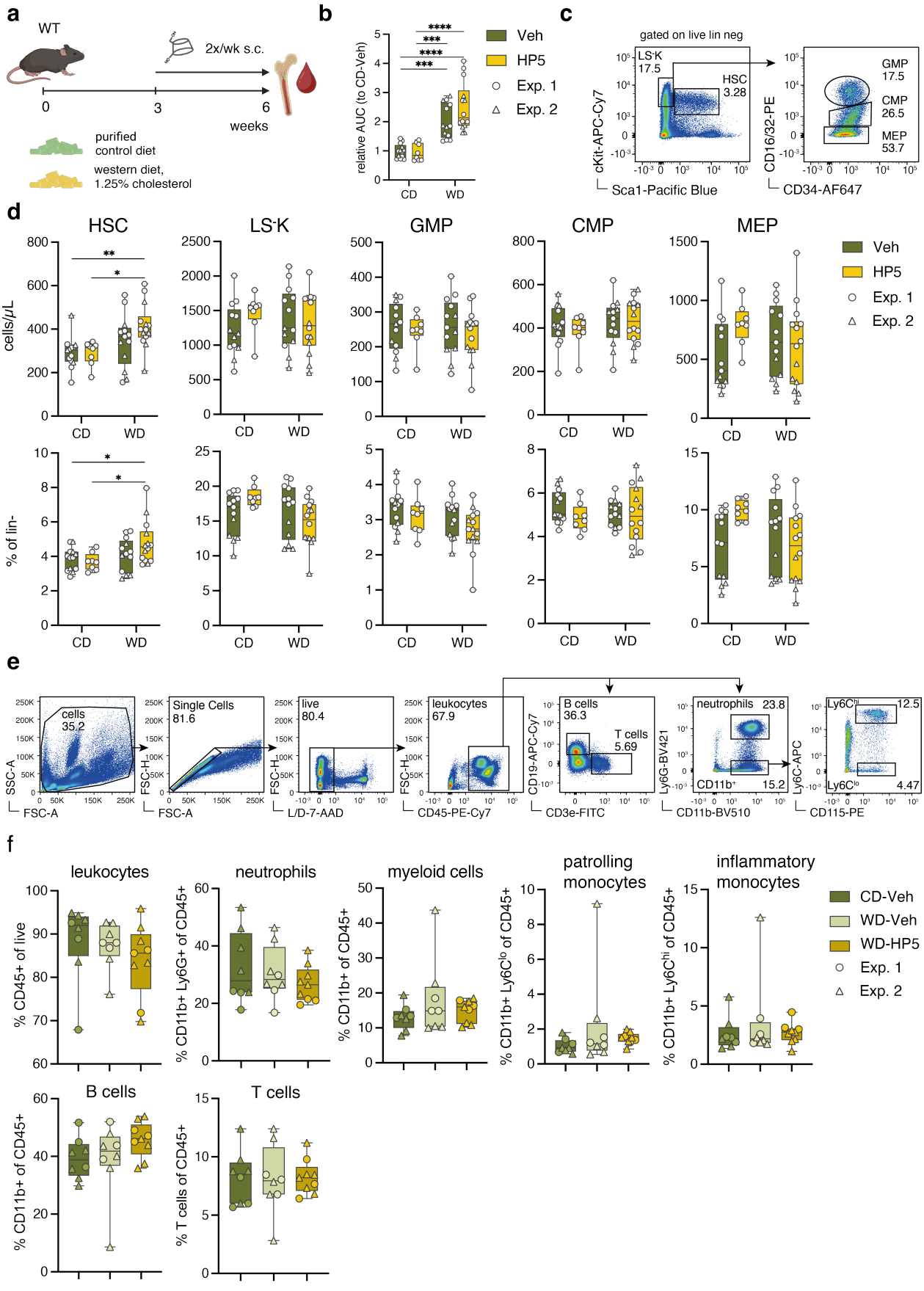
a
WT
2x/wk s.c.
0
3
6
weeks
purified
control diet
western diet,
1.25% cholesterol
b
relative AUC (to CD-Veh)
Veh
HP5
Exp. 1
Exp. 2
CD
WD
c
gated on live lin neg
LS-K
17.5
HSC
3.28
cKit-APC-Cy7
Sca1-Pacific Blue
CD16/32-PE
CD34-AF647
GMP
17.5
CMP
26.5
MEP
53.7
d
HSC
LS-K
GMP
CMP
MEP
cells/μL
% of lin-
e
cells
35.2
Single Cells
81.6
live
80.4
leukocytes
67.9
B cells
36.3
T cells
5.69
neutrophils
23.8
CD11b+
15.2
Ly6Chi
12.5
Ly6Clo
4.47
SSC-A
FSC-A
FSC-H
L/D-7-AAD
CD45-PE-Cy7
CD19-APC-Cy7
CD3e-FITC
Ly6G-BV421
CD11b-BV510
Ly6C-APC
CD115-PE
f
leukocytes
neutrophils
myeloid cells
patrolling
monocytes
inflammatory
monocytes
% CD45+ of live
% CD11b+ Ly6G+ of CD45+
% CD11b+ of CD45+
% CD11b+ Ly6Clo of CD45+
% CD11b+ Ly6Chi of CD45+
B cells
T cells
% T cells of CD45+
CD-Veh
WD-Veh
WD-HP5
Exp. 1
Exp. 2

Fig. 8: Effects of HPβCD-HP5 on immune cells in bone marrow and blood of WD-fed WT mice. a) Study design: male WT mice were fed a WD for 6 weeks and treated with HPβCD-HP5 (HP5; 2 g/kg BW) or PBS (Veh) via s.c. injection for the last three weeks prior to euthanasia. Blood and bone marrow were collected for downstream analysis. b) Quantified BW changes expressed as AUC over the course of WD feeding. c), e) Representative flow cytometry gating strategy for analysis of c) bone marrow HSPC populations and e) circulating immune cells in the blood. d), f) Frequencies of HSPC and circulating immune cell subsets. Statistical analysis was performed by two-way ANOVA and Tukey's multiple comparisons post hoc test; displayed *p*-values are adjusted for multiple testing. *n* = 8-14 mice per group from two independent experiments (indicated by circle or triangle symbol shape of data points).

The results showed that the highest concentration of Pam3CysK4 (100 ng/mL) was required to induce cytokine secretion under both dietary conditions. For LPS, stimulation with 10 ng/mL and 100 ng/mL induced measurable cytokine levels. Most samples showed slightly higher cytokine levels with increasing LPS concentrations, whereas some showed lower or markedly higher responses, resulting in greater variability and a lack concentration dependence. For R848, IL-6 levels increased in concentration-dependent manner, whereas TNFα showed only minor changes. For CpG, 1 µM induced high cytokine responses, which were variably attenuated or further increased at 5 µM. As WD did not substantially alter cytokine secretion (**Fig. 9b**), it appears unnecessary to include all different stimuli concentrations in future experiments.

3.2.3 Effects of HPβCD-HP5 on systemic cytokine responses

To investigate the effects of WD and HPβCD-HP5 on systemic inflammation, cytokine levels were quantified using the Olink Target 48 Mouse Cytokine panel. Plasma samples of the first mouse experiment, which included all four treatment groups, were analyzed. The comparison of the WD-Veh vs CD-Veh group revealed significantly enriched levels of IL-17A and IL-17F only (**Fig. 10a-b, e**). In contrast, comparing WD-HP5 vs CD-HP5 showed multiple highly significantly upregulated chemokines, such as CCL4, CXCL2, and CCL2 and also significantly upregulated cytokines, such as TNFα, IFNγ, and IL-17F (**Fig. 10a-b, e**), along with the growth factors FGF21 and hepatocyte growth factor (HGF) (**Fig. 10a-b, f**). One significantly downregulated analyte was found, which was macrophage colony stimulating factor (M-CSF) (**Fig. 10a-b**), a cytokine inducing differentiation of hematopoietic stem cells into macrophages (Mossadegh-Keller et al., 2013).

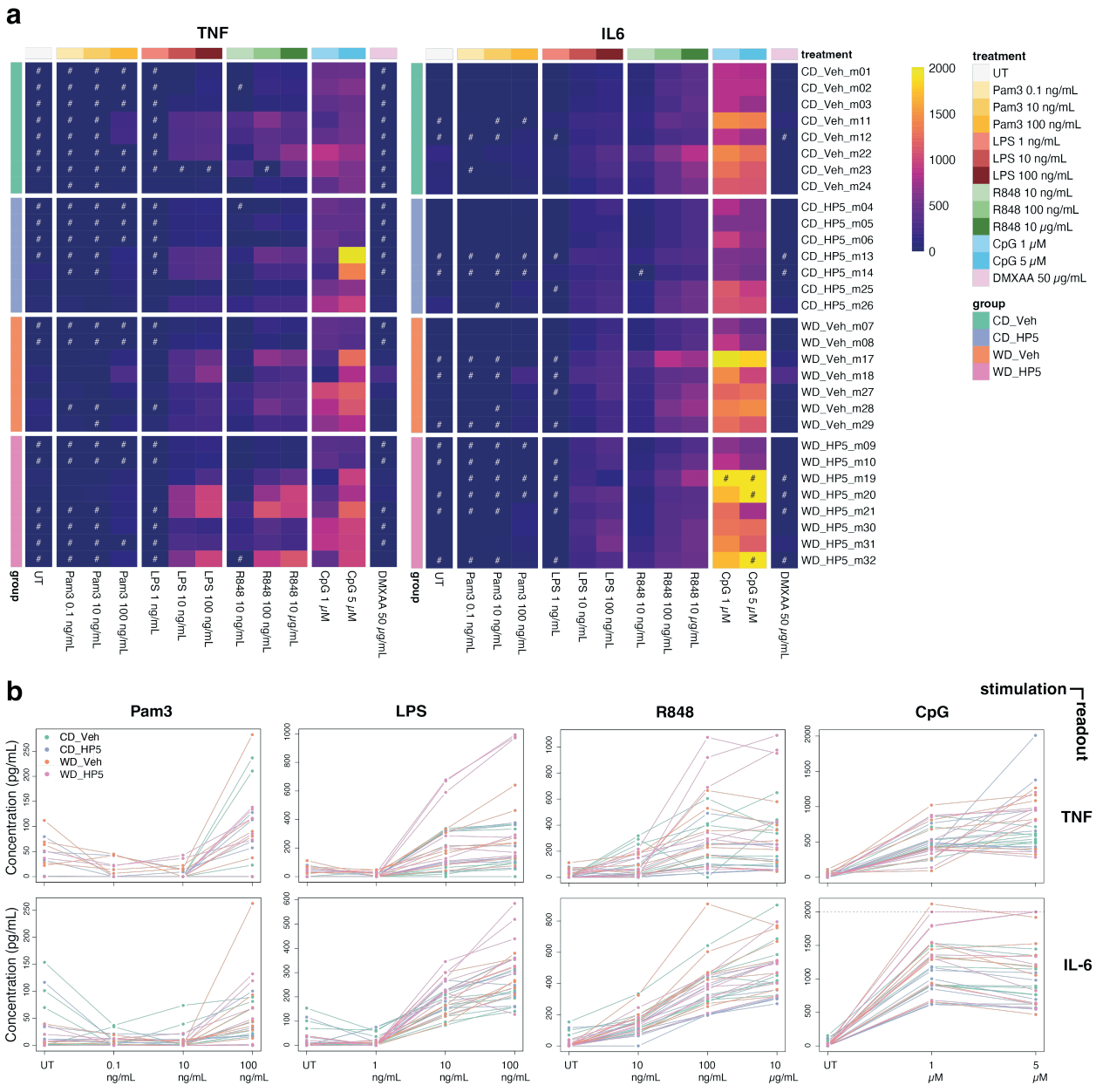

Fig. 9: Cytokine secretion of *ex vivo*-stimulated bone marrow of WD-fed, HPβCD-HP5-treated WT mice. Bone marrow cells isolated from WD- or CD-fed, HPβCD-HP5 (HP5)- or Veh-treated mice were stimulated *ex vivo* with various TLR agonists for 24 h. TNFα and IL-6 secretion in culture supernatants was quantified by ELISA. a) Heat map and b) line graphs showing cytokine concentrations. '#' indicates values below the lower limit of detection (set to 0) or above the upper limit (set to the maximum value of the standard curve).

The comparison of CD-HP5 vs CD-Veh showed no significant changes. The comparison of WD-HP5 vs WD-Veh showed a similar trend to WD-HP5 vs CD-HP5, with several cytokines (e.g., IL-17A, IL-17F, IL-6, GM-CSF) showing lower levels without reaching

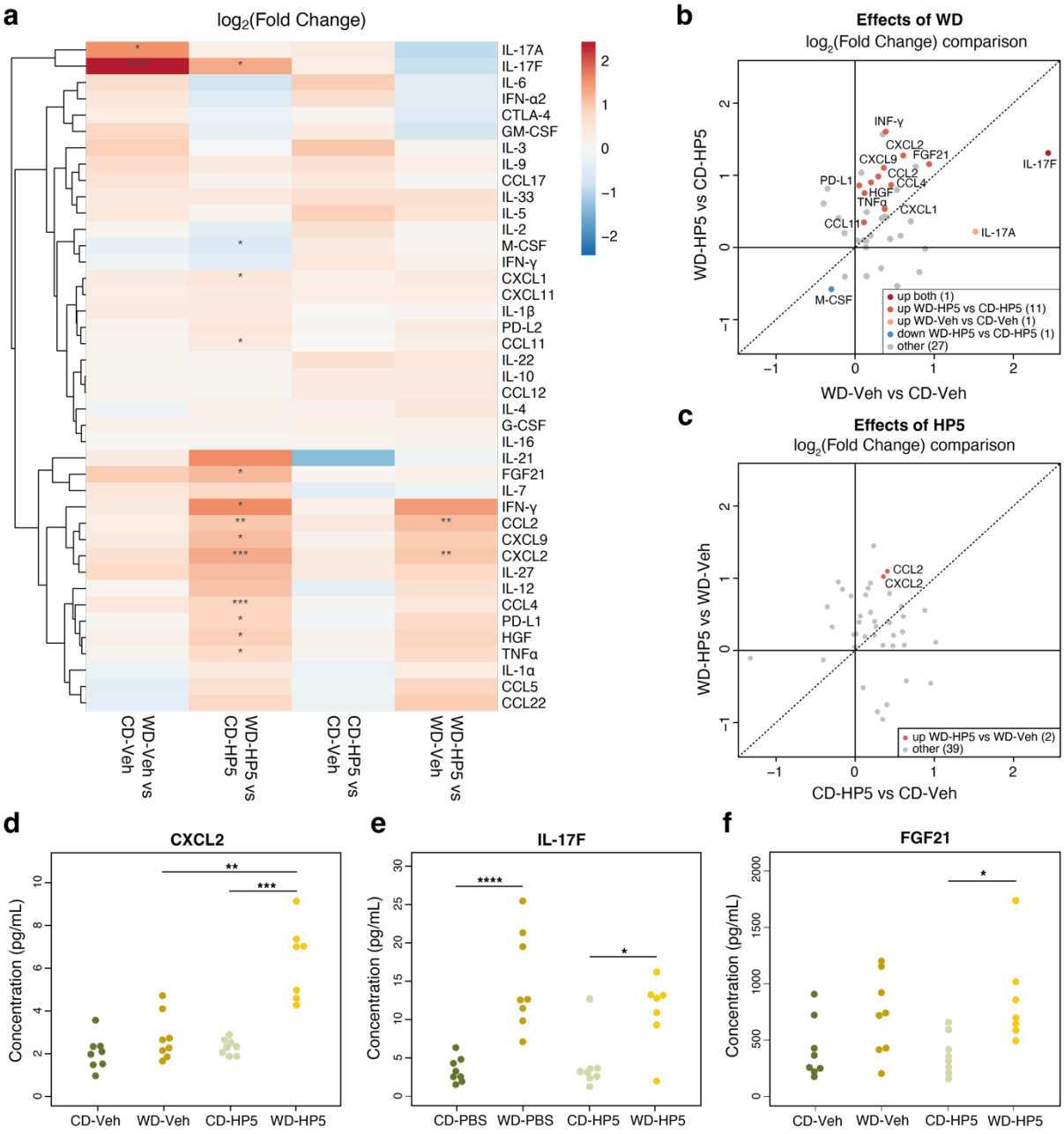

Fig. 10: Plasma cytokine profiling in WD-fed, HPβCD-HP5-treated WT mice. Cytokines were measured using the Olink Target 48 Mouse Cytokine panel. a) Heat map showing the FC of detected cytokines across indicated comparisons. b), c) log_2FC comparison plots illustrating the effects of b) WD feeding and c) HP5 treatment on plasma cytokine concentrations. Proteins are highlighted if they meet the significance threshold in one or both of the comparisons indicated. d-f) Individual plots for d) CXCL2, e) IL-17F, and f) FGF21 are shown. Statistical analysis was performed using empirical Bayes moderated *t*-tests followed by a correction for multiple testing using the Benjamini Hochberg FDR method. Significantly changed cytokines are indicated by asterisks. *n* = 7-8 mice per group.

statistical significance (**Fig. 10a, c, e**). A few analytes displayed increased levels, of which only CXCL2, CCL2 were significantly altered (**Fig. 10a, c-d**). Overall, WD alone induced only mild cytokine effects, which was markedly amplified under HPβCD-HP5 treatment conditions; HPβCD-HP5 alone only had minimal effects.

3.3 Effects of HPβCD-HP7 and HPβCD-HP5 on atherosclerosis, inflammation and the adipose tissue in *Apoe*$^{-/-}$ mice

Previous experiments in *Ldlr*$^{-/-}$ and WT mice did not reveal overt inflammatory effects of WD feeding. To further investigate diet-induced inflammation, we therefore utilized the *Apoe*$^{-/-}$ model, which exerts a higher degree of systemic inflammation and atherosclerosis compared to other murine models (Emini Veseli et al., 2017b; Oppi et al., 2019) Different study designs were employed to study prophylactic (prevention model) (**Fig. 11a**) or therapeutic (regression model) effects (**Fig. 11b**) of HPβCD-HP7 and HPβCD-HP5 on atherogenesis development. Within the prevention model design, we added a control group of mice fed SC to account for the investigation of potential diet effects.

3.3.1 HPβCD-HP5 and HPβCD-HP7 effectively reduce atherosclerosis

In both models, atherosclerotic plaques size was reduced by HPβCD treatment in male mice (**Fig. 11c-d**). In the prevention model, plaque area was reduced by approximately 10 % (**Fig. 11c)** and in the regression model by about 13 % (**Fig. 11d**) compared with the untreated WD group. The average plaque area of untreated mice was approximately 25 % in the prevention model and 38 % in the regression model, and it was comparable between male and female mice. However, no plaque reduction was observed in female mice following HPβCD treatment. In the prevention model, HPβCD-HP5 even led to a significant increase in plaque area (**Fig. 11c**); indicating a clear sex-dependent interaction with the treatment modality.

To characterize lipid metabolism parameters relevant to atherosclerosis progression, total cholesterol, the cholesterol metabolite 27-OHC (shown to be induced by HPβCD-HP5 in an LXR-dependent manner (Zimmer et al., 2016)), and triacylglycerides (TAG) were measured. As expected, In the prevention model, total cholesterol was highly induced by WD compared to SC in both male and female mice (**Fig. 11e**), which could not be shown

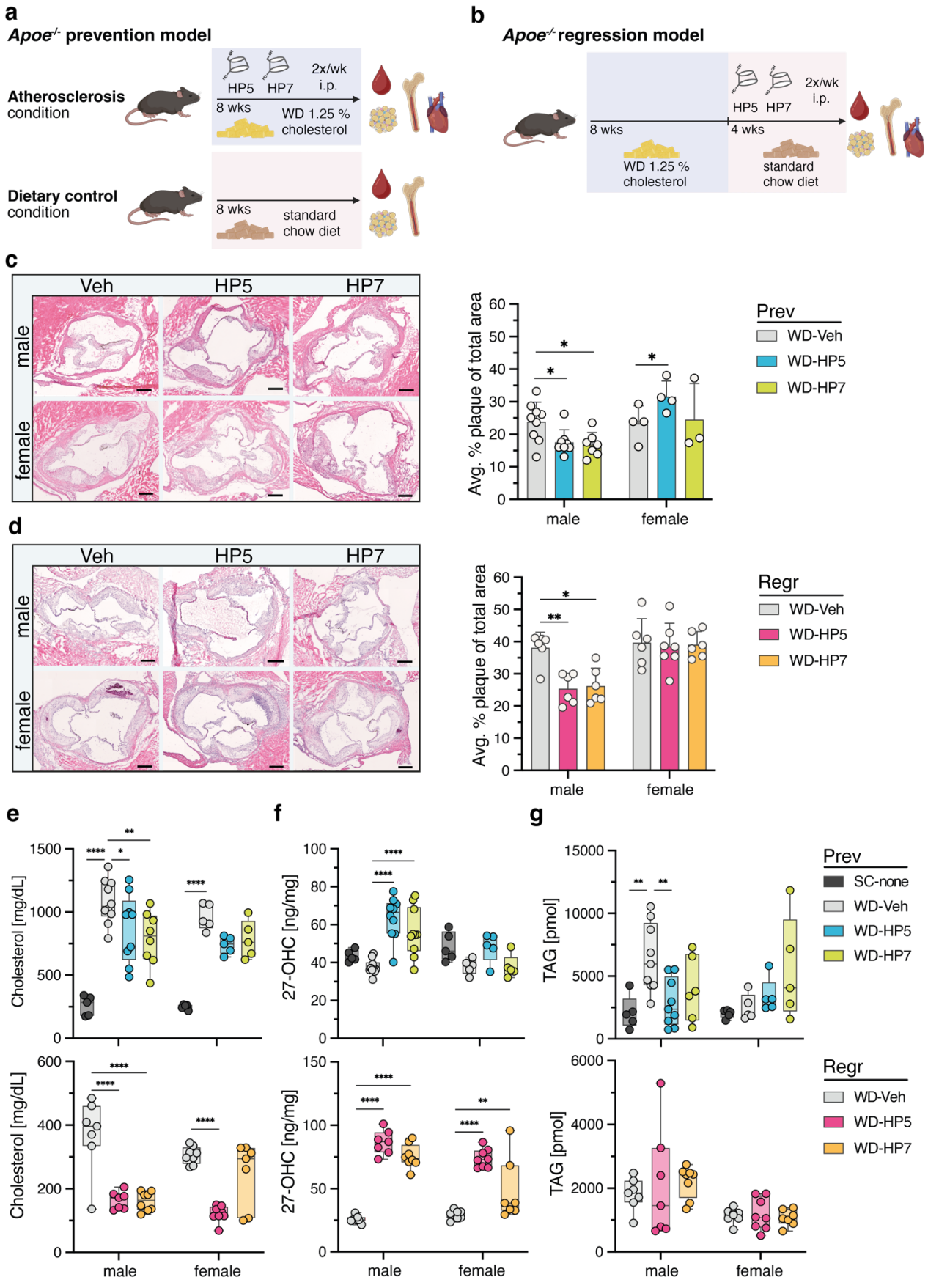
a
Apoe-/- prevention model
Atherosclerosis condition
HP5
HP7
2x/wk i.p.
8 wks
WD 1.25 % cholesterol
Dietary control condition
8 wks
standard chow diet
b
Apoe-/- regression model
HP5
HP7
2x/wk i.p.
8 wks
4 wks
WD 1.25 % cholesterol
standard chow diet
c
Veh
HP5
HP7
male
female
Avg. % plaque of total area
Prev
WD-Veh
WD-HP5
WD-HP7
d
Veh
HP5
HP7
male
female
Avg. % plaque of total area
Regr
WD-Veh
WD-HP5
WD-HP7
e
Cholesterol [mg/dL]
male
female
f
27-OHC [ng/mg]
male
female
g
TAG [pmol]
male
female
Prev
SC-none
WD-Veh
WD-HP5
WD-HP7
Regr
WD-Veh
WD-HP5
WD-HP7

Fig. 11: Effects of HPβCD-HP5 and HPβCD-HP7 on atherosclerosis in the *Apoe*$^{-/-}$ model. a), b) Study design: male and female *Apoe*$^{-/-}$ mice were fed a WD for eight weeks and either a) treated with HPβCD-HP5 (HP5) or HPβCD-HP7 (HP7) (2 g/kg BW) or NaCl (Veh) via i.p. injection twice weekly (atherosclerosis prevention model, Prev), or b) switched to SC for four additional weeks with HPβCD treatment as described above (atherosclerosis regression model, Regr). A dietary control cohort (SC-fed, untreated) was included for comparison in the prevention model. Heart, blood, bone marrow, and adipose tissues were collected for analysis. c), d) Plaque burden: representative HE-stained sections of the aortic root area in the heart and quantification of the average atherosclerotic plaque area in the c) prevention and d) regression models. e-g) Plasma lipids: e) total cholesterol, f) 27-OHC, and g) TAG. Statistical analysis was performed by two-way ANOVA followed by Dunnett's multiple comparisons test. Displayed *p*-values are adjusted for multiple testing. *n* (males) = 5-10, *n* (females) = 3-6 mice per group.

for the regression model as a SC-control group was not included. The average cholesterol levels (median) of the control group (WD-Veh) were about 2.5-fold lower in the regression model, as compared to the prevention model (approx. 1,000 mg/dL vs. 400 mg/dL), which is likely due to the switch from atherogenesis induction with WD (eight weeks) to the regression phase with SC (four weeks) prior to euthanasia. In the prevention model, both HPβCD compounds decreased total plasma cholesterol in both sexes, with a significant reduction observed only in the male group. In the males of the regression model, there was a reduction of cholesterol upon HPβCD therapy of >2-fold, which was higher compared to the prevention model (up to approximately 1.3-fold). In the female groups, the effects of HPβCD-HP5 and HPβCD-HP7 differed markedly. HPβCD-HP5 significantly reduced cholesterol levels, whereas HPβCD-HP7 was less effective resulting in values comparable to those of the Veh group. In contrast, 27-OHC levels were markedly increased by HPβCD treatment in males of both models and in females of the regression model (**Fig. 11f**). HPβCD-HP5 appeared to be a slightly more potent inducer of 27-OHC in females, as there was a trend toward higher levels in the prevention model that was absent with HPβCD-HP7. Moreover, in the regression model, the increase in 27-OHC among females was significantly greater with HPβCD-HP5 than with HPβCD-HP7.

WD feeding increased TAG levels in male mice in the prevention model, which were significantly lowered by HPβCD-HP5; a similar trend was observed for HPβCD-HP7 despite lacking significance ($p = 0.1105$). In female mice, HPβCD treatment appeared with a slight increase of TAG levels. In the regression model, no differences were seen between control and treatment groups. The baseline levels of the mice treated with NaCl

(WD-Veh) were similar to those of the mice fed SC in the prevention model. This suggests that switching from WD to SC was sufficient to reduce TAGs to “normal” levels.

To assess systemic inflammatory effects, cytokines in the plasma were measured. A customized panel of 19 cytokines was created, of which eight (CXCL1, GDF-15, CCL2, S100A9, ICAM-1, G-CSF, CCL3, and PCSK9) could be reliably measured (**Fig. 12**). In the prevention model, the values of the treatment groups were mostly unchanged compared to the Veh group (**Fig. 12a**). The SC-fed group showed overall lower cytokine levels, with GDF-15 and CCL3 showing particularly low levels compared to the WD-fed control group. In the regression model, not all samples could be measured due to limited assay capacity. We therefore decided to include mainly male mice, as plaque regression was observed in those groups earlier (**Fig. 12b**). Overall, there was no difference in cytokine levels compared to the control group.

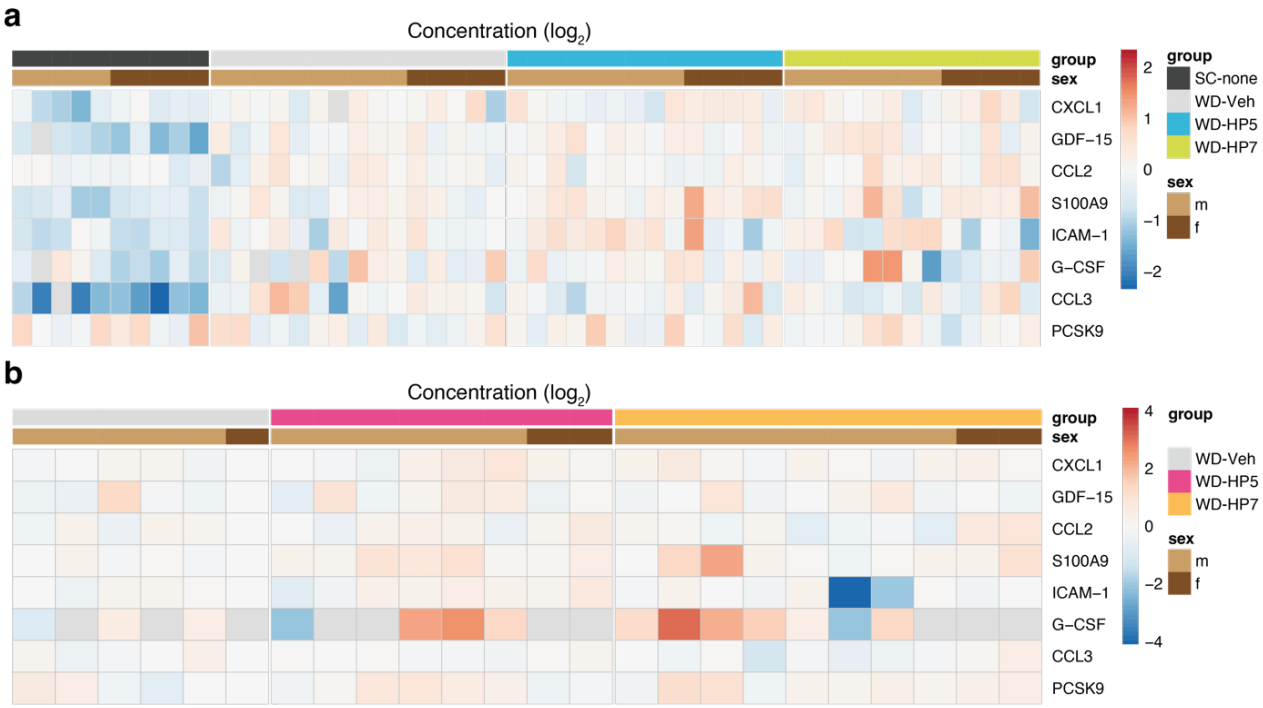

Fig. 12: Effects of HPβCD-HP5 and HPβCD-HP7 on plasma cytokine levels in WD-fed, *Apoe*$^{-/-}$ mice. Cytokines, chemokines, and other atherosclerosis-related proteins were measured using a multiplex Luminex assay. Data are shown as log_2-transformed concentrations, normalized to the mean of the WD-Veh controls (calculated separately for each sex). a), b) prevention and regression models, respectively. *n* = 5-10 (prevention model), *n* = 1-6 (regression model).

3.3.2 Effects of HPβCD-HP5 and HPβCD-HP7 on hematopoiesis

To investigate alterations on HSPC populations, we conducted flow cytometry-based phenotyping. An extended panel allowed us to analyze sub populations of LSK (lineage$^-$ Sca1$^+$ cKit$^+$) cells, including short-term (ST; LSK FLT3$^-$ CD150$^-$ CD48$^-$), long-term (LT; LSK FLT3$^-$ CD150$^+$ CD48$^-$) HSC, and multipotent progenitor populations (MPP), which can differentiate into distinct lineages (**Fig. 13a**). MPP2 (LSK FLT3$^-$ CD150$^+$ CD48$^+$), MPP3 (LSK FLT3$^-$ CD150$^-$ CD48$^+$), and MPP4 (LSK FLT3$^+$ CD150$^-$), display lineage biases toward megakaryocyte/erythrocyte, myeloid, and lymphoid differentiation, respectively (Pietras et al., 2015; Solomon et al., 2020).

In the prevention model, no significant differences between SC- and WD-fed control mice were observed regarding lineage$^-$ Sca1$^-$ cKit$^+$ (LS$^-$K) cells which encompass the committed sub populations GMP, common myeloid progenitors (CMP) and MEP (**Fig. 13b**). In males, HSC and MPP2-4 populations were significantly lower in the SC-fed group compared to WD-Veh group. This was not observed in the females, despite showing similar trends. ST- and LT-HSC also appeared less frequent in SC-fed mice, but lacking significance. In the absence of statistically significant differences, the effects observed following HPβCD treatment are considered indicative trends: Across the LS$^-$K population and its subpopulations, HPβCD-HP5 and HPβCD-HP7 treatment resulted in frequencies similar to the WD-Veh group in males. In females, however, most populations showed modest increases, except for the CMP subset. This trend is reflected, to some extent, in the relative frequencies of MPP2-4. Male mice treated with HPβCD-HP5 or HPβCD-HP7 displayed similar frequencies of ST- and LT-HSC as the WD-Veh group, whereas female mice showed slight increases.

In general, the SC-fed mice exhibited a smaller spread of the data compared to the WD-fed mice. This suggests that WD and perhaps the HPβCD treatment induced variable effect sizes, indicating interindividual variability in response. The effects observed here are also largely reflected in absolute cell counts per µL (**Fig. S4a, b**). The difference between LSK counts in male mice of the SC-fed group compared to the WD-Veh group is apparent (**Fig. S4b**).

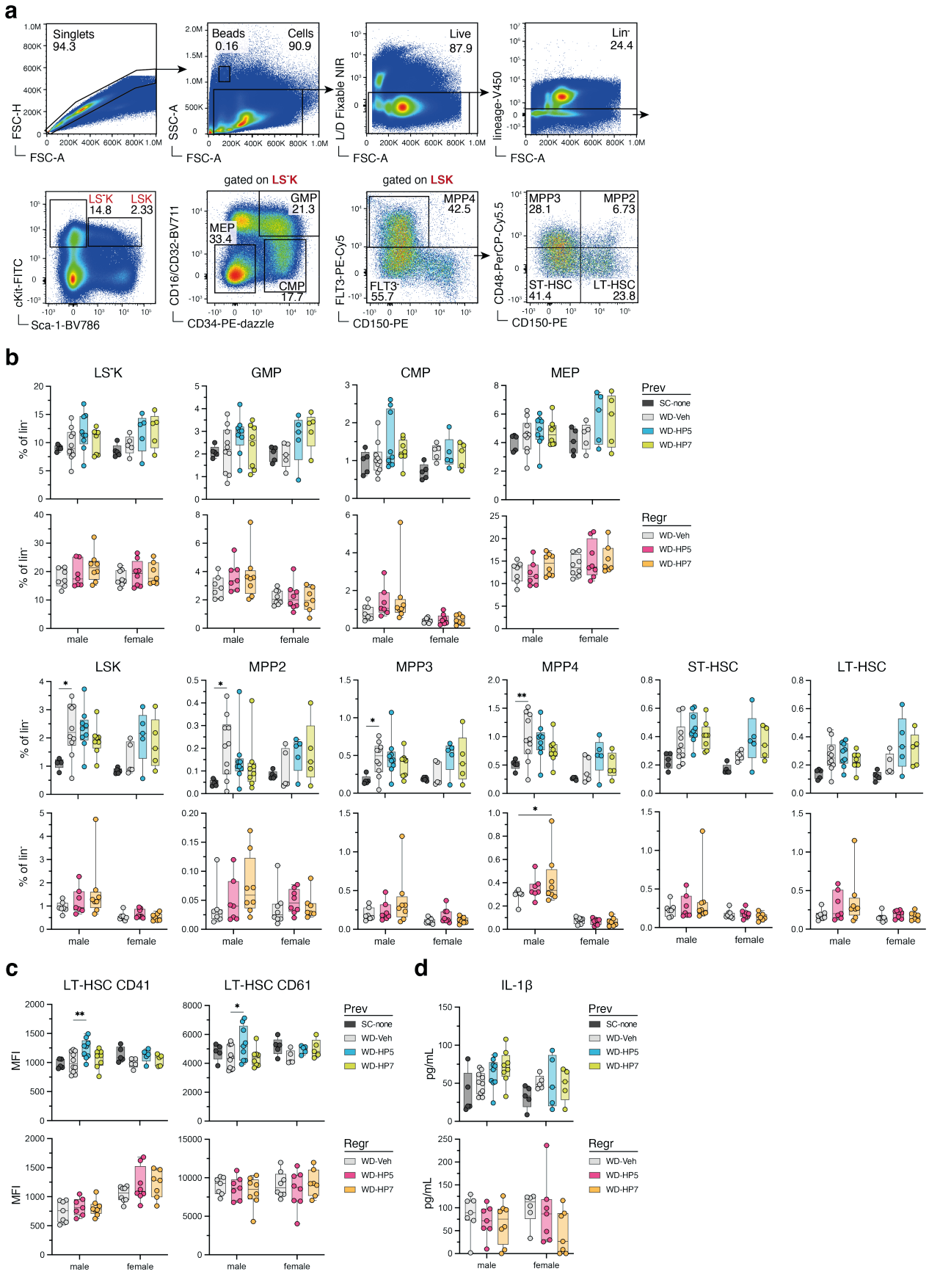
a
Singlets
94.3
FSC-H
FSC-A
Beads
0.16
Cells
90.9
SSC-A
FSC-A
Live
87.9
L/D Fixable NIR
FSC-A
Lin-
24.4
lineage-V450
FSC-A
LS-K
14.8
LSK
2.33
cKit-FITC
Sca-1-BV786
gated on LS-K
GMP
21.3
MEP
33.4
CMP
17.7
CD16/CD32-BV711
CD34-PE-dazzle
gated on LSK
MPP4
42.5
FLT3-PE-Cy5
FLT3-
55.7
CD150-PE
MPP3
28.1
MPP2
6.73
ST-HSC
41.4
LT-HSC
23.8
CD48-PerCP-Cy5.5
CD150-PE
b
LS-K
GMP
CMP
MEP
% of lin-
Prev
SC-none
WD-Veh
WD-HP5
WD-HP7
Regr
WD-Veh
WD-HP5
WD-HP7
male
female
LSK
MPP2
MPP3
MPP4
ST-HSC
LT-HSC
c
LT-HSC CD41
LT-HSC CD61
MFI
d
IL-1β
pg/mL

Fig. 13: Effects of HPβCD-HP5 and HPβCD-HP7 on bone marrow hematopoietic cells of WD-fed *Apoe*$^{-/-}$ mice. a) Representative flow cytometry gating strategy for analysis of bone marrow hematopoietic cells. b) Frequencies of HSPC. c) MFI of CD41 and CD61 on LT-HSC. D) IL-1β concentrations in the bone marrow supernatants after flushing. Statistical analysis was performed by two-way ANOVA followed by Dunnett's multiple comparisons test. Displayed *p*-values are adjusted for multiple testing. *n* (males) = 5-10, *n* (females) = 5-8 mice per group.

In the regression model, the HPβCD treatment does not change frequencies of most of the HSPC populations in both male and female mice (**Fig. 13b**). However, there is a significant increase of MPP4 in the males with HPβCD-HP7. This is not reflected in absolute cell counts (**Fig. S4b**). Here, HPβCD-HP7 induced a significant increase of CMP, LSK, LT-HSC and MPP3 (**Fig. S4a, b**) and a non-significant elevation of MPP2.

To further characterize LT-HSC, we measured CD41 and CD61, surface markers that hint toward myeloid cell polarization (CD41) (Gekas and Graf, 2013) and increased immune responses to inflammation (CD61) (Mann et al., 2018). WD alone did not lead to a higher Mean Fluorescence Intensity (MFI) of those biomarkers (**Fig. 9c**). However, HPβCD-HP5 treatment induced a significant increase of both CD41 and CD61 in male mice in the prevention model. Overall, increased frequencies of CD41^{+} LT-HSC were observed (**Fig. S4c**). No changes on MFI level were seen in the regression model; however, cell counts of CD41^{+} LT-HSC were significantly increased following HPβCD-HP7 treatment in male mice (**Fig. S4c**).

Since the bone marrow cytokine milieu can influence (hematopoietic) stem cell differentiation, it may be indicative of the inflammatory status; for example, by increased lineage-skewing stimuli such as IL-1β (Mitchell et al., 2023; Pietras, 2017). We measured IL-1β in the supernatant of freshly isolated bone marrow cells (**Fig. 13d**). In the prevention model, SC feeding resulted in lower levels of IL-1β relative to WD-Veh control mice, although not significantly. HPβCD-HP5 or HPβCD-HP7 treatment slightly increased IL-1β levels in male mice, whereas females remained unchanged. In the regression model, both HPβCD treatments showed an opposite trend, with mildly reduced IL-1β levels compared with WD-Veh controls.

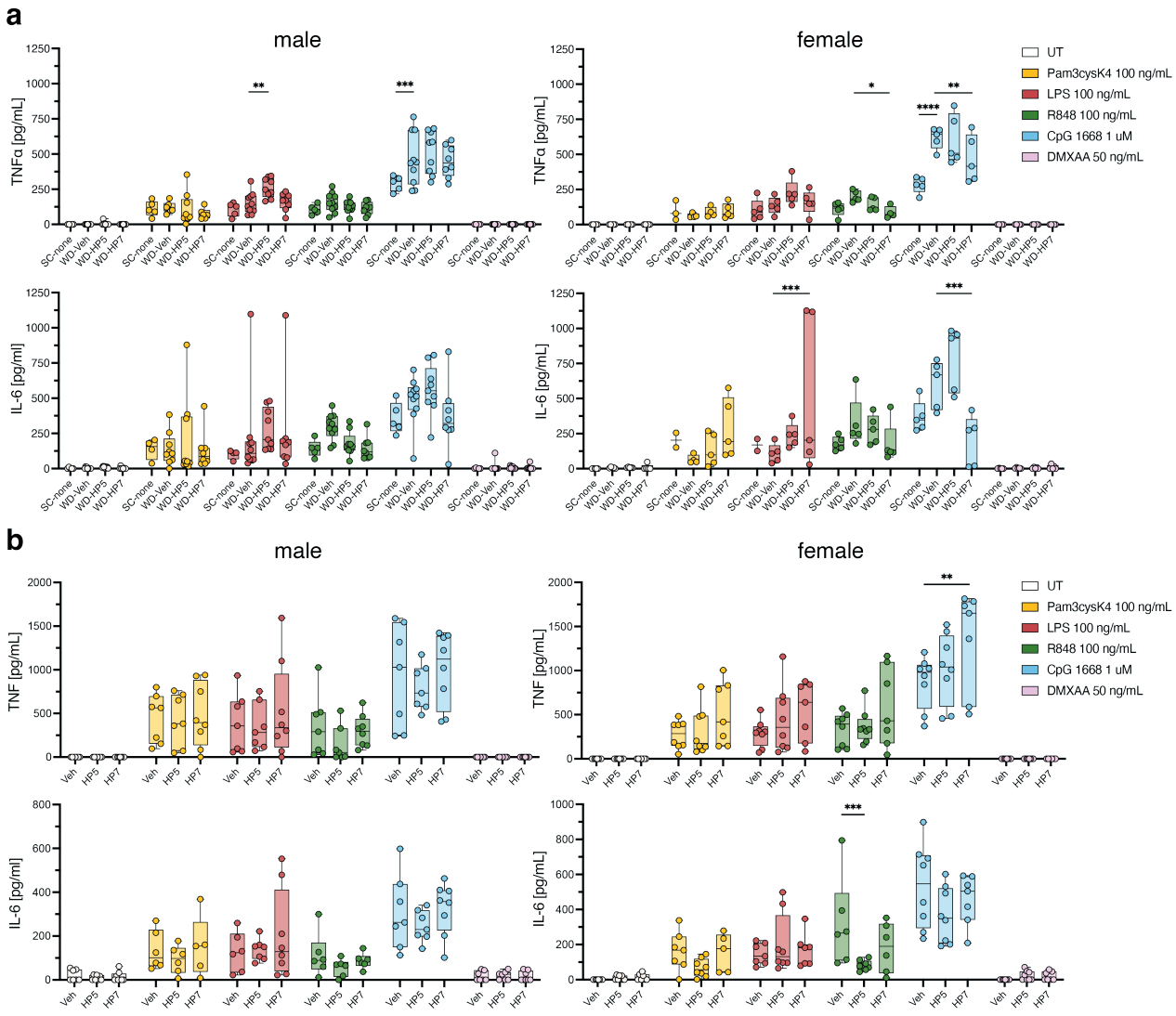

Fig. 14: Effect of HPβCD-HP5 and HPβCD-HP7 on cytokine secretion by *ex vivo* TLR ligand-stimulated bone marrow cells. Flushed bone marrow cells were counted and seeded into plates pre-filled with the indicated stimuli for 24h. Cytokine levels were measured by a) ELISA or b) HTRF. a), b) TNFα and IL-6 concentrations from the a) prevention and b) regression model separated by sex. Statistical analysis was performed by two-way ANOVA followed by Dunnett's multiple comparisons test. Displayed *p*-values are adjusted for multiple testing. *n* (males) = 5-10, *n* (females) = 2-8 mice per group.

Beside flow cytometric analyses, we investigated TI effects on bone marrow cells following WD feeding by *ex vivo* re-stimulation and subsequent cytokine level measurement. We stimulated isolated BM cells with TLR stimuli (Pam3CysK4, LPS, R848, CpG, and DMXAA) at concentrations selected from previous results (**Fig. 9**) and measured TNFα and IL-6 in the supernatant using ELISA and HTRF. In the prevention model, CpG (TLR9) stimulation induced a significant increase in TNFα in the WD-Veh group, with a similar,

but nonsignificant trend for R848 (TLR7/8), while other stimuli had no effect (**Fig. 14a**). HPβCD-HP5 and HPβCD-HP7 exerted differential effects depending on sex and stimulus. In males, HPβCD-HP5 amplified the LPS (TLR4)-induced increase in TNFα, whereas in the females, HPβCD-HP7 attenuated the R848- and CpG-induced TNFα responses. IL-6 displayed a similar overall pattern to TNFα. In the regression model, HPβCD-HP7 significantly increased LPS- and CpG-induced TNFα levels in males and in females an upward trend was seen (**Fig. 14b**). A significant decrease of Pam3CysK4 (TLR2) induced IL-6 was observed with HPβCD-HP5 in males and a similar trend was seen in females.

To conclude, the effects of WD on the bone marrow were mostly restricted to increased frequencies of hematopoietic stem cells relative to SC-fed mice and small effects on cytokine secretion after *ex vivo* stimulation and IL-1β in the bone marrow. No WD-induced increase of GMP was observed. HPβCD displayed sex- and treatment model-dependent effects on stem cell frequencies (e.g. increased $CD41^+$ and $CD61^+$ LT-HSC) in the bone marrow and cytokine secretion after *ex vivo* stimulation. In general, the effects were rather pro-inflammatory than anti-inflammatory.

3.3.3 Effects of HPβCD-HP5 and HPβCD-HP7 on circulating immune cells

Circulating immune cells were analyzed by flow cytometry using the antibody panel and gating strategy shown above (**Fig. 8e**). The cell population frequencies were similar across treatments. in the prevention experiment, leukocytes ($CD45^+$ of live) showed a high variation, which may account for batch effects from the three different sacrifice days. This is demonstrated in the graph, each symbol shape indicating a different day (**Fig. 15**). HPβCD-HP5 significantly lowered (HPβCD-HP7 trending) inflammatory monocytes ($CD11b^+$ $Ly6C^{hi}$ of $CD45^+$) in females in the regression model. This effect was not seen for males or in the prevention model. T cells were significantly increased by HPβCD-HP7 in the prevention model, and by HPβCD-HP5 in the regression model. In absolute cell numbers, other observations were made, in fact HPβCD-HP7 induced significant increase of all analyzed cell types in the males from the prevention model (**Fig. S5**).

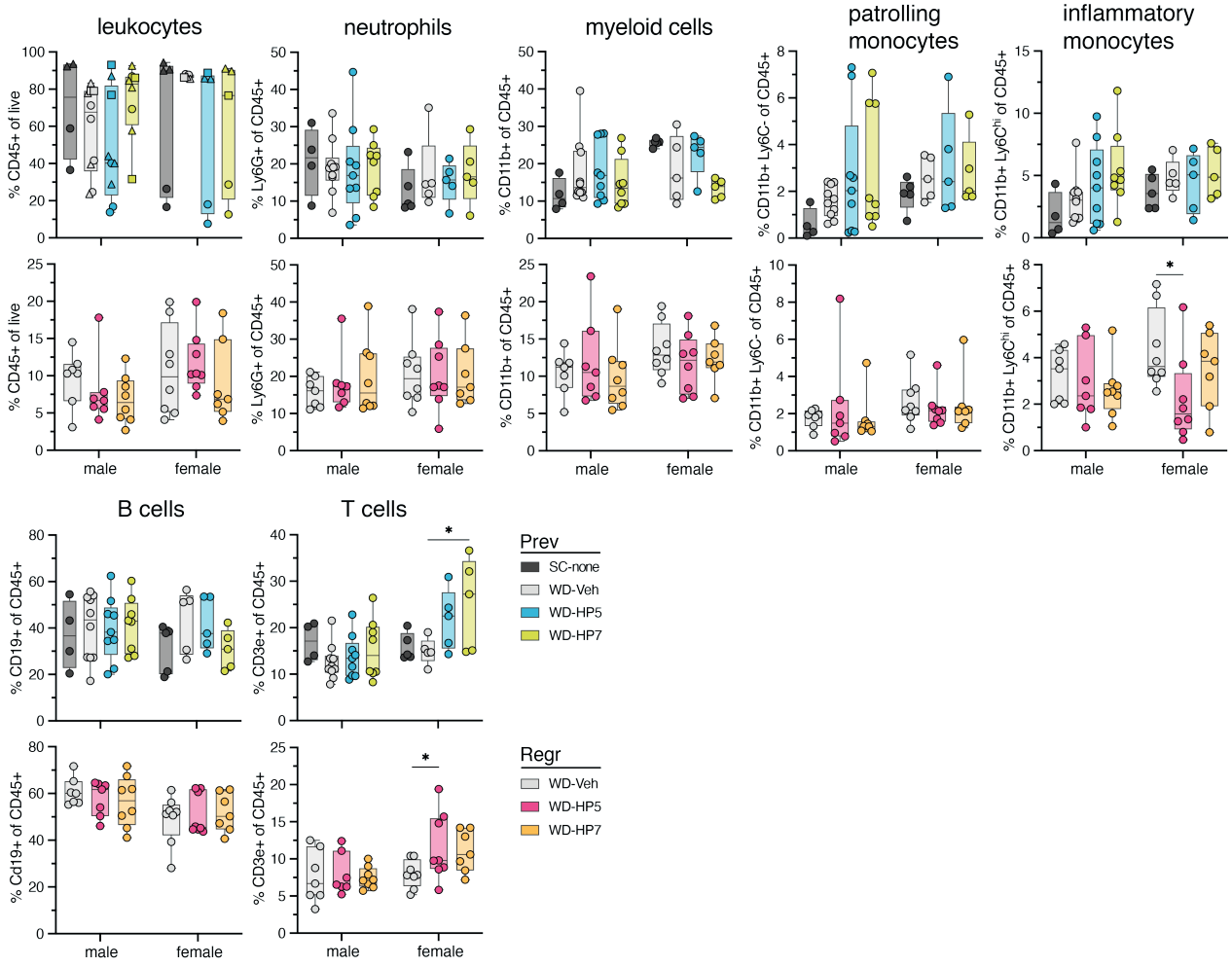

Fig. 15: Effect of HPβCD-HP5 and HPβCD-HP7 on circulating immune cells in the blood. Frequencies of myeloid and lymphoid cells in the circulation, analyzed by flow cytometry. In the prevention model, single data points for leukocytes indicate a different day of sacrifice (circle, triangle, rectangle). Statistical analysis was performed by two-way ANOVA followed by Dunnett's multiple comparisons test. Displayed *p*-values are adjusted for multiple testing. *n* (males) = 4-10, *n* (females) = 5-8 mice per group.

3.3.4 Effects of HPβCD-HP5 and HPβCD-HP7 on weight gain and ATM

Given the close relationship between atherosclerosis and metabolic alterations, particularly those involving lipid metabolism (Libby, 2021; Stroope et al., 2024), we next analyzed the effects of HPβCD on the AT depot. The gWAT was of particular interest, as it is the largest visceral fat depot in mice and exhibits a high degree of immunological responsiveness to increased energy availability, e.g. through macrophage infiltration and TNFα secretion (Kolb, 2022; Weisberg et al., 2003b; H. Xu et al., 2003). The inguinal fat

tissue (iWAT) lies subcutaneously and is less responsive at the cellular and metabolic level (van Beek et al., 2015).

To evaluate diet-induced obesity effects, including increases in body and fat-pat weight (de Moura e Dias et al., 2021), BW was examined both as an absolute endpoint and as a longitudinal measure expressed as AUC (g * week) (**Fig. 16a**). SC-fed mice were added as a dietary control group, but since they were not part of the actual experiment, there was no weight data recorded over time. In the prevention model, SC-fed mice displayed a significantly reduced BW relative to the WD-Veh group, but there was no difference between the WD-HPβCD conditions compared to the Veh group. Notably, the difference of SC and WD was higher within the males than the females. In the regression model, there were no significant changes, although HPβCD-HP5 showed a strong tendency for increased BW changes in males (p=0.0590).

We next weighed metabolic organs and normalized them to BW. In the prevention model, SC-fed mice showed significantly lower gWAT/BW and iWAT/BW ratios than WD-Veh mice (**Fig. 16b**). HPβCD-HP5 and HPβCD-HP7 reduced gWAT/BW and HPβCD-HP5 significantly lowered iWAT/BW in males. Liver/BW ratios were reduced in SC-fed mice, but not altered with HPβCD treatment. In the regression model, across all conditions and in both sexes, gWAT/BW and iWAT/BW ratios showed no significant differences. For liver/BW ratios, no major effects were detected except for HPβCD-HP7, which increased liver/BW in males (**Fig. 16b**).

To elucidate which effects HPβCD-HP5 and HPβCD-HP7 have on ATM in the gWAT, we isolated the SVF and analyzed the percentage of different populations using flow cytometry (Silva Ribeiro et al., 2024) (**Fig. 16 c, d**). Macrophage (mΦ; $CD11b^+$ $F4/80^+$ of $CD45^+$ lin^-) frequencies were significantly reduced in males by HPβCD-HP5 in both the prevention and the regression model, whereas HPβCD-HP7 reduced the frequencies significantly only in the prevention model (**Fig. 16d**). Monocyte-derived macrophages ($CD11b^+$ $F4/80^+$ $TIM4^{lo}$ $CD45^+$ lin^-) were slightly increased in WD-fed mice in the prevention model, which is in line with the literature (Weisberg et al., 2003a). Both HPβCD reduced the frequency of monocyte-derived macrophages to the level of SC-fed mice, although this effect was only significant for HPβCD-HP5 and $CD11c^-$ macrophages.

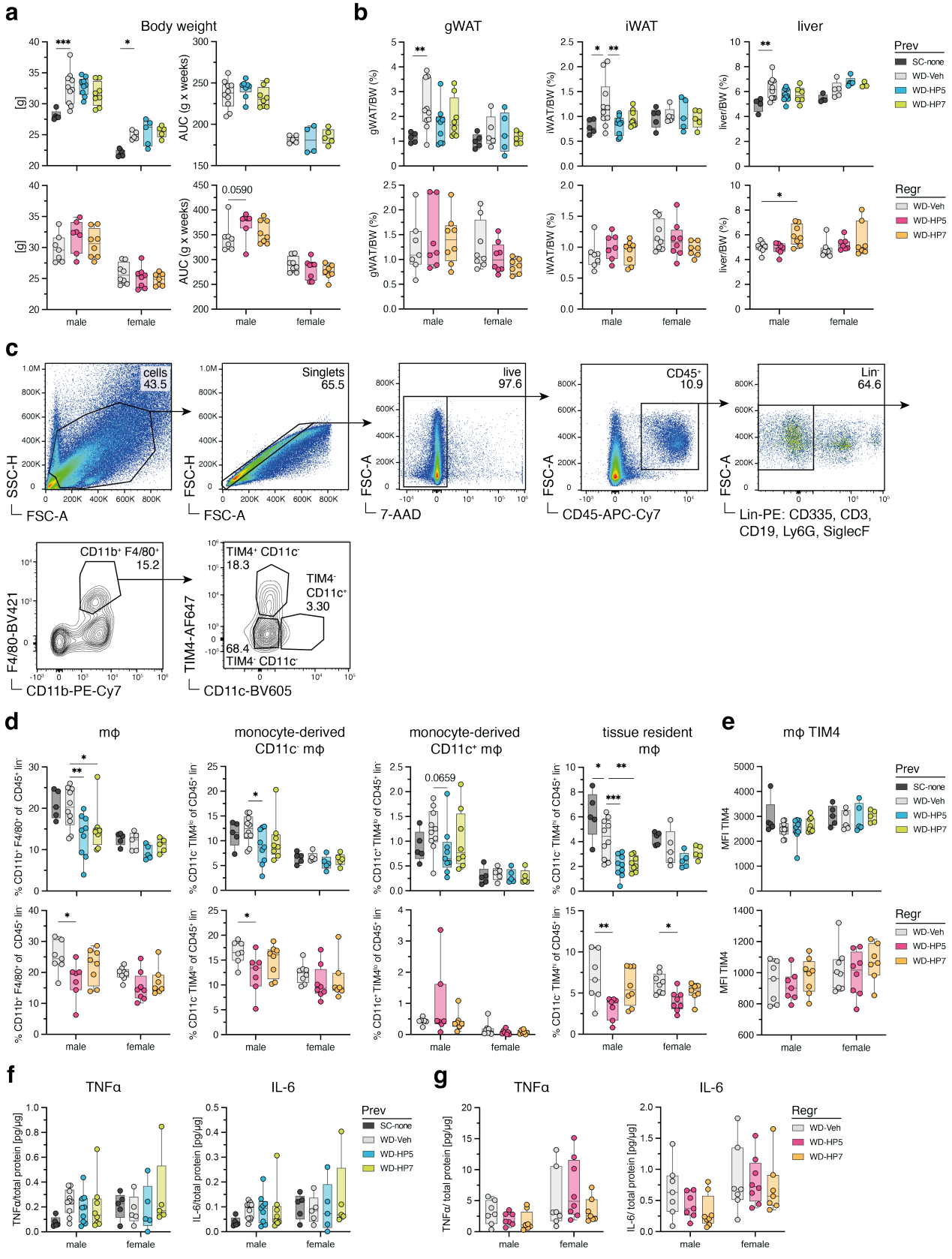
a
Body weight
[g]
AUC (g x weeks)
0.0590
male
female
b
gWAT
iWAT
liver
gWAT/BW (%)
iWAT/BW (%)
liver/BW (%)
Prev
SC-none
WD-Veh
WD-HP5
WD-HP7
Regr
WD-Veh
WD-HP5
WD-HP7
c
cells
43.5
Singlets
65.5
live
97.6
CD45+
10.9
Lin-
64.6
SSC-H
FSC-A
FSC-H
7-AAD
CD45-APC-Cy7
Lin-PE: CD335, CD3, CD19, Ly6G, SiglecF
CD11b+ F4/80+
15.2
TIM4+ CD11c-
18.3
TIM4- CD11c+
3.30
68.4
TIM4- CD11c-
F4/80-BV421
TIM4-AF647
CD11b-PE-Cy7
CD11c-BV605
d
mϕ
monocyte-derived CD11c- mϕ
monocyte-derived CD11c+ mϕ
tissue resident mϕ
0.0659
% CD11b+ F4/80+ of CD45+ lin-
% CD11c- TIM4lo of CD45+ lin-
% CD11c+ TIM4lo of CD45+ lin-
e
mϕ TIM4
MFI TIM4
f
TNFα
IL-6
TNFα/total protein [pg/µg]
IL-6/total protein [pg/µg]
g
TNFα
IL-6
TNFα/ total protein [pg/µg]
IL-6/ total protein [pg/µg]

Fig. 16: Effects of HPβCD-HP5 and HPβCD-HP7 on BW, metabolic organs and ATM. *Apoe*$^{-/-}$ mice of the prevention (Prev) and regression (Regr) atherosclerosis models were fed with WD and treated with HPβCD-HP5 (HP5) and HPβCD-HP7 (HP7) (2x/week). a) BW as absolute values and longitudinal measurement as AUC b) Tissue weights of iWAT, gWAT, and liver. c) Representative flow cytometry gating strategy of the isolated SVF from gWAT. d) Frequency of macrophage populations. e) MFI of TIM4 on total macrophages, f), g) TNFα and IL-6 concentrations from the e) prevention and f) regression model. Statistical analysis was performed using two-way ANOVA followed by Dunnett's multiple comparisons test. Displayed *p*-values are adjusted for multiple testing. *n* (males) = 5-10, *n* (females) = 5-8 mice per group.

In the regression model, there was a reduction of specifically CD11c^{-}, but not CD11c^{+} monocyte-derived ATM. No effects were observed in the females; however, the frequencies of total and monocyte-derived ATM were lower in females as compared to males. The frequency of tissue-resident ATM was lower in the males of the WD-Veh group compared to the SC-fed group. HPβCD-HP5 and HPβCD-HP7 treatment significantly lowered cell frequencies in males of the prevention model. In the regression model, the effect of HPβCD-HP5 was similar, and it was also observed in the females. The expression of TIM4, a marker of tissue-resident ATM (Huh and Kim, 2021; Magalhaes et al., 2021), on total macrophages was similar across treatments (**Fig. 16e**).

As macrophages shape the cytokine milieu around them, we tested whether pro-inflammatory cytokines changed upon loss of ATM in the gWAT (**Fig. 16f, g**). In the prevention model, TNFα and IL-6 had the tendency of increased levels in the males of the WD-Veh group relative to the SC group (**Fig. 16f**). Females already showed these levels already at baseline level (SC) and did not show further increases upon WD feeding. HPβCD treatment marginally lowered the increased TNFα levels in males, but had no effects in females. In the regression model, similar trends were observed, albeit at generally higher cytokine levels relative to the total protein concentrations (**Fig. 16g**).

In summary, the frequencies of ATM were reduced by HPβCD treatment in male mice, independent of their origin, which did not correlate with reduced cytokine levels in the AT.

3.3.5 Effects of HPβCD-HP5 and HPβCD-HP7 on adipocyte morphology

The major cell type in the AT are adipocytes, and we thus investigated whether we find structural changes in the gWAT architecture following HPβCD treatment (**Fig. 17a, b**).

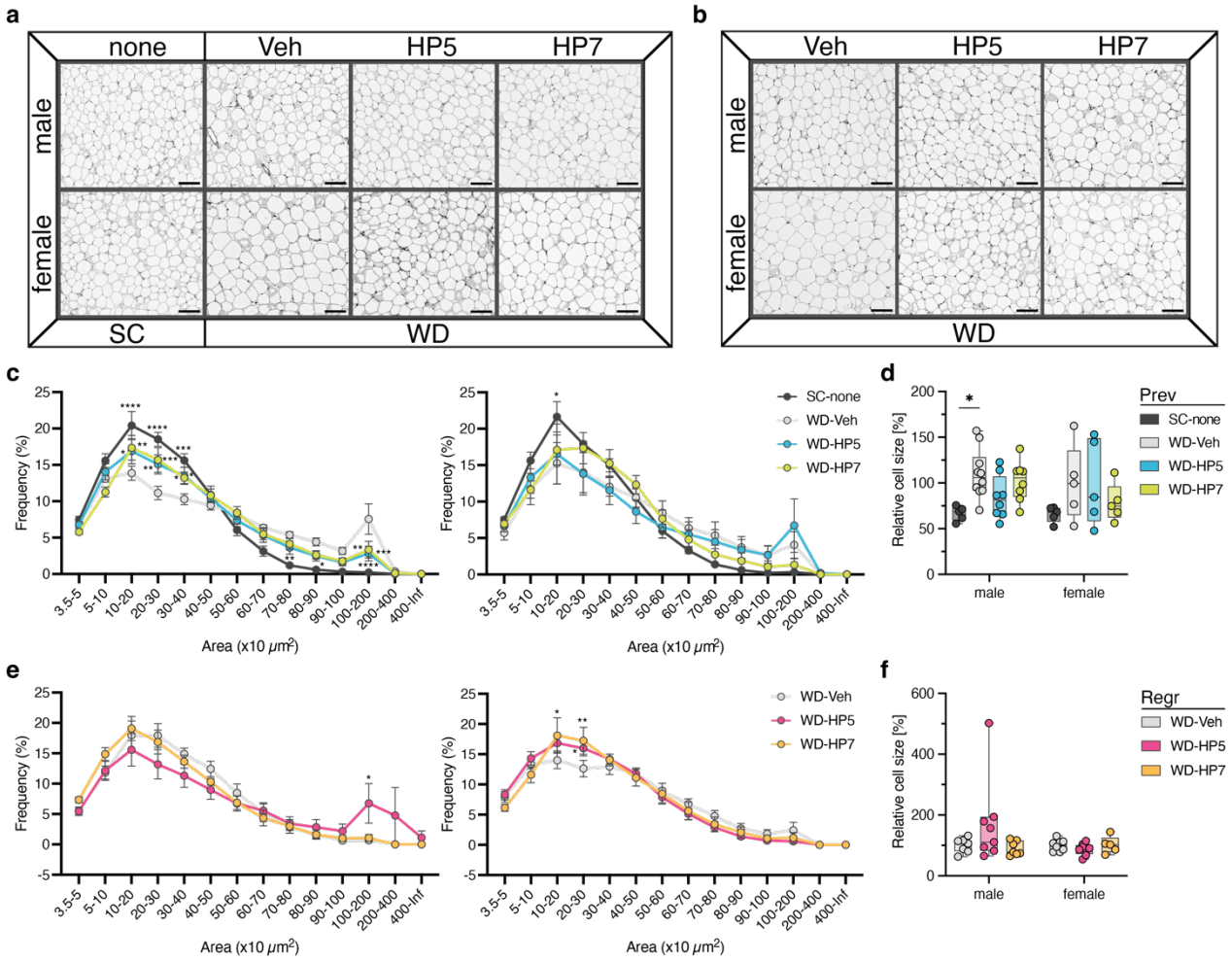

Fig. 17: Effects of HPβCD-HP5 and HPβCD-HP7 on adipocyte morphology in the *Apoe*$^{-/-}$ prevention and regression model. a), b) Representative HE-stained sections of gWAT from the a) prevention (Prev) and b) regression (Regr) model. Scale bar = 50 µm. c), e) Adipocyte size distribution quantified from images as shown in a) and b) for the c) Prev and e) Regr model. d), f) Relative adipocyte cell size, normalized to the mean value of the WD-Veh group of the respective experiment. Statistical analysis was performed using two-way ANOVA followed by Dunnett's multiple comparisons test. Displayed *p*-values are adjusted for multiple testing. *n* (males) = 5-10, *n* (females) = 5-8 mice per group.

As expected, adipocytes from mice fed a WD showed an increased cell size phenotype in both male and female mice, compared to the SC-fed mice (**Fig. 17c**). This is evident from the reduced frequency of smaller-adipocytes (e.g., 10-20 x10 µm^2) and the increased size of larger adipocytes (e.g., 100-200 x10 µm^2). This finding is further reflected in an increased average cell size (**Fig. 17d**). In contrast, HPβCD-HP5 and HPβCD-HP7-treated males, but not females, showed a reduced size gain in the prevention model. In the regression model, HPβCD-HP5 treatment increased the proportion of 100-200 x10 µm^2

cells in males, whereas HPβCD-HP5 and HPβCD-HP7 increased the proportion of 10-30 x10 μm^2 cells in females (**Fig. 17e**). These effects had no major impact on average cell size (**Fig. 17f**).
To conclude, HPβCD-HP5 and HPβCD-HP7 reduced the hypertrophic cell phenotype induced by WD, and enabled hyperplasia in male mice in the prevention model. This means, that the adipose tissue grew by increasing cell frequency instead of cell growth which is usually associated with a lean and healthy tissue (Horwitz and Birk, 2023).

As HPβCD treatment induced changes in the fat tissue, especially the gWAT, we measured a set of hormones and other markers, which are secreted by the adipose tissue, and are commonly dysregulated during obesity, inflammation, and metabolic syndrome (Hotamisligil, 2017). In the prevention model, WD feeding induced increased levels of insulin, leptin, total PAI-1, and resistin in the gWAT in both male and female mice, with more pronounced effects in the males (**Fig. 18a**). In the males, leptin and total PAI-1 were significantly elevated upon WD, as compared to SC. No effects were seen with HPβCD treatment, the values remained similar to the WD-Veh group. Plasma adiponectin, which exerts atheroprotective effects and is reduced in plasma under conditions of chronically high insulin, was measured (**Fig. 18b**). In the prevention model, adiponectin was reduced in the WD-fed females compared to the SC-fed group, but no treatment effects were observed. In the males no effects were seen either. In the regression model, not all samples could be measured; therefore, mainly male samples were selected, as they also showed the plaque area reduction. However, just a trend toward reduced adiponectin plasma levels were seen. In summary, HPβCD did not affect general adipokine secretion levels in the gWAT or the circulation.

As the morphological changes, which were seen in the histological analysis, could have various origins, we tested the HPβCD-HP5 and HPβCD-HP7 treatment efffects on lipolysis in adipocytes, i.e. the breakdown from triacylglycerides to glycerol and fatty acids (Zechner et al., 2012) (**Fig. 18d**), which may account for a reduction in fat mass.

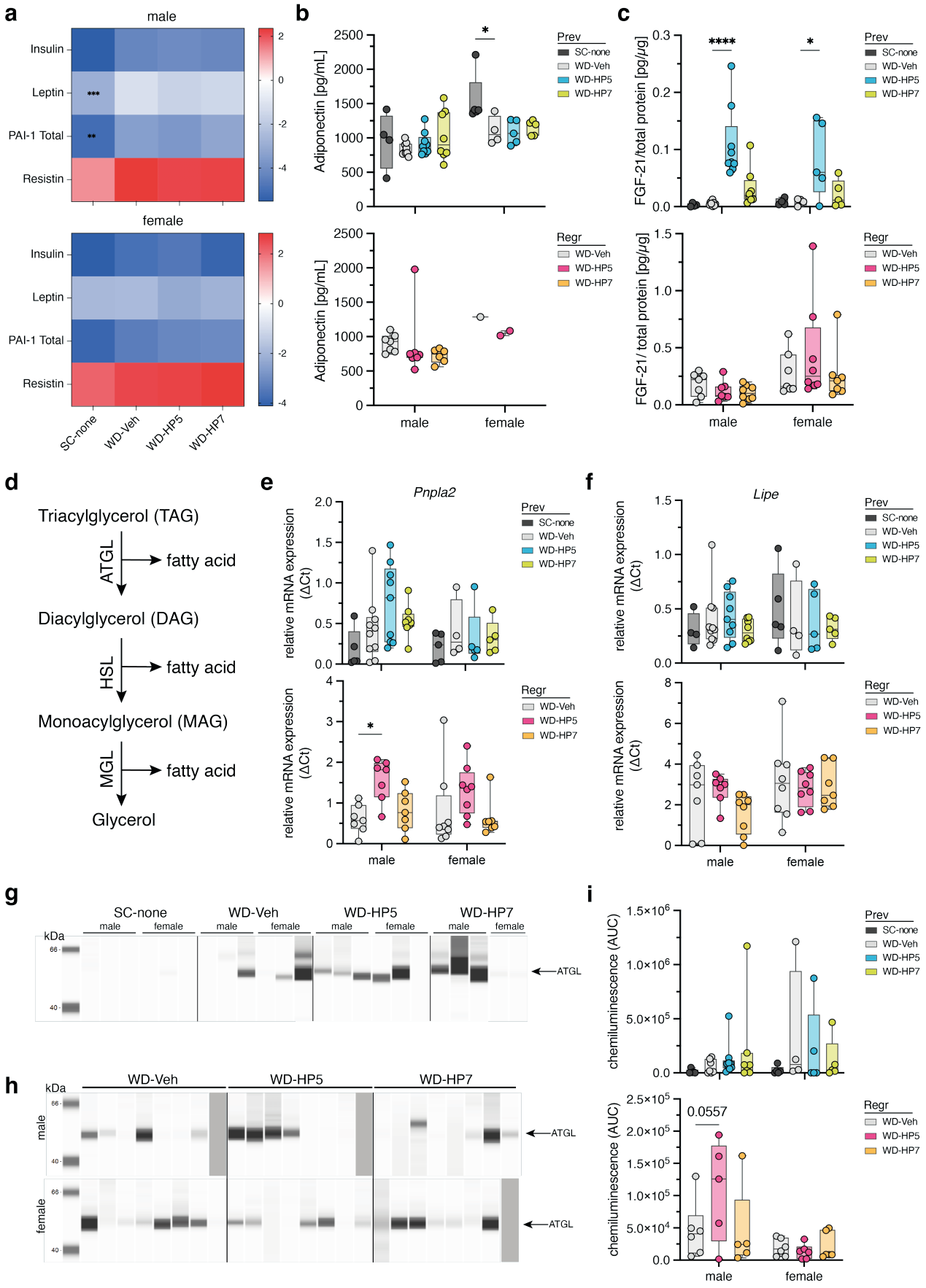
a
male
Insulin
Leptin
PAI-1 Total
Resistin
***
**
2
0
-2
-4
female
SC-none
WD-Veh
WD-HP5
WD-HP7
b
Adiponectin [pg/mL]
*
Prev
SC-none
WD-Veh
WD-HP5
WD-HP7
Regr
WD-Veh
WD-HP5
WD-HP7
male
female
c
FGF-21/total protein [pg/µg]
****
*
FGF-21/ total protein [pg/µg]
d
Triacylglycerol (TAG)
ATGL
fatty acid
Diacylglycerol (DAG)
HSL
fatty acid
Monoacylglycerol (MAG)
MGL
fatty acid
Glycerol
e
Pnpla2
relative mRNA expression (ΔCt)
f
Lipe
g
SC-none
WD-Veh
WD-HP5
WD-HP7
kDa
66
40
ATGL
h
i
chemiluminescence (AUC)
0.0557

Fig. 18: Effects of HPβCD-HP5 and HPβCD-HP7 on adipokines and lipolysis markers in the gWAT of WD-fed *Apoe*$^{-/-}$ mice. a) Heat maps of adipokines measured in the gWAT from mice of the prevention model using a multiplex Luminex assay. b) Adiponectin concentration in the plasma measured by a single-plex Luminex assay. c) FGF21 levels in gWAT measured by ELISA. d) Lipolysis steps and involved enzymes e), f) Relative mRNA expression of e) *Pnpla2* and f) *Lipe* in the gWAT, normalized to the reference gene *Hprt*. g), h) Representative Wes (ProteinSimple) images showing ATGL protein expression in the gWAT of the (g) prevention model and h) regression model i) Quantification of the protein expression shown in g), h), expressed as AUC. Statistical analysis was performed using two-way ANOVA followed by Dunnett's multiple comparisons test. Displayed p-values are adjusted for multiple testing. n (males) = 4-10, n (females) = 5-8 mice per group. Read about missing values for adiponectin in methods.

One factor, which induces lipolysis, is FGF21 (Inagaki et al., 2007), which was shown to be induced by HPβCD-HP5 in the WT model used earlier (**Fig. 10f**). Therefore, we analyzed FGF21 in protein lysates generated from gWAT tissue and found that HPβCD-HP5 induced highly significant increases of FGF21 levels in the prevention model, predominantly in the male group (**Fig. 18c**). HPβCD-HP7 showed a tendency for increased FGF21 levels. In the regression model, no effects were observed.

To validate whether the lipolysis (**Fig. 18d**) was induced in the gWAT, we measured the mRNA and protein expression of adipose triglyceride lipase (ATGL, gene name *Pnpla2*), which is the enzyme that catalyzes the first hydrolysis step, removing one fatty acid and resulting in a diacylglyceride (Zimmermann et al., 2004). In the prevention model, WD feeding induced minor upregulations of both mRNA and protein levels in males and females. HPβCD-HP5 treatment induced a slight increase of *Pnpla2* mRNA level in the males (**Fig. 18e**), but this was not reflected on protein level (**Fig. 18g, i**). In the regression model, HPβCD-HP5 induced a significant upregulation of *Pnpla2* mRNA levels (**Fig. 18e**) and a moderate increase in ATGL protein levels (**Fig. 18h, i**) in the males. In females, a trend of increasing *Pnpla2* mRNA levels was seen, however, without changes on protein level. The second step of the lipolysis reaction is catalyzed by hormone-sensitive lipase (HSL, gene name *Lipe*), which creates a monoacylglyceride and a free fatty acid. *Lipe* mRNA levels were overall unchanged in both models across all conditions (**Fig. 14f**). To conclude, HPβCD-induced lipolysis in the gWAT could not entirely be confirmed.

3.3.6 Effects of HPβCD-HP5 and HPβCD-HP7 on *ex vivo* lipolysis

As previous observations suggested potential induction of lipolysis, the ability of HPβCD-HP5 and HPβCD-HP7 to stimulate this process was tested in a more controlled setting. Using an *ex vivo* lipolysis assay on gWAT from adult WT mice, we observed a dose-dependent increase in lipolysis, indicated by elevated release of free glycerol into the medium. This effect was primarily observed in incubated tissue samples from male mice (**Fig. 19a**) rather than female mice (**Fig. 19b**). However, as most of the results did not reach statistical significance, these findings should be considered a trend. Nevertheless, they are consistent with the sex-dependent effects on lipolysis observed in the *in vivo* models (**Fig. 19**).

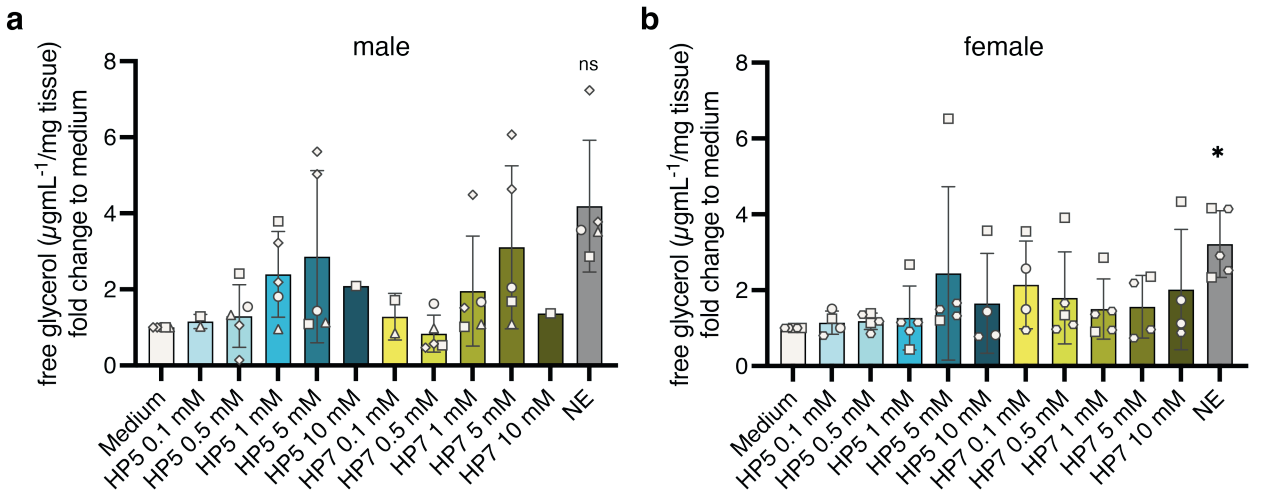

Fig. 19: Lipolytic capacity of HPβCD-HP5 and HPβCD-HP7 in gWAT explants of male and female WT mice. Isolated gWAT from adult WT mice was cut into pieces and stimulated with the respective concentrations of HPβCD-HP5 (HP5) and HPβCD-HP7 (HP7) for 2 h. a) Free glycerol levels were measured in the supernatant. *NE*, norepinephrine. Data represents mean ± SEM of three independent experiments. If male and female gWAT was treated within the same experiment, the same symbol shape is used. Statistical analysis was performed using two-way ANOVA followed by Dunnett's multiple comparisons test. Displayed p-values are adjusted for multiple testing. *n* (males) = 2-5, *n* (females) = 4-5 mice per group.

3.4 Modulation of adipocyte differentiation by HPβCD-HP5 and HPβCD-HP7

3.4.1 The effects of HPβCD-HP5 and HPβCD-HP7 on adipogenesis *in vitro*

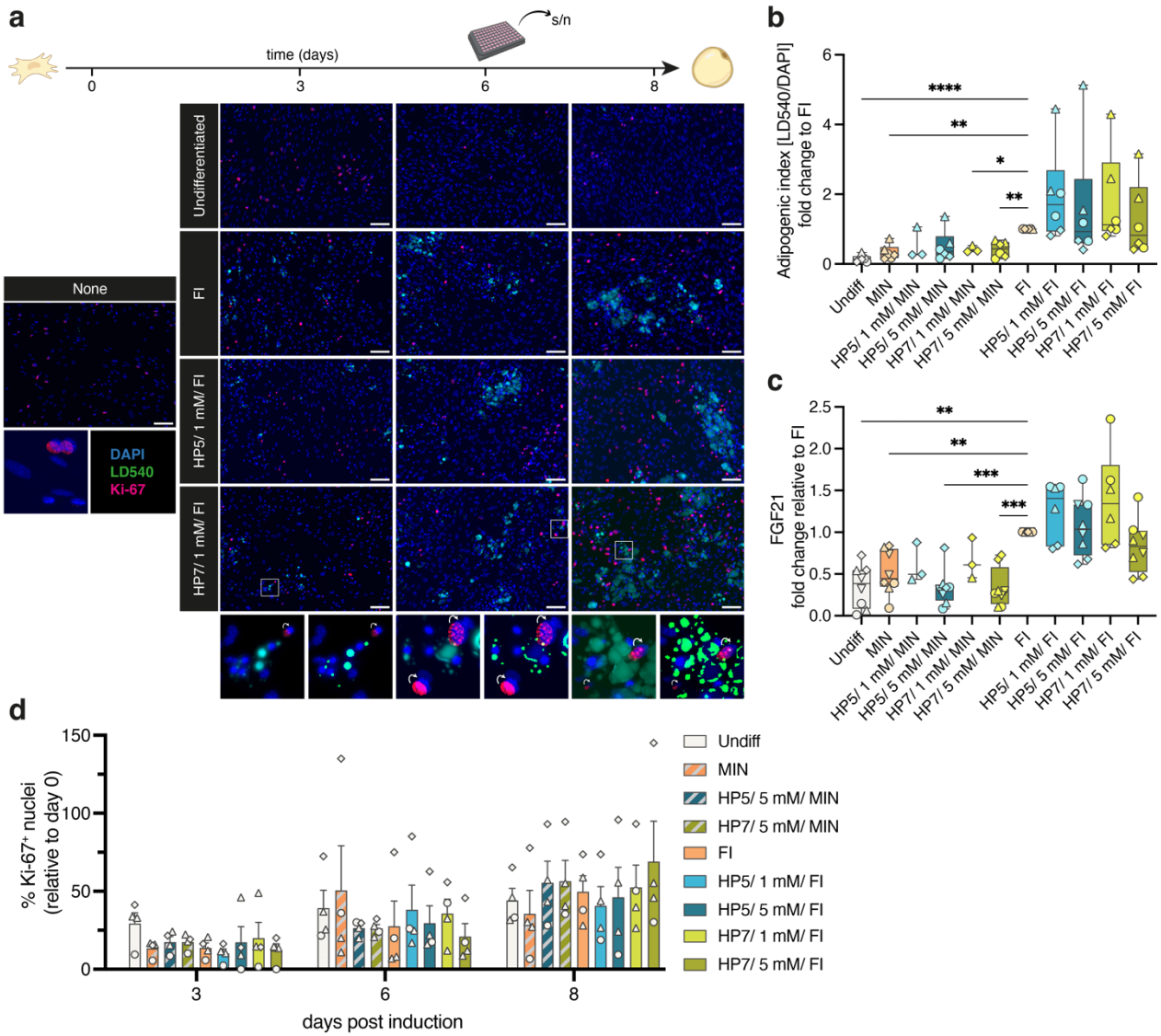

Fig. 20: Effects of HPβCD-HP5 and HPβCD-HP7 on *ex vivo* adipogenesis of SVF cells. a) Isolated SVF from gWAT of WT mice were cultured and adipogenesis was induced in pre-adipocyte cells. Cells were fixed on the day of induction (day 0), as well as on day 3, 6 and 8. Cells were stained with DAPI, LD540 and Ki-67. Representative images showing adipogenesis and cell proliferation. Scale bar = 100 µm b) Adipogenic index as lipid area relative to nuclei area. c) FGF21 levels in the cell supernatants on day 6 measured by ELISA. d) Ki-67$^+$ nuclei indicating proliferating cells. Statistical analysis was performed using two-way ANOVA followed by Dunnett's multiple comparisons test. Displayed p-values are adjusted for multiple testing. n=3-6 mice per condition; similar shapes of the data points indicate different mice from the same experiment. Undiff=undifferentiated, MIN=minimal induction, FI=full induction

As reduced adipocyte size could result not only from enhanced lipolysis of stored fat but also from altered adipocyte differentiation, we investigated whether HPβCD-HP5 and HPβCD-HP7 treatment interferes with the maturation of preadipocytes into mature lipid-

storing adipocytes. We therefore cultured the SVF (Lin^-) of WT mice, and added HPβCD-HP5 or HPβCD-HP7 to the adipogenesis induction cocktail to assess effects on lipid droplet formation (**Fig. 20a**). Both HPβCD exhibited a similar response pattern, with the lower concentration (1 mM) showing a tendency toward a higher adipogenic index compared with the higher concentration (5 mM), although this difference was not statistically significant (**Fig. 20b**). The addition of HPβCD to the minimal induction cocktail, which lacks rosiglitazone - an activator of PPARγ and master regulator of adipocyte differentiation - also resulted in a slight increase in adipogenic indices.

To test whether FGF21-inducing effects of HPβCD-HP5 and HPβCD-HP7 in AT could be reproduced *in vitro*, we measured FGF21 levels in day-6 cell supernatants by ELISA. FGF21 secretion levels generally rose with adipocyte differentiation, correlating positively with the adipogenic index (**Fig. 20c**). FGF21 secretion may primarily reflect adipogenesis rather than a direct effect from cyclodextrin treatment, as no increase of FGF21 was observed when HPβCD were added to the minimal induction medium.

Lastly, we investigated effects of HPβCD-HP5 and HPβCD-HP7 on the proliferation of adipocyte precursor cells. We therefore assessed the frequency of Ki-67^+ nuclei over four different time points (day 0, 3, 6 and 8) (**Fig. 20d**). Ki-67 is an antigen solely expressed in proliferating cells, but not in quiescent or resting cells in the G0 phase of the cell cycle (Gerdes et al., 1984). In general, the proliferation was highest on day 0 before the addition of any induction medium. On day 3, the proliferation rate had dropped by about 4-fold relative to day 0 and was slightly higher in the undifferentiated control cells compared to the treated condition. The frequency of proliferating cells increased over time, and the difference between undifferentiated and differentiated cells disappeared. However, HPβCD had no measurable effect on proliferation. Off note, Ki-67+ nuclear counts did not differ by the end of differentiation, further supporting the absence of an effect on cell proliferation (**Fig. S6**).

3.4.2 The effects of HPβCD-HP5 and HPβCD-HP7 on adipogenesis in *ex vivo* explants

Another way to study the effects on adipocyte differentiation is the use of explants from adipose precursor tissue. This approach is independent of the artificial application of an

induction cocktail to trigger adipogenesis, and may therefore better reflect physiological conditions (Han et al., 2011). A limitation of this approach is the availability of precursor tissue exclusively from male pups, as it is anatomically connected to the testis and cannot be readily identified in females.

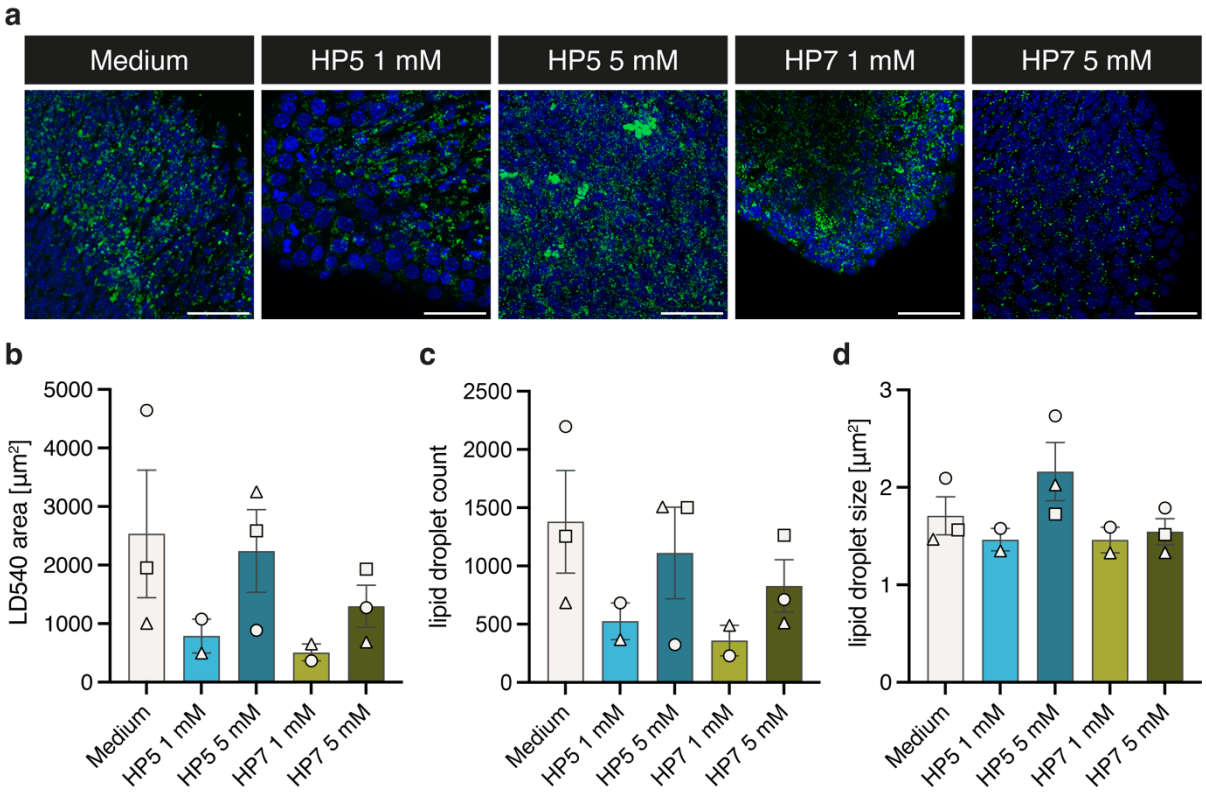

Fig. 21: Effect of HPβCD-HP5 and HPβCD-HP7 on lipid droplet formation in precursor gWAT. Precursor gWAT was isolated from male P4 pups (WT) and treated with HPβCD-HP5 (HP5) or HPβCD-HP7 (HP7) for 5 days. Tissues were fixed and stained with LD540 and DAPI. a) Representative images of the lipid droplets (LD540) and nuclei (DAPI). Scale bar = 50 µm. b), c) Quantification of lipid droplet b) area and c) counts. d) Average lipid droplet size, calculated as total LD540^{+} area divided by droplet count within each image. Data represent mean ± SEM of three independent experiments. Statistical analysis was performed using two-way ANOVA followed by Dunnett's multiple comparisons test. n=2-3 independent experiments

Lipid droplets were analyzed by area and count, as the normalization to the nuclei area was not possible. HPβCD-HP5 and HPβCD-HP7 appeared to reduce both the LD540-positive lipid droplets area and the droplet counts (**Fig. 21b, c**). However, this analysis did not account for dark regions in the image lacking cells. Consequently, the results were skewed by unequal distribution of empty regions within the imaged fields (**Fig. 21a**). Due

to the difficulty in identifying appropriate regions within the tissue, these results were not further processed, and additional replicates will be required to draw reliable conclusions. This also applies for the analysis of lipid droplet sizes, which are at least independent of tissue distribution artefacts, but may still not have been consistently derived from the correct tissue area (**Fig. 21d**).

3.5 Effects of HPβCD-HP5 and HPβCD-HP7 on the liver

FGF21 is mainly produced in the liver and secreted into the circulation (Flippo and Potthoff, 2021). We measured the FGF21 protein levels from liver lysates of the atherosclerosis prevention and regression models. In the prevention model, slightly elevated concentrations were detected in the WD-Veh group compared with the SC group in both sexes (**Fig. 22a**). FGF21 levels increased in males following treatment with both HPβCD, although the effect reached significance only with HPβCD-HP7. No treatment effects were observed in the females. In the regression model, small trends toward increased FGF21 levels were seen with HPβCD-HP7 but not with HPβCD-HP5, and similarly to the prevention model, no effects were observed in females.

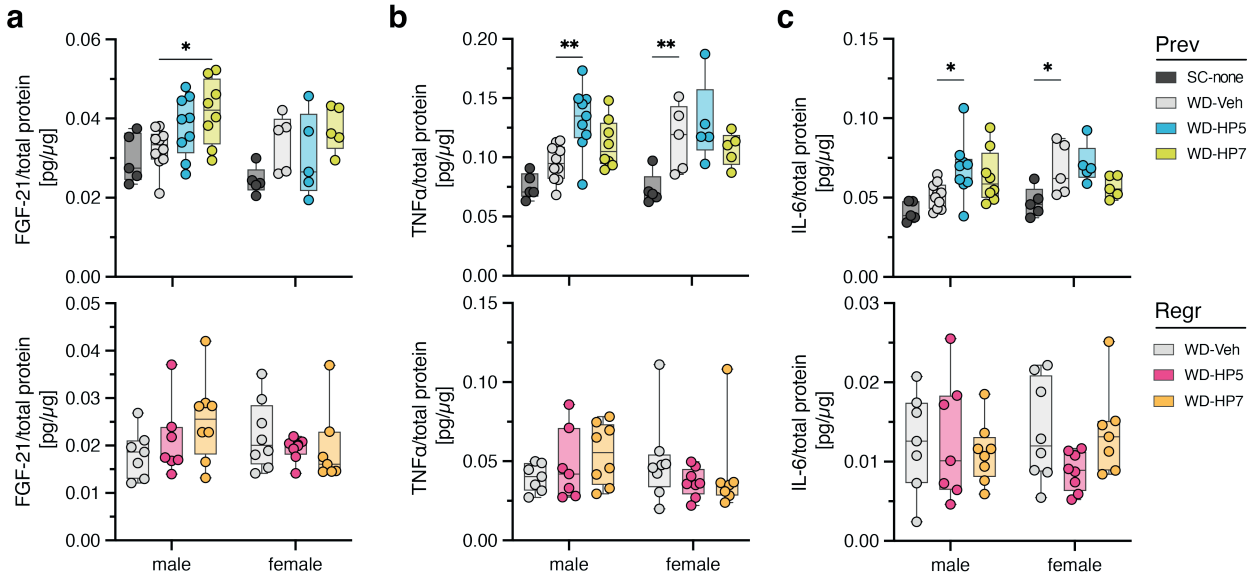

Fig. 22: FGF21 and cytokine expression in the liver of WD-fed *Apoe*$^{-/-}$ mice, treated with HPβCD-HP5 or HPβCD-HP7. a)-c) protein levels of a) FGF21 b) TNFα and c) IL-6 in the liver. Statistical analysis was performed using two-way ANOVA followed by Dunnett's multiple comparisons test. Displayed *p*-values are adjusted for multiple testing. *n* (males) = 5-10, *n* (females) = 5-8 mice per group.

The liver serves as a central hub for systemic inflammation (Kostallari et al., 2025). We assessed pro-inflammatory cytokine secretion in the liver protein extracts by ELISA. In the prevention model, WD feeding increased TNFα and IL-6 in both sexes, reaching significance only in females (**Fig. 22b, c**). However, HPβCD-HP5 significantly enhanced this effect in males, particularly for TNFα, which was affected by both diet and HPβCD-HP5 treatment. In the regression model, no clear trends were observed, and cytokine levels were generally lower than those in the prevention model.

In summary, WD induced both FGF21 and pro-inflammatory cytokines in the liver of mice in the atherosclerosis prevention model. Both HPβCD showed distinct effects, with HPβCD-HP7 primarily inducing FGF21 and HPβCD-HP5 enhancing a proinflammatory signature with elevated TNFα and IL-6 levels in males.

4. Discussion

New therapies that can simultaneously reduce excess cholesterol and dampen inflammation are highly desirable for treating patients with atherosclerosis. The aim of this thesis was to investigate the therapeutic effects of HPβCD derivatives (HPβCD-HP5 and HPβCD-HP7) in modulating bone marrow hematopoiesis and adipose tissue (AT) composition in the context of metaflammation and atherosclerosis. We show that both derivatives reduce atherosclerotic plaque burden in male *Apoe*$^{-/-}$ mice, in both preventive and therapeutic treatment setting. This effect was accompanied by a marked decrease in total cholesterol and an increase in the oxysterol 27-OHC. In the prevention setting, triacylglycerides (TAG) were also lowered. Additionally, we observed changes in gonadal white adipose tissue (gWAT) morphology, a reduction of adipose tissue macrophages (ATM), and elevated FGF21 levels in gWAT. Phenotyping of hematopoietic stem and progenitor cells (HSPC) indicated that HPβCD induced only mild alterations in myeloid reprogramming. Notably, most of these findings were observed in male, but not female mice, highlighting a sex-dependent response to HPβCD treatment. Together, these findings provide new insight into how cyclodextrin derivatives can modulate metabolic inflammation. In particular the reduction of TAG is clinically relevant, as elevated TAG levels represent a recognized risk factor for ASCVD (Akivis et al., 2024).

4.1 Comparison between HPβCD-HP5 and HPβCD-HP7 treatment effects

The original study by Zimmer et al. (2016) used HPβCD-HP5. In our work, we initially tested HPβCD-HP7, which has a higher degree of hydroxypropyl substitution than HPβCD-HP5 and therefore provides higher solubility and protection against enzymatic degradation by amylases (Ashland, 2016). Because we examined not only s.c. injection but also oral administration, HPβCD-HP7 was selected for the *Ldlr*$^{-/-}$ study. In subsequent studies with WT mice, we switched to HPβCD-HP5 as no effects were seen with HPβCD-HP7. However, under conditions of WD-induced metaflammation, neither HPβCD appeared to influence bone marrow parameters. Given these results, it was reasonable to include both derivatives in the *Apoe*$^{-/-}$ atherosclerosis studies, to be able to compare their anti-atherosclerotic activity with regards to the known effects shown by Zimmer et al. (2016), and further evaluate the effects on bone marrow and AT, which has not been looked at before.

In addition to confirming the plaque-reducing effect of HPβCD-HP5, we now demonstrate that HPβCD-HP7 also decreases atherosclerotic plaque burden. Although both HPβCD effectively reduced plaque area, total cholesterol, and TAG levels, differences emerged with regard to their effects on ATM, FGF21 and ATGL induction in gWAT, and cytokine responses in the bone marrow and liver. Overall, HPβCD-HP5 appeared to exert stronger effects across those biomarkers.

The underlying reason likely relates to slightly different chemical properties**.** Compared to the parental β-cyclodextrin, other derivatives such as sulfobutylether-β-cyclodextrin (SBEβCD), or even α-cyclodextrins with six or γ-cyclodextrins with eight glucose units, the two forms of HPβCD that we used, are quite similar. However, while both HPβCD-HP5 and HPβCD-HP7 share the same cavity of a β-cyclodextrin, that enables preferential binding of cholesterol, they differ in the number of substitution groups, molecular weight and solubility. Compared to HPβCD-HP5, HPβCD-HP7 has a higher degree of hydroxypropyl substitution, which increases its solubility by enhancing the molecule's amphiphilic character - combining a lipophilic carbon backbone with polar hydroxyl groups (Ashland, 2016). In theory, this allows for better interaction with lipophilic groups, e.g., lipids in the adipose tissue or circulating lipoproteins. Because administration was

performed intraperitoneally, the injected HPβCD was in close proximity to gWAT, further supporting the possibility of depot-specific effects. These chemical distinctions may therefore contribute to the similar, but not identical, outcomes observed across tissues. Nevertheless, the mechanism of how these structural differences result in comparable effects on plaque reduction and hematopoiesis, but divergent responses in adipose tissue and liver, remain unclear.

For future clinical translation, a more detailed characterization of atherosclerotic lesions in response to different HPβCD variants may help resolve the observed difference between HPβCD-HP5 and HPβCD-HP7. Attributes such as plaque composition (fibrous vs lipid-rich), cap thickness, inflammation, calcification, and arterial wall elasticity are clinically relevant measures beyond plaque size alone, and may reveal variant-specific therapeutic signatures.

4.2 Reproducibility of WD-induced bone marrow reprogramming

A central question raised by using WD models was that WD not only leads to atherosclerotic plaques formation, but also induces broader changes in hematopoiesis, which is consistent with the principle of trained immunity (TI). Previous reports have suggested that WD triggers epigenetic reprogramming of bone marrow progenitor cells with the expansion of GMP, which leads to an increased inflammatory state within the myeloid compartment (Christ et al., 2018). Across the different models we employed - *Ldlr* $^{-/-}$**,** WT**,** and *Apoe*$^{-/-}$ - we could neither consistently detect the anticipated GMP expansion in response to WD feeding, nor did sorted GMP reveal a transcriptional shift in RNA- and ATAC-seq profiles.

This divergence from previously reported observations underscores potential limitations in the reproducibility of WD-induced TI and suggests that dietary cues may be substantially more context-dependent, influenced by genetic background, facility-specific microbiota, or housing conditions.

One relevant factor is the use of a different control diet compared with the original publication. In our *Ldlr*$^{-/-}$ and WT studies, we used a purified control diet matched to the

WD in vitamins, trace elements, and amino acid composition, whereas the original study employed a standard chow diet (Christ et al., 2018). In WT mice, one additional confounding factor is their efficient cholesterol clearance due to high HDL levels, which prevents them from developing severe hypercholesterolemia as observed in *Ldlr* $^{-/-}$ or *Apoe*$^{-/-}$ mice (Gisterå et al., 2022). Although WT mice are used in atherosclerosis studies employing proatherogenic diets (1.25 % cholesterol, 0.5 % cholic acid, and 15 % fat), these diets induce only early fatty streaks after prolonged feeding of 10-14 weeks. After five weeks of feeding, plasma cholesterol levels remain below 320 mg/dL (Paigen et al., 1985), which corresponds to the baseline levels of *Ldlr*$^{-/-}$ (200-400 mg/dL) and is substantially lower than those of *Apoe*$^{-/-}$ mice (600-700 mg/dL). This markedly lower cholesterol and lipid burden reduces the amount of oxLDL, a key trigger of TI (Bekkering et al., 2014).

In our *Apoe*$^{-/-}$ atherosclerosis prevention experiment, which included a standard chow (SC)-fed control group, we did not observe a WD-induced expansion of GMP, as compared to the SC-fed mice. However, we detected significant increases in MPP populations - particularly the myeloid-biased MPP3 subset - and a trend toward elevated HSC frequencies, suggesting enhanced leukocyte production. During emergency myelopoiesis, MPP that have different lineage biases, shifts toward a myeloid differentiation, including the lymphoid-biased MPP4 subset (Olson et al., 2020; Pietras et al., 2015). The combination of increased HSPC, together with the absence of GMP expansion and the lack of changes in circulating mature myeloid cells in response to WD feeding may therefore reflect a state of emergency hematopoiesis, in which differentiation is simultaneously retained. This is in part reflected in lower circulating cell counts of WD-fed mice, compared to SC-fed mice. Notably, *Apoe*$^{-/-}$ mice show significantly increased HSPC proliferation after ten weeks of WD feeding, whereas *Ldlr*$^{-/-}$ mice do not (Murphy et al., 2011), underscoring model-specific differences in inflammatory responses.

4.2.1 Modulation of TI by HPβCD-HP5 and HPβCD-HP7

The above mentioned limitations have implications for interpreting the effects of cyclodextrin treatments. If WD feeding does not reliably induce a detectable hematopoietic shift, potential “reversal” effects of HPβCD-HP5 or HPβCD-HP7 cannot be meaningfully

evaluated at the progenitor level. As a result, our conclusions regarding the role of cyclodextrins in TI must remain cautious.

The first approach to evaluate TI was done in WD-fed *Ldlr*$^{-/-}$ mice, from which GMP were sorted for transcriptomic and epigenetic analysis. The results from RNA- and ATAC-seq showed no increase of LXR target genes by HPβCD-HP7 compared to the respective Veh group. A few DE genes were identified; however, they were not consistent among the two treatment groups that differed in the route of administration (oral: *Hmox*, *mt-Atp6*, and *mt-Nd4* (up) vs s.c.: *mt-Atp6*, *Ftl1*, *C1qc* (down), and *Ifitm3* (up)). This highlights that the route of drug administration influences the effect on the target organ.

The interpretation of subtle changes is further complicated by the underlying statistical framework. Differences in statistical approaches – specifically, the use of unadjusted *p*-values (Christ et al., 2018) versus multiple testing correction in our RNA-seq and ATAC-seq analyses – may contribute to the divergent outcomes in DE gene and DOR identification. However, even when analyzing our unadjusted data, we did not observe increases in key marker genes such as *Abca1* or *Tlr4*.

To evaluate bone marrow niche inflammation, we measured IL-1β in the supernatants of flushed bone marrow cells. We observed marginal increases following HPβCD treatment within the prevention model, but not in the regression model, which may be a result of increased frequencies of HPβCD injections (eight vs four weeks). IL-1β is a key driver of TI amplification (Li et al., 2022; Simats et al., 2024; Teufel et al., 2022) and future studies are needed to monitor effects of HPβCD on inflammation of the bone marrow niche, which also affects central (maladaptive) TI and hematopoietic aging.

Together, these observations suggest that WD-induced hematopoietic reprogramming is not uniformly reproducible across mouse models or dietary backgrounds. Based on the cumulative evidence from our experiments, the *Ldlr*$^{-/-}$ mouse model, combined with standard chow (SC) rather than purified control diet (CD), appears to be the most promising system for future studies investigating TI effects in the bone marrow, as this setting - at least in the oral group – yielded measurable and significant increases of GMP frequencies.

4.3 Reduction of adipocyte size in the gWAT by HPβCD treatment

In our *Apoe*$^{-/-}$ atherosclerosis prevention model, but not in the regression model, we observed the morphological shift from larger to smaller sized adipocytes in the gWAT. This is a striking observation, as it may represent an important mechanistic link between AT-driven metaflammation and atherogenesis. Several hypotheses may explain this phenotype.

4.3.1 FGF21-induced lipolysis

One potential mechanism involves fibroblast growth factor 21 (FGF21), an adipokine with pleiotropic metabolic functions (Flippo and Potthoff, 2021; Velingkar et al., 2023), and the ability to promote lipolysis during fasting (Inagaki et al., 2007). Lipolysis helps to source energy by the release of free fatty acids that then undergo β-oxidation to produce acetyl-CoA and electron carriers (Bartlett and Eaton, 2004). The acetyl-CoA can enter the tricarboxylic acid (TCA) cycle and the electron carriers deliver electrons to the mitochondrial electron transport chain, thereby sustaining cellular energy demands (Houten and Wanders, 2010). In the prevention model, HPβCD-HP5 robustly increased FGF21 levels in males, with HPβCD-HP7 showing only a moderate induction. However, these elevations did not correlate with increased expression of lipolytic markers like ATGL. Conversely, in the regression model, HPβCD-HP5 did not elevate FGF21 or induce detectable morphological changes in adipocytes, yet did increase ATGL expression. The morphological change was likely not observed, because switching from a WD to SC alone was sufficient to restore normal adipocyte sizes, potentially masking moderate HPβCD effects. Because the two experiments substantially differed in feeding duration (8 vs. 12 weeks) and dietary scheme (continuous WD vs. WD followed by SC), their metabolic contexts are not directly comparable. Nevertheless, our collective findings do **not** support the hypothesis that FGF21 is a primary driver of the observed lipolysis-related effects. This may not be as surprising, as the literature itself presents conflicting evidence regarding the role of FGF21 in lipolysis induction; whereas Hotta et al. (2009) and Inagaki et al. (2007) support the hypothesis, Arner et al. (2008) and Li et al. (2009) present opposing findings. Those discrepancies likely arise from differences in experimental systems (FGF21 transgenic mice, *Fgf21*$^{-/-}$ mice, ob/ob mice, 3T3-L1 adipocytes, and

human AT; *in vitro* vs *in vivo*), different lipolysis readouts (free fatty acids, free glycerol, mRNA levels of lipolytic enzymes, p-nitrophenyl laurate, total lipase activity assay) and different stimuli (fasting, ketogenic diet, FGF21 injection/stimulation). Importantly, the role of FGF21 in lipolysis has not yet been examined in *Apoe*$^{-/-}$ mice, likely because the profound lipid-metabolic alterations, inherent to this genotype, make it challenging to dissect additional regulatory effects.

4.3.2 Direct lipolytic effects of HPβCD and enhanced cholesterol mobilization

Our *ex vivo* lipolysis assay demonstrated a trend toward HPβCD-induced lipolysis within 2h, which suggests direct and rapid effect, rather than an indirect one that would require transcriptional or translational changes in lipolysis-supporting molecules such as FGF21. A direct inducer of lipolysis is norepinephrine, which acts via β-adrenergic signaling. Binding to its receptor, norepinephrine leads to a cascade of G-protein coupled receptor (GPCR) activation, increased levels of the second messenger cyclic adenosine monophosphate (cAMP), activation of the protein kinase A (PKA) and phosphorylation of HSL and perilipins, which open the droplet surface for lipases (Collins, 2012, 2025). So far, we have no evidence, that HPβCD induces lipolysis via this pathway. However, LXRα is an activator of *Atgl*, binding to an LXR response element within the promoter region (Y. Chen et al., 2023), and could likely induce lipolysis the oxysterol-LXR axis. Induction of the metabolization of cholesterol to oxysterols has been shown to be a mode of action of HPβCD (Zimmer et al., 2016). Oxysterols not only passively diffuse through the cell membrane, thereby reducing cholesterol content of the cell, but are also endogenous ligands of the LXR transcription factor, which targets genes involved in lipid and cholesterol metabolism, as well as inflammation. Induction of the LXR by HPβCD could hence indirectly activate lipolysis, although this rather applies for time periods above 2 h.

HPβCD is a potent cholesterol-scavenging molecule, raising the possibility that it actively facilitates cholesterol efflux from adipocytes, similar to what has been demonstrated for macrophages (Zimmer et al., 2016). Our *in vitro* adipogenesis assay primarily examined the differentiation of pre-adipocytes into mature adipocytes, but could be adapted to assess whether HPβCD reduces pre-existing lipid droplets rather than preventing their formation. Lipolysis markers could then be evaluated in cultured adipocytes using qPCR,

Wes™, or by incorporating fluorescently labeled antibodies into the microscopic analysis. In addition, cholesterol levels could be quantified in cells and in the supernatant, as HPβCD is as a sink for cholesterol (Atger et al., 1997; Kilsdonk et al., 1995), which is stored as cholesterol esters inside the lipid droplets.

We could also investigate whether lysosomal lipolysis contributes to HPβCD-mediated effects, since this pathway represents a noncanonical mode of lipid mobilization in adipocytes, particularly during fasting and cold exposure (Yeh et al., 2025). Lysosomal acid lipase (LAL) hydrolyzes triacylglycerol and cholesteryl esters that reach lysosomes either through receptor-mediated endocytosis (Goldstein et al., 1975) or via lipophagy, the autophagic degradation of intracellular lipid droplets (R. Singh et al., 2009). In atherosclerosis, foam cells rely on lysosomal lipolysis to convert stored cholesteryl esters into free cholesterol, which is subsequently exported through ABCA1 and ABCG1 (Ouimet et al., 2011). Inhibition of LAL prevents the accumulation of unesterified cholesterol in lysosomes of NPC-mutant cells (Rosenbaum et al., 2010). Moreover, in a murine NPC model, a single dose of HPβCD alleviated disease manifestations by promoting redistribution of lysosomal free cholesterol into the cytosol, where it was metabolized and excreted (B. Liu et al., 2009). This treatment also activated LXR target genes, including *Abcg1* and *Cyp7a1*, while reducing endogenous sterol synthesis. Together, these findings support the idea of HPβCD to similarly modulate lysosomal lipolysis in our atherosclerosis model.

4.3.3 No effect of HPβCD on adipocyte differentiation *in vitro*

Our *in vitro* adipogenesis experiments, HPβCD neither altered the development of lipid droplets, nor did it change adipocyte proliferation (equivalent to hyperplasia). However, for both HPβCD moieties a trend toward increased lipid droplet area was observed.
HPβCD-induced metabolization of cholesterol to oxysterols with subsequent LXR activation may potentially be a link to increased lipid droplet formation. Juvet et al. (2003) demonstrated augmented fat accumulation in murine 3T3-L1 cells and in human adipocytes following stimulation with an PPARγ agonist, which directly controlled the expression of LXRα.

However, the role of LXRα in adipocytes is ambiguous according to the literature. Ross et al. (2002) reported that LXRα activation suppresses adipocyte differentiation and reduces lipid accumulation in cultured preadipocytes, if inappropriately expressed and activated. Activation of LXRα increased basal glucose uptake and glycogen synthesis in 3T3-L1 adipocytes elevated cholesterol synthesis, and promoted the release of non-esterified fatty acids. In mice, LXRα agonists increased serum glycerol and fatty acid levels, indicating enhanced adipose tissue lipolysis. In accordance with this, Matsushita et al. (2016) showed that LXRα regulates adipocyte formation by acting as a negative regulator of adipogenesis in bone marrow-derived MSC. MSC, isolated from LXRα/β$^{-/-}$ mice, display enhanced lipid droplet accumulation and adipogenic gene expression, whereas LXRα overexpression *in vitro* suppresses adipocyte differentiation. Mechanistically, LXRα maintains Wnt/β-catenin signaling, a pathway that inhibits the adipogenic program.

These findings highlight a functional link between LXR signaling and adipogenesis and suggest that LXRα activation may contribute to white adipose tissue (WAT) remodeling in our atherosclerosis model, although the effects of HPβCD on MSC remain unclear. This could be explored further using our *in vitro* adipogenesis assay by assessing HPβCD-induced mRNA expression changes.

4.4 Implications of HPβCD-induced ATM reduction

A notable finding is the consistent reduction of ATM across both atherosclerosis models, especially by HPβCD-HP5 treatment. As ATM accumulate in obesity and are associated with the development of insulin resistance, macrophage reduction appeared as a beneficial aspect of HPβCD, especially of monocyte-derived TIM4^{-} CD11c^{+} cells. Nevertheless, the following questions remain: 1) How is this reduction mediated by HPβCD? 2) What is the impact on metabolic parameters? 3) Why is the effect sex-specific?

Regarding the first question, one must note that we did not measure cell counts, but only looked at population frequencies. Consequently, as macrophage frequencies declined, several other immune cell populations increased, which were excluded by the lineage gate, including T cells (CD3^{+}), B cells (CD19^{+}), neutrophils (Ly6G^{+}), NK cells (CD335^{+}),

and eosinophils ($CD170^+$)**.** In theory, we might therefore not look at a decrease of macrophages, but an increase of another immune cell population.

It should be noted that our gating strategy was based on CD11c and F4/80, which are not fully macrophage-specific and may also capture dendritic cells. However, gating on $F4/80^+$ cells likely enriches predominantly for macrophages, as dendritic cells typically show higher CD11c expression (Gautier et al., 2012). For increased specificity, future studies should incorporate additional macrophage markers such as MerTK and CD64 (Gautier et al., 2012).

Regarding the second question, we hypothesized that reduction of macrophages could alter the inflammatory milieu due to lower pro-inflammatory cytokine production, which could affect systemic metabolic effects like insulin resistance (Hotamisligil et al., 1993; Weisberg et al., 2006). However, our data do not show altered IL-6 and TNFα levels. In addition, insulin, leptin, and resistin were not changed; neither was adiponectin in the plasma, which was shown to be induced by methyl-β-cyclodextrin in 3T3-L1-derived adipocytes (Chiang et al., 2023). Further studies may include glucose and insulin tolerance tests to directly study the effects of HPβCD, although the *Apoe*$^{-/-}$ model might not be suitable, as these mice already perform better in glucose tolerance test, as compared to WT mice (Y. Zhang et al., 2023), which could mask the effect of HPβCD. Similar results are seen for *Ldlr*$^{-/-}$ mice (Ngai et al., 2010). The use of db/db mice, a model for T2D, could be used, if the focus was mainly on effects of HPβCD on hyperglycemia.

Ablation of $TIM4^+$ macrophages could be affecting lipid homeostasis, as $Lyve1^+$ $TIM4^+$ ATM express high levels of Abca1 and aid in the post-prandial cholesterol transport (Magalhaes et al., 2021). Blocking $TIM4^+$, or its lysosomal function with chloroquine, leads to inhibition of post-prandial HDL-C release. Notably, these cells do not express *Nr1h3* (gene name of LXRα), but rather *Klf4*, an endothelial cell transcription factor that induces *Abca1* transcription. Loss of these ATM could, in principle, disrupt cholesterol and lipoprotein handling within the gWAT. However, our data provide no evidence of impaired cholesterol metabolism; instead, systemic cholesterol levels were reduced, suggesting an overall improvement rather than dysregulation.

Regarding the third question, several studies report that high-fat diet induces a more pronounced macrophage infiltration into gWAT of male rather than female mice, with males showing more crown-like structures and pro-inflammatory ATM (K.-H. E. Chen et al., 2021; Lainez et al., 2018; Medrikova et al., 2012; Pettersson et al., 2012). Our finding of reduced macrophage infiltration is therefore in line with the literature. As we do not know the reason for macrophage reduction in males, it is difficult to speculate which effect prevents macrophage reduction in females. Generally, sex hormones, genetic differences (X chromosome dosage effects), and nervous signaling from the brain play a role in sex-dependent differences that shape the adipose tissue (Fuente-Martín et al., 2013).

4.5 The connection between HPβCD, FGF21, and atherosclerosis

FGF21 and its role in atherosclerosis and metabolic diseases have been extensively studied in the past years and several mechanisms of antiatherosclerotic effects have been suggested, predominantly in mice (Jin et al., 2016; Tan et al., 2023). Mechanistically, FGF21 mainly acts on the adipose tissue and liver, but not directly by targeting arterial walls. FGF21 signaling induces adiponectin, which improves endothelial dysfunction (Lin et al., 2015), and improved cholesterol metabolism. This was explained by reduced cholesterol synthesis through the inhibition of hepatic SREBP-2 (Lin et al., 2015), and via adipose tissue browning which accelerates clearance of cholesterol-rich lipoproteins (C. Liu et al., 2022). FGF21 also exerts cardioprotective effects by preventing cardiomyocyte injury and apoptosis through FGFR1/β-Klotho/Akt and adiponectin-dependent pathways (Joki et al., 2015; S. Q. Liu et al., 2013), and by reducing cardiac lipid accumulation in diabetic cardiomyopathy (Yan et al., 2015).

Clinical studies have reported mixed results regarding the role of FGF21 in ASCVD. FGF21 has been linked to cardiovascular risk, with several studies reporting that circulating FGF21 predicts adverse outcomes or incident coronary artery disease (CAD) in statin-treated patients and individuals with type 2 diabetes (Gan et al., 2020; Lee et al., 2017; Ong, Hui, et al., 2019). However, one multiethnic cohort did not confirm its predictive value in atherosclerosis patients without CVD (Ong, Campbell, et al., 2019). Nonetheless, evidence suggests that FGF21 may serve as a biomarker for CAD primary prevention, particularly in subclinical atherosclerosis, in patients without NAFLD or diabetes, and in

women without prior CVD (Basurto et al., 2019; J. S. Wang et al., 2017; L. Wu et al., 2020). Whether and how FGF21 induction causally contributes to the observed reduction in atherosclerosis in our model remains elusive, especially as we could not detect FGF21 in the plasma.

One plausible mechanism of HPβCD-induced FGF21 secretion involves endoplasmic reticulum (ER) stress. Cholesterol extraction from cellular membranes by HPβCD may disturb membrane homeostasis, triggering ER stress pathways that activate ATF4 (CREB-2), a transcriptional driver of *Fgf21* (Schaap et al., 2013; Wan et al., 2014). In the liver, *Fgf21* is also induced downstream of PPARα, which senses free fatty acids that are released upon lipolysis in the AT. Thus, both ER stress/ATF4 signaling and PPARα activation could converge on increased FGF21 expression following HPβCD treatment. However, the underlying mechanism of FGF21 upregulation through HPβCD could not be identified in this study, especially the much higher increase in the gWAT compared with the liver, the main source of FGF21.

4.6 Sex differences

Sex differences were frequently observed across our studies, including atherosclerosis reduction, alterations in ATM, FGF21 induction, and WAT remodeling. Intriguingly, we did not observe sex-dependent differences in baseline plaque size, which are usually reported to be larger in female mice (Man et al., 2020).

Preclinical studies examining sex as a biological variable in atherosclerosis are limited and require enhanced investigations, especially of the underlying mechanisms (Man et al., 2020). Nonetheless, we can speculate on several factors that may contribute to the divergent responses in our models. First, genetic differences linked to sex chromosomes, including X-linked gene dosage, shape metabolic responses, e.g. differences in weight gain upon WD feeding (Link et al., 2013; Reue, 2017; Wiese et al., 2023). It could be that a relatively high weight gain is necessary for treatment success. Second, the different steroid sex hormones, could be interfering with HPβCD-function, as they are derived from cholesterol (Miller and Auchus, 2011) and are bound by HPβCD, with preference to testosterone over estradiol (Albers and Müller, 1992; Schwarz et al., 2017). However, as

cholesterol is much more abundant, a scavenging of these steroids is rather limited. Depletion of cholesterol from the plasma membrane through HPβCD, however, reduces steroid synthesis (Deng et al., 2019). Third, sex-dependent pharmacodynamics or pharmacokinetics of HPβCD could further modulate tissue exposure and biological effects, although this might be less reasonable, as HPβCD is not metabolized, and excreted via glomerular filtration. Thus, its kinetics depend primarily on kidney function, which does not typically show strong sex differences in mice under normal conditions.

In humans, the plaques between men and women are different. Men rather display atheromatous plaques with a thin fibrous cap, which is prone to rupture, while women have smaller, fibrous plaques with thicker fibrous caps, high collagen and smooth muscle cell content (Sangiorgi et al., 2013; N. Singh et al., 2017; Vrijenhoek et al., 2013; Wendorff et al., 2015; Willem E. Hellings et al., 2007). These plaques are prone to erosion and thrombus formation on the plaque (Ralapanawa and Sivakanesan, 2021). A recent study reviewing genetic and epigenetic studies revealed 40 candidate genes that may explain, at least in part, sex differences in vascular remodeling, lipid metabolism and endothelial dysfunction. These potentially act through smooth muscle cells, endothelial cells, and potentially, macrophages (Sakkers et al., 2023). Aging also plays a role, as women develop an increased risk in advanced age compared to men (Hakamaa et al., 2024).

More research is required that also involves adequate representation of female participants in clinical trials (Tobb et al., 2022). In addition, socio-cultural/economic factors (gender) need to be addressed, to account for the complexity of human lifestyle. Even though premenopausal females appear protected from atherosclerosis by sex hormones and chromosomes, they face a higher risk of adverse outcomes due to late diagnosis and less guideline-directed treatment (Roeters van Lennep et al., 2025).

In conclusion, sex-dependent differences in human atherosclerosis are well documented, including variations in the age of disease onset and in plaque characteristics. Underlying mechanisms may partially be explained by X-chromosome dosage effects, which influence pathways relevant to atherosclerosis development such as lipid metabolism. Because sex-specific mechanisms in *Apoe*$^{-/-}$ mice are not well characterized, we can only speculate about the factors underlying the divergent responses to HPβCD treatment

observed in our study. A deeper understanding of HPβCD actions could clarify why we see differences in male and female mice, and what implications this could have for therapeutic use in men and women.

Notably, a sex-specific pattern has been reported in NPC mouse studies, where female *Npc1*$^{-/-}$ mice benefited more strongly from HPβCD therapy than males, e.g. in the prevention of weight loss and reduction of required anesthetics (Holzmann et al., 2021). The proposed explanation involves sex- and genotype-dependent differences in estradiol and testosterone, and a possible normalization of these hormones by HPβCD.

4.7 No reduced inflammation by HPβCD treatment

Across all *in vivo* experiments, we did not observe a reduction in inflammatory biomarkers; conversely, inflammation appeared to increase. This was evident in circulating cytokine profiles, *ex vivo* stimulated immune cells, bone marrow IL-1β expression, and liver as well as AT-derived cytokines. Despite significant plaque reductions, systemic inflammation did not decrease, which is in strong contrast to the findings of Zimmer et al. (2016). One explanation could be of technical nature: IL-6, IL-1β, and TNF-α were below detection limits in our Luminex assay, and more sensitive methods, such as Olink may be required. However, even in previous assays using the highly sensitive Olink platform we did not observe consistent anti-inflammatory effects either, suggesting this discrepancy may not be methodological alone.

The RNA-seq analysis of sorted GMP from HPβCD-HP7-treated *Ldlr*$^{-/-}$ mice showed an upregulation of *Hmox*, an indicator of homeostasis restoration, which in macrophages is upregulated by a plethora of stimuli (Vijayan et al., 2018). As such, HPβCD might be an inducer of oxidative stress, and could potentially increase pro-inflammatory signatures. In the same experiment, the ATAC-seq analysis showed that *Jun* was more accessible upon HPβCD-HP7 treatment. Interaction of Jun-c with the transcription factor PU.1 is critical for myeloid development (Zhao et al., 2022), and indicates a potential skewing toward myelopoiesis, also supporting the proinflammatory signature.

The literature provides some evidence suggesting that HPβCD may have inflammatory effects. Although HPβCD has shown less nephrotoxicity than the parental β-cyclodextrin,

a study by Scantlebery et al. (2019) found nephrotoxic effects, which are easily overlooked if the kidneys are not evaluated. This could potentially lead to systemic low-grade inflammation. Further, Houben et al. (2021) reported time and concentration-dependent pro-inflammatory effects of HPβCD *in vivo*, studying *Ldlr*$^{-/-}$ mice transplanted with bone marrow of *Npc1*$^{-/-}$ (*Npc1*^{nih}) mice, and *in vitro,* using human and murine macrophages (RAW, THP-1, and WT bone marrow-derived macrophages). This indicates the importance of the optimization of HPβCD dosage, balancing out the most antiatherosclerotic with the least pro-inflammatory effects. In addition, polymerization of HPβCD may reduce inflammation, as demonstrated in the context of NPC (Kulkarni et al., 2018; Tamura and Yui, 2018), and it may further allow for reduced dosage of HPβCD, because the polymer accumulates in the atherosclerotic plaque instead of the kidneys, which prevents fast elimination from the body (H. Kim et al., 2020).

4.8 Conclusion

Both HPβCD-HP5 and HPβCD-HP7 demonstrated prophylactic and therapeutic efficacy in male *Apoe*$^{-/-}$ mice, and the therapeutic (regression) model is particularly promising for translation to human disease, as lifestyle modifications - such as dietary improvement - are commonly recommended alongside pharmacological therapy. Although the underlying effects could not be conclusively resolved, our data indicate HPβCD-induced changes in the gWAT, while bone marrow HSPC populations remained largely unaltered.

Future studies should address several outstanding questions, including the origin and mechanisms underlying the subtle, but persistent proinflammatory signature observed with HPβCD treatment, the pathways through which HPβCD induces FGF21 and the relevance for the induction for atherosclerosis, and, importantly, the sex-dependent differences in treatment response.

Translating these findings into clinical application will require careful monitoring of FGF21 levels and inflammatory markers, particularly given the unresolved role of FGF21 in human atherosclerosis and the chronic low-grade inflammation in patients with established disease. Further investigation will be essential to fully evaluate the therapeutic potential and safety profile of HPβCD in human cardiovascular disease.

5. Abstract

The modern Western lifestyle offers many conveniences - sedentary routines, abundant processed food, and digital rather than in-person contact. The immune system has not yet adapted to these rapid socioeconomic changes. Evolution has shaped the immune system for pathogen defense, but was never optimized for sterile, lifestyle-related stimuli that fuel metaflammation, a chronic low-grade inflammatory condition in metabolic diseases. This inflammatory state accelerates non-communicable diseases (NCD), including atherosclerotic cardiovascular disease (ASCVD). Atherosclerosis is marked by cholesterol accumulation and immune cell infiltration in the arterial wall, and is profoundly shaped by metabolic and inflammatory imbalance.

Here, we set out to determine whether the known antiatherosclerotic effects of 2-hydroxypropyl-β-cyclodextrin (HPβCD), a cyclic oligosaccharide, can be explained through its effects on the white adipose tissue (WAT), a key site of metaflammation. We further aimed to investigate potential effects on the hematopoietic phenotype, specifically whether HPβCD counteracts Western diet (WD)-induced myeloid reprogramming in the bone marrow, with a particular focus on the monocytic progenitor lineage, which is known to enter both the adipose tissue and the arterial wall, thereby promoting inflammatory disease progression.

We used two derivates of HPβCD with different degree of substitution, HPβCD-HP5 and HPβCD-HP7, in the *Apoe*$^{-/-}$ atherosclerosis mouse model. The data show significant reduction in atherosclerotic plaque burden, accompanied with reduced cholesterol and increased oxysterol, in both a prevention and therapeutic setting. In the prevention study, both HPβCD increased FGF21 levels in gonadal WAT, reduced adipose tissue macrophages (ATM), and was associated with reduced adipocyte size. Interestingly, none of the HPβCD effects applied to female mice.

In summary, our study demonstrates that the investigated HPβCD derivatives modulate adipose tissue morphology, reduce ATM, and stimulate FGF21 secretion from gWAT in males. These findings offer new insight into how cyclodextrins may influence metabolic inflammation and may contribute to their atheroprotective effects.

6. List of figures

7. List of tables

8. References

Akivis, Y., Alkaissi, H., McFarlane, S. I., & Bukharovich, I. (2024). The Role of Triglycerides in Atherosclerosis: Recent Pathophysiologic Insights and Therapeutic Implications. *Current Cardiology Reviews*, *20*(2). https://doi.org/10.2174/011573403x272750240109052319

Albers, E., & Müller, B. W. (1992). Complexation of steroid hormones with cyclodextrin derivatives: Substituent effects of the guest molecule on solubility and stability in aqueous solution. *Journal of Pharmaceutical Sciences*, *81*(8), 756–761. https://doi.org/10.1002/jps.2600810808

Ambrosi, T. H., Scialdone, A., Graja, A., Gohlke, S., Jank, A. M., Bocian, C., Woelk, L., Fan, H., Logan, D. W., Schürmann, A., Saraiva, L. R., & Schulz, T. J. (2017). Adipocyte Accumulation in the Bone Marrow during Obesity and Aging Impairs Stem Cell-Based Hematopoietic and Bone Regeneration. *Cell Stem Cell*, *20*(6). https://doi.org/10.1016/j.stem.2017.02.009

Arner, P., Pettersson, A., Mitchell, P. J., Dunbar, J. D., Kharitonenkov, A., & Rydén, M. (2008). FGF21 attenuates lipolysis in human adipocytes - A possible link to improved insulin sensitivity. *FEBS Letters*, *582*(12), 1725–1730. https://doi.org/10.1016/j.febslet.2008.04.038

Arts, R. J. W., Novakovic, B., ter Horst, R., Carvalho, A., Bekkering, S., Lachmandas, E., Rodrigues, F., Silvestre, R., Cheng, S. C., Wang, S. Y., Habibi, E., Gonçalves, L. G., Mesquita, I., Cunha, C., van Laarhoven, A., van de Veerdonk, F. L., Williams, D. L., van der Meer, J. W. M., Logie, C., … Netea, M. G. (2016). Glutaminolysis and Fumarate Accumulation Integrate Immunometabolic and Epigenetic Programs in Trained Immunity. *Cell Metabolism*, *24*(6). https://doi.org/10.1016/j.cmet.2016.10.008

Ashland, Cavitron™ and Cavasol* hydroxypropyl-β-cyclodextrins, Product Overview, https://www.ashland.com/file_source/Ashland/Product/Documents/Pharmaceutical/PC_11734_Cavitron_Cavasol.pdf, created 08.10.2015, modified 23.02.2016, accessed on 24.11.25

Atger, V. M., De La, M., Moya, L., Stoudt, G. W., Rodrigueza, W. V, Phillips, M. C., & Rothblat, G. H. (1997). Cyclodextrins as Catalysts for the Removal of Cholesterol from Macrophage Foam Cells. In *J. Clin. Invest* (Vol. 99, Issue 4).

Bartlett, K., & Eaton, S. (2004). Mitochondrial β-oxidation. In *European Journal of Biochemistry* (Vol. 271, Issue 3, pp. 462–469). https://doi.org/10.1046/j.1432-1033.2003.03947.x

Basurto, L., Gregory, M. A., Hernández, S. B., Sánchez-Huerta, L., Martínez, A. D., Manuel-Apolinar, L., Avelar, F. J., Alonso, L. A. M., & Sánchez-Arenas, R. (2019). Monocyte chemoattractant protein-1 (MCP-1) and fibroblast growth factor-21 (FGF-21) as biomarkers of subclinical atherosclerosis in women. *Experimental Gerontology*, *124*. https://doi.org/10.1016/j.exger.2019.05.013

Bekkering, S., Arts, R. J. W., Novakovic, B., Kourtzelis, I., van der Heijden, C. D. C. C., Li, Y., Popa, C. D., ter Horst, R., van Tuijl, J., Netea-Maier, R. T., van de Veerdonk, F. L., Chavakis, T., Joosten, L. A. B., van der Meer, J. W. M., Stunnenberg, H., Riksen, N. P., & Netea, M. G. (2018). Metabolic Induction of Trained Immunity through the Mevalonate Pathway. *Cell*, *172*(1–2), 135-146.e9. https://doi.org/10.1016/j.cell.2017.11.025

Bekkering, S., Domínguez-Andrés, J., Joosten, L. A. B., Riksen, N. P., & Netea, M. G. (2021). *Trained Immunity: Reprogramming Innate Immunity in Health and Disease*. *41*. https://doi.org/10.1146/annurev-immunol-102119

Bekkering, S., Quintin, J., Joosten, L. A. B., Van Der Meer, J. W. M., Netea, M. G., & Riksen, N. P. (2014). Oxidized low-density lipoprotein induces long-term proinflammatory cytokine production and foam cell formation via epigenetic reprogramming of monocytes. *Arteriosclerosis, Thrombosis, and Vascular Biology*, *34*(8), 1731–1738. https://doi.org/10.1161/ATVBAHA.114.303887

Bhargavi, G., & Subbian, S. (2024). The causes and consequences of trained immunity in myeloid cells. In *Frontiers in Immunology* (Vol. 15). Frontiers Media SA. https://doi.org/10.3389/fimmu.2024.1365127

Blaszczak, A. M., Bernier, M., Wright, V. P., Gebhardt, G., Anandani, K., Liu, J., Jalilvand, A., Bergin, S., Wysocki, V., Somogyi, A., Bradley, D., & Hsueh, W. A. (2020). Obesogenic Memory Maintains Adipose Tissue Inflammation and Insulin Resistance. *Immunometabolism (United States)*, *2*(3). https://doi.org/10.20900/immunometab20200023

Boring, L., Gosling, J., Cleary, M., & Charo, I. (1998). *Decreased lesion formation in CCR2-/- mice reveals a rolefor chemokines in the initiation of atherosclerosis*.

Buenrostro, J. D., Giresi, P. G., Zaba, L. C., Chang, H. Y., & Greenleaf, W. J. (2013). Transposition of native chromatin for fast and sensitive epigenomic profiling of open chromatin, DNA-binding proteins and nucleosome position. *Nature Methods*, *10*(12), 1213–1218. https://doi.org/10.1038/nmeth.2688

Burberry, A., Zeng, M. Y., Ding, L., Wicks, I., Inohara, N., Morrison, S. J., & Núñez, G. (2014). Infection mobilizes hematopoietic stem cells through cooperative NOD-like receptor and toll-like receptor signaling. *Cell Host and Microbe*, *15*(6), 779–791. https://doi.org/10.1016/j.chom.2014.05.004

Cave, E., & Crowther, N. J. (2019). The Use of 3T3-L1 Murine Preadipocytes as a Model of Adipogenesis. In *Methods in Molecular Biology* (Vol. 1916, pp. 263–272). Humana Press Inc. https://doi.org/10.1007/978-1-4939-8994-2_25

Cawthorn, W. P., Scheller, E. L., & MacDougald, O. A. (2012). Adipose tissue stem cells meet preadipocyte commitment: Going back to the future. In *Journal of Lipid Research* (Vol. 53, Issue 2, pp. 227–246). https://doi.org/10.1194/jlr.R021089

Challa, R., Ahuja, A., Ali, J., & Khar, R. K. (2005). *Cyclodextrins in Drug Delivery: An Updated Review*. http://www.aapspharmscitech.org

Chavakis, T., Mitroulis, I., & Hajishengallis, G. (2019). Hematopoietic progenitor cells as integrative hubs for adaptation to and fine-tuning of inflammation. In *Nature Immunology* (Vol. 20, Issue 7, pp. 802–811). Nature Publishing Group. https://doi.org/10.1038/s41590-019-0402-5

Chen, K.-H. E., Lainez, N. M., & Coss, D. (2021). Sex Differences in Macrophage Responses to Obesity-Mediated Changes Determine Migratory and Inflammatory Traits. *The Journal of Immunology*, *206*(1), 141–153. https://doi.org/10.4049/jimmunol.2000490

Chen, Y., Jiang, H., Zhan, Z., Lu, J., Gu, T., Yu, P., Liang, W., Zhang, X., Liu, S., Bi, H., Zhong, S., & Tang, L. (2023). Restoration of lipid homeostasis between TG and PE by the LXRα-ATGL/EPT1 axis ameliorates hepatosteatosis. *Cell Death and Disease*, *14*(2). https://doi.org/10.1038/s41419-023-05613-6

Chiang, Y. T., Wu, Y. Y., Lin, Y. C., Huang, Y. Y., & Lu, J. C. (2023). Cyclodextrin-Mediated Cholesterol Depletion Induces Adiponectin Secretion in 3T3-L1 Adipocytes. *International Journal of Molecular Sciences*, *24*(19). https://doi.org/10.3390/ijms241914718

Choi, J., Baldwin, T. M., Wong, M., Bolden, J. E., Fairfax, K. A., Lucas, E. C., Cole, R., Biben, C., Morgan, C., Ramsay, K. A., Ng, A. P., Kauppi, M., Corcoran, L. M., Shi, W., Wilson, N., Wilson, M. J., Alexander, W. S., Hilton, D. J., & De Graaf, C. A. (2019). Haemopedia RNA-seq: A database of gene expression during haematopoiesis in mice and humans. *Nucleic Acids Research*, *47*(D1), D780–D785. https://doi.org/10.1093/nar/gky1020

Christ, A., Günther, P., Lauterbach, M. A. R., Duewell, P., Biswas, D., Pelka, K., Scholz, C. J., Oosting, M., Haendler, K., Baßler, K., Klee, K., Schulte-Schrepping, J., Ulas, T., Moorlag, S. J. C. F. M., Kumar, V., Park, M. H., Joosten, L. A. B., Groh, L. A., Riksen, N. P., … Latz, E. (2018). Western Diet Triggers NLRP3-Dependent Innate Immune Reprogramming. *Cell*, *172*(1–2). https://doi.org/10.1016/j.cell.2017.12.013

Coats, B. R., Schoenfelt, K. Q., Barbosa-Lorenzi, V. C., Peris, E., Cui, C., Hoffman, A., Zhou, G., Fernandez, S., Zhai, L., Hall, B. A., Haka, A. S., Shah, A. M., Reardon, C. A., Brady, M. J., Rhodes, C. J., Maxfield, F. R., & Becker, L. (2017). Metabolically Activated Adipose Tissue Macrophages Perform Detrimental and Beneficial

Functions during Diet-Induced Obesity. *Cell Reports*, *20*(13), 3149–3161. https://doi.org/10.1016/j.celrep.2017.08.096

Collins, S. (2012). β-Adrenoceptor signaling networks in adipocytes for recruiting stored fat and energy expenditure. In *Frontiers in Endocrinology* (Vol. 3, Issue JAN). https://doi.org/10.3389/fendo.2011.00102

Collins, S. (2025). β-Adrenergic Receptors and Adipose Tissue Metabolism: Evolution of an Old Story. *Annual Review of Physiology Downloaded from Www.Annualreviews.Org. Guest*, *46*, 42. https://doi.org/10.1146/annurev-physiol-060721

Cox, N., Crozet, L., Holtman, I. R., Loyher, P. L., Lazarov, T., White, J. B., Mass, E., Stanley, E. R., Elemento, O., Glass, C. K., & Geissmann, F. (2021). Diet-regulated production of PDGFcc by macrophages controls energy storage. *Science*, *373*(6550). https://doi.org/10.1126/science.abe9383

Cronstein, B. N., Molad, Y., Reibman, J., Balakhane, E., Levin, R. 1, & Weissmann, G. (1996). *Colchicine Alters the Quantitative and Qualitative Display of Selectins on Endothelial Cells and Neutrophils Key words: E-selectin * L-selectin * integrins *-microtubules * tumor necrosis factor a * interleukin-1*.

Dalbeth, N., Lauterio, T. J., & Wolfe, H. R. (2014). Mechanism of action of colchicine in the treatment of gout. In *Clinical Therapeutics* (Vol. 36, Issue 10, pp. 1465–1479). Excerpta Medica Inc. https://doi.org/10.1016/j.clinthera.2014.07.017

Davis, M. E., & Brewster, M. E. (2004). Cyclodextrin-based pharmaceutics: Past, present and future. In *Nature Reviews Drug Discovery* (Vol. 3, Issue 12). https://doi.org/10.1038/nrd1576

de Moura e Dias, M., dos Reis, S. A., da Conceição, L. L., Sediyama, C. M. N. de O., Pereira, S. S., de Oliveira, L. L., Gouveia Peluzio, M. do C., Martinez, J. A., & Milagro, F. I. (2021). Diet-induced obesity in animal models: points to consider and influence on metabolic markers. In *Diabetology and Metabolic Syndrome* (Vol. 13, Issue 1). BioMed Central Ltd. https://doi.org/10.1186/s13098-021-00647-2

Demel, U. M., Lutz, R., Sujer, S., Demerdash, Y., Sood, S., Grunschlager, F., Kuck, A., Werner, P., Blaszkiewicz, S., Uckelmann, H. J., Haas, S., & Essers, M. A. G. (2022). A complex proinflammatory cascade mediates the activation of HSCs upon LPS

exposure in vivo. *Blood Advances*, *6*(11), 3513–3528. https://doi.org/10.1182/bloodadvances.2021006088

Del Valle, E. M. M. (2004). Cyclodextrins and their uses: A review. In *Process Biochemistry* (Vol. 39, Issue 9, pp. 1033–1046). https://doi.org/10.1016/S0032-9592(03)00258-9

Deng, B., Shen, W. J., Dong, D., Azhar, S., & Kraemer, F. B. (2019). Plasma membrane cholesterol trafficking in steroidogenesis. *FASEB Journal*, *33*(1). https://doi.org/10.1096/fj.201800697RRR

Díez-Díez, M., Ramos-Neble, B. L., de la Barrera, J., Silla-Castro, J. C., Quintas, A., Vázquez, E., Rey-Martín, M. A., Izzi, B., Sánchez-García, L., García-Lunar, I., Mendieta, G., Mass, V., Gómez-López, N., Espadas, C., González, G., Quesada, A. J., García-Álvarez, A., Fernández-Ortiz, A., Lara-Pezzi, E., … Fuster, J. J. (2024). Unidirectional association of clonal hematopoiesis with atherosclerosis development. *Nature Medicine*. https://doi.org/10.1038/s41591-024-03213-1

Ding, J., Wang, K., Liu, W., She, Y., Sun, Q., Shi, J., Sun, H., Wang, D. C., & Shao, F. (2016). Pore-forming activity and structural autoinhibition of the gasdermin family. *Nature*, *535*(7610), 111–116. https://doi.org/10.1038/nature18590

Dong, Z., Hou, L., Luo, W., Pan, L. H., Li, X., Tan, H. P., Wu, R. Da, Lu, H., Yao, K., Mu, M. Di, Gao, C. S., Weng, X. Y., & Ge, J. B. (2024). Myocardial infarction drives trained immunity of monocytes, accelerating atherosclerosis. *European Heart Journal*, *45*(9). https://doi.org/10.1093/eurheartj/ehad787

Dos Santos, A. R. de O., Zanuso, B. de O., Miola, V. F. B., Barbalho, S. M., Santos Bueno, P. C., Flato, U. A. P., Detregiachi, C. R. P., Buchaim, D. V., Buchaim, R. L., Tofano, R. J., Mendes, C. G., Tofano, V. A. C., & Dos Santos Haber, J. F. (2021). Adipokines, myokines, and hepatokines: Crosstalk and metabolic repercussions. In *International Journal of Molecular Sciences* (Vol. 22, Issue 5, pp. 1–23). MDPI AG. https://doi.org/10.3390/ijms22052639

Drucker, D. J. (2016). The Cardiovascular Biology of Glucagon-like Peptide-1. In *Cell Metabolism* (Vol. 24, Issue 1, pp. 15–30). Cell Press. https://doi.org/10.1016/j.cmet.2016.06.009

Duewell, P., Kono, H., Rayner, K. J., Sirois, C. M., Vladimer, G., Bauernfeind, F. G., Abela, G. S., Franchi, L., Nũez, G., Schnurr, M., Espevik, T., Lien, E., Fitzgerald, K. A., Rock,

K. L., Moore, K. J., Wright, S. D., Hornung, V., & Latz, E. (2010). NLRP3 inflammasomes are required for atherogenesis and activated by cholesterol crystals. *Nature*, *464*(7293), 1357–1361. https://doi.org/10.1038/nature08938

Durinck, S., Moreau, Y., Kasprzyk, A., Davis, S., De Moor, B., Brazma, A., & Huber, W. (2005). BioMart and Bioconductor: A powerful link between biological databases and microarray data analysis. *Bioinformatics*, *21*(16), 3439–3440. https://doi.org/10.1093/bioinformatics/bti525

Durinck, S., Spellman, P. T., Birney, E., & Huber, W. (2009). Mapping identifiers for the integration of genomic datasets with the R/ Bioconductor package biomaRt. *Nature Protocols*, *4*(8), 1184–1191. https://doi.org/10.1038/nprot.2009.97

Dykstra, B., Olthof, S., Schreuder, J., Ritsema, M., & Haan, G. De. (2011). Clonal analysis reveals multiple functional defects of aged murine hematopoietic stem cells. *Journal of Experimental Medicine*, *208*(13), 2691–2703. https://doi.org/10.1084/jem.20111490

Emini Veseli, B., Perrotta, P., De Meyer, G. R. A., Roth, L., Van der Donckt, C., Martinet, W., & De Meyer, G. R. Y. (2017a). Animal models of atherosclerosis. *European Journal of Pharmacology*, *816*, 3–13. https://doi.org/10.1016/j.ejphar.2017.05.010

Emini Veseli, B., Perrotta, P., De Meyer, G. R. A., Roth, L., Van der Donckt, C., Martinet, W., & De Meyer, G. R. Y. (2017b). Animal models of atherosclerosis. *European Journal of Pharmacology*, *816*. https://doi.org/10.1016/j.ejphar.2017.05.010

Essers, M. A. G., Offner, S., Blanco-Bose, W. E., Waibler, Z., Kalinke, U., Duchosal, M. A., & Trumpp, A. (2009). IFNα activates dormant haematopoietic stem cells in vivo. *Nature*, *458*(7240), 904–908. https://doi.org/10.1038/nature07815

Félix, I., Jokela, H., Karhula, J., Kotaja, N., Savontaus, E., Salmi, M., & Rantakari, P. (2021). Single-Cell Proteomics Reveals the Defined Heterogeneity of Resident Macrophages in White Adipose Tissue. *Frontiers in Immunology*, *12*. https://doi.org/10.3389/fimmu.2021.719979

Ferreira, A. V., Domínguez-Andrés, J., Merlo Pich, L. M., Joosten, L. A. B., & Netea, M. G. (2024). Metabolic Regulation in the Induction of Trained Immunity. *Seminars in Immunopathology*, *46*(3–4), 7. https://doi.org/10.1007/s00281-024-01015-8

Feuerer, M., Herrero, L., Cipolletta, D., Naaz, A., Wong, J., Nayer, A., Lee, J., Goldfine, A. B., Benoist, C., Shoelson, S., & Mathis, D. (2009). Lean, but not obese, fat is

enriched for a unique population of regulatory T cells that affect metabolic parameters. *Nature Medicine*, *15*(8), 930–939. https://doi.org/10.1038/nm.2002

Flippo, K. H., & Potthoff, M. J. (2021). Metabolic Messengers: FGF21. In *Nature Metabolism* (Vol. 3, Issue 3, pp. 309–317). Nature Research. https://doi.org/10.1038/s42255-021-00354-2

Fuente-Martín, E., Argente-Arizón, P., Ros, P., Argente, J., & Chowen, J. A. (2013). Sex differences in adipose tissue. *Adipocyte*, *2*(3), 128–134. https://doi.org/10.4161/adip.24075

Fuster, J. J., MacLauchlan, S., Zuriaga, M. A., Polackal, M. N., Ostriker, A. C., Chakraborty, R., Wu, C. L., Sano, S., Muralidharan, S., Rius, C., Vuong, J., Jacob, S., Muralidhar, V., Robertson, A. A. B., Cooper, M. A., Andrés, V., Hirschi, K. K., Martin, K. A., & Walsh, K. (2017). Clonal hematopoiesis associated with TET2 deficiency accelerates atherosclerosis development in mice. *Science*, *355*(6327), 842–847. https://doi.org/10.1126/science.aag1381

Gan, F., Huang, J., Dai, T., Li, M., & Liu, J. (2020). Serum level of fibroblast growth factor 21 predicts long-term prognosis in patients with both diabetes mellitus and coronary artery calcification. *Annals of Cardiothoracic Surgery*, *9*(2), 368–374. https://doi.org/10.21037/apm.2020.03.28

Ganjali Koli, M., & Fogolari, F. (2023). Exploring the role of cyclodextrins as a cholesterol scavenger: a molecular dynamics investigation of conformational changes and thermodynamics. *Scientific Reports*, *13*(1). https://doi.org/10.1038/s41598-023-49217-8

Gautiar, E. L., Shay, T., Miller, J., Greter, M., Jakubzick, C., Ivanov, S., Helft, J., Chow, A., Elpek, K. G., Gordonov, S., Mazloom, A. R., Ma'Ayan, A., Chua, W. J., Hansen, T. H., Turley, S. J., Merad, M., Randolph, G. J., Best, A. J., Knell, J., … Benoist, C. (2012). Gene-expression profiles and transcriptional regulatory pathways that underlie the identity and diversity of mouse tissue macrophages. *Nature Immunology*, *13*(11), 1118–1128. https://doi.org/10.1038/ni.2419

Gautier, E. L., Shay, T., Miller, J., Greter, M., Jakubzick, C., Ivanov, S., Helft, J., Chow, A., Elpek, K. G., Gordonov, S., Mazloom, A. R., Ma'Ayan, A., Chua, W. J., Hansen, T. H., Turley, S. J., Merad, M., Randolph, G. J., Best, A. J., Knell, J., … Benoist, C. (2012). Gene-expression profiles and transcriptional regulatory pathways that

underlie the identity and diversity of mouse tissue macrophages. *Nature Immunology*, *13*(11), 1118–1128. https://doi.org/10.1038/ni.2419

Gekas, C., & Graf, T. (2013). *CD41 expression marks myeloid-biased adult hematopoietic stem cells and increases with age Key Points*. https://doi.org/10.1182/blood-2012-09

Genovese, G., Kähler, A. K., Handsaker, R. E., Lindberg, J., Rose, S. A., Bakhoum, S. F., Chambert, K., Mick, E., Neale, B. M., Fromer, M., Purcell, S. M., Svantesson, O., Landén, M., Höglund, M., Lehmann, S., Gabriel, S. B., Moran, J. L., Lander, E. S., Sullivan, P. F., … McCarroll, S. A. (2014). Clonal Hematopoiesis and Blood-Cancer Risk Inferred from Blood DNA Sequence. *New England Journal of Medicine*, *371*(26), 2477–2487. https://doi.org/10.1056/nejmoa1409405

Gerdes, J., Lemke, H., Baisch, H., Wacker, H. H., Schwab, U., & Stein, H. (1984). Cell cycle analysis of a cell proliferation-associated human nuclear antigen defined by the monoclonal antibody Ki-67. *The Journal of Immunology*, *133*(4). https://doi.org/10.4049/jimmunol.133.4.1710

Ghaben, A. L., & Scherer, P. E. (2019). Adipogenesis and metabolic health. In *Nature Reviews Molecular Cell Biology* (Vol. 20, Issue 4, pp. 242–258). Nature Publishing Group. https://doi.org/10.1038/s41580-018-0093-z

Gisterå, A., Ketelhuth, D. F. J., Malin, S. G., & Hansson, G. K. (2022). Animal Models of Atherosclerosis–Supportive Notes and Tricks of the Trade. *Circulation Research*, *130*(12), 1869–1887. https://doi.org/10.1161/circresaha.122.320263

Goldstein, J. L., Dana, S. E., Faust, J. R., Beaudet, A. L., & Brown, M. S. (1975). Role of lysosomal acid lipase in the metabolism of plasma low density lipoprotein. Observations in cultured fibroblasts from a patient with cholesteryl ester storage disease. *Journal of Biological Chemistry*, *250*(21), 8487–8495. https://doi.org/10.1016/s0021-9258(19)40786-2

Gomez, D. F., Bekkering, S., Horst, R. ter, Cossins, B., van den Munckhof, I. C. L., Rutten, J. H. W., Joosten, L. A. B., Netea, M. G., & Riksen, N. P. (2024). The effect of leptin on trained innate immunity and on systemic inflammation in subjects with obesity. *Journal of Leukocyte Biology*, *115*(2), 374–384. https://doi.org/10.1093/jleuko/qiad118

Gong, J. S., Kobayashi, M., Hayashi, H., Zou, K., Sawamura, N., Fujita, S. C., Yanagisawa, K., & Michikawa, M. (2002). Apolipoprotein E (ApoE) isoform-

dependent lipid release from astrocytes prepared from human ApoE3 and ApoE4 knock-in mice. *The Journal of Biological Chemistry*, *277*(33), 29919–29926. https://doi.org/10.1074/jbc.M203934200

Gould, S., & Scott, R. C. (2005). 2-Hydroxypropyl-β-cyclodextrin (HP-β-CD): A toxicology review. In *Food and Chemical Toxicology* (Vol. 43, Issue 10). https://doi.org/10.1016/j.fct.2005.03.007

Greenbaum, A., Hsu, Y. M. S., Day, R. B., Schuettpelz, L. G., Christopher, M. J., Borgerding, J. N., Nagasawa, T., & Link, D. C. (2013). CXCL12 in early mesenchymal progenitors is required for haematopoietic stem-cell maintenance. *Nature*, *495*(7440), 227–230. https://doi.org/10.1038/nature11926

Griffiths, W. J., & Wang, Y. (2020). Oxysterols as lipid mediators: Their biosynthetic genes, enzymes and metabolites. In *Prostaglandins and Other Lipid Mediators* (Vol. 147). Elsevier Inc. https://doi.org/10.1016/j.prostaglandins.2019.106381

Groenen, A. G., Halmos, B., Tall, A. R., & Westerterp, M. (2021). Cholesterol efflux pathways, inflammation, and atherosclerosis. In *Critical Reviews in Biochemistry and Molecular Biology* (Vol. 56, Issue 4, pp. 426–439). Taylor and Francis Ltd. https://doi.org/10.1080/10409238.2021.1925217

Gumuser, E. D., Schuermans, A., Cho, S. M. J., Sporn, Z. A., Uddin, M. M., Paruchuri, K., Nakao, T., Yu, Z., Haidermota, S., Hornsby, W., Weeks, L. D., Niroula, A., Jaiswal, S., Libby, P., Ebert, B. L., Bick, A. G., Natarajan, P., & Honigberg, M. C. (2023). Clonal Hematopoiesis of Indeterminate Potential Predicts Adverse Outcomes in Patients With Atherosclerotic Cardiovascular Disease. *Journal of the American College of Cardiology*, *81*(20), 1996–2009. https://doi.org/10.1016/j.jacc.2023.03.401

Haczeyni, F., Bell-Anderson, K. S., & Farrell, G. C. (2018). Causes and mechanisms of adipocyte enlargement and adipose expansion. In *Obesity Reviews* (Vol. 19, Issue 3, pp. 406–420). Blackwell Publishing Ltd. https://doi.org/10.1111/obr.12646

Hakamaa, E., Goebeler, S., Martiskainen, M., Louhelainen, A. M., Ahinko, K., Lehtimäki, T., & Karhunen, P. (2024). Sex differences in coronary atherosclerosis during the pre- and postmenopausal period: The Tampere Sudden Death Study. *Atherosclerosis*, *390*. https://doi.org/10.1016/j.atherosclerosis.2024.117459

Han, J., Lee, J. E., Jin, J., Lim, J. S., Oh, N., Kim, K., Chang, S. I., Shibuya, M., Kim, H., & Koh, G. Y. (2011). The spatiotemporal development of adipose tissue. *Development*, *138*(22), 5027–5037. https://doi.org/10.1242/dev.067686

Hansson, G. K., & Libby, P. (2006). The immune response in atherosclerosis: A double-edged sword. In *Nature Reviews Immunology* (Vol. 6, Issue 7, pp. 508–519). https://doi.org/10.1038/nri1882

Hildebrand, S., & Pfeifer, A. (2025). The obesity pandemic and its impact on non-communicable disease burden. In *Pflugers Archiv European Journal of Physiology* (Vol. 477, Issue 5, pp. 657–668). Springer Science and Business Media Deutschland GmbH. https://doi.org/10.1007/s00424-025-03066-8

Hilgendorf, I., Swirski, F. K., & Robbins, C. S. (2015). Monocyte fate in atherosclerosis. *Arteriosclerosis, Thrombosis, and Vascular Biology*, *35*(2), 272–279. https://doi.org/10.1161/ATVBAHA.114.303565

Hilgendorf, K. I., Johnson, C. T., Mezger, A., Rice, S. L., Norris, A. M., Demeter, J., Greenleaf, W. J., Reiter, J. F., Kopinke, D., & Jackson, P. K. (2019). Omega-3 Fatty Acids Activate Ciliary FFAR4 to Control Adipogenesis. *Cell*, *179*(6), 1289-1305.e21. https://doi.org/10.1016/j.cell.2019.11.005

Holzmann, C., Witt, M., Rolfs, A., Antipova, V., & Wree, A. (2021). Gender-specific effects of two treatment strategies in a mouse model of niemann-pick disease type c1. *International Journal of Molecular Sciences*, *22*(5), 1–32. https://doi.org/10.3390/ijms22052539

Horwitz, A., & Birk, R. (2023). Adipose Tissue Hyperplasia and Hypertrophy in Common and Syndromic Obesity—The Case of BBS Obesity. In *Nutrients* (Vol. 15, Issue 15). https://doi.org/10.3390/nu15153445

Hotamisligil, G. S. (2017). Inflammation, metaflammation and immunometabolic disorders. In *Nature* (Vol. 542, Issue 7640). https://doi.org/10.1038/nature21363

Hotamisligil, G. S., Shargill, N. S., & Spiegelman, B. M. (1993). Adipose Expression of Tumor Necrosis Factor-α: Direct Role in Obesity-Linked Insulin. In *New Series* (Vol. 259, Issue 5091).

Hotta, Y., Nakamura, H., Konishi, M., Murata, Y., Takagi, H., Matsumura, S., Inoue, K., Fushiki, T., & Itoh, N. (2009). Fibroblast growth factor 21 regulates lipolysis in white

adipose tissue but is not required for ketogenesis and triglyceride clearance in liver. *Endocrinology*, *150*(10), 4625–4633. https://doi.org/10.1210/en.2009-0119

Houten, S. M., & Wanders, R. J. A. (2010). A general introduction to the biochemistry of mitochondrial fatty acid β-oxidation. In *Journal of Inherited Metabolic Disease* (Vol. 33, Issue 5, pp. 469–477). https://doi.org/10.1007/s10545-010-9061-2

Huh, J. Y., & Kim, J. B. (2021). TIM4+ adipose tissue-resident macrophages: new modulators of adiposity. *Nature Reviews Endocrinology*, *17*(11), 645–646. https://doi.org/10.1038/s41574-021-00554-6

Inagaki, T., Dutchak, P., Zhao, G., Ding, X., Gautron, L., Parameswara, V., Li, Y., Goetz, R., Mohammadi, M., Esser, V., Elmquist, J. K., Gerard, R. D., Burgess, S. C., Hammer, R. E., Mangelsdorf, D. J., & Kliewer, S. A. (2007). Endocrine Regulation of the Fasting Response by PPARα-Mediated Induction of Fibroblast Growth Factor 21. *Cell Metabolism*, *5*(6), 415–425. https://doi.org/10.1016/j.cmet.2007.05.003

Ishibashi, S., Brown, M. S., Goldstein, J. L., Gerard, R. D., Hammer, R. E., & Herz, J. (1993). *Hypercholesterolemia in Low Density Lipoprotein Receptor Knockout Mice and its Reversal by Adenovirus-mediated Gene Delivery*.

Ishibashi, S., Goldstein, J. L., Brown, M. S., Herz, J., & Burns, D. K. (1994). Massive xanthomatosis and atherosclerosis in cholesterol-fed low density lipoprotein receptor-negative mice. *Journal of Clinical Investigation*, *93*(5). https://doi.org/10.1172/JCI117179

Jais, A., & Brüning, J. C. (2017). Hypothalamic inflammation in obesity and metabolic disease. *Journal of Clinical Investigation*, *127*(1), 24–32. https://doi.org/10.1172/JCI88878

Jaiswal, S., & Ebert, B. L. (2019). Clonal hematopoiesis in human aging and disease. In *Science* (Vol. 366, Issue 6465). American Association for the Advancement of Science. https://doi.org/10.1126/science.aan4673

Jaiswal, S., Fontanillas, P., Flannick, J., Manning, A., Grauman, P. V., Mar, B. G., Lindsley, R. C., Mermel, C. H., Burtt, N., Chavez, A., Higgins, J. M., Moltchanov, V., Kuo, F. C., Kluk, M. J., Henderson, B., Kinnunen, L., Koistinen, H. A., Ladenvall, C., Getz, G., … Ebert, B. L. (2014). Age-Related Clonal Hematopoiesis Associated with Adverse Outcomes. *New England Journal of Medicine*, *371*(26), 2488–2498. https://doi.org/10.1056/nejmoa1408617

Jin, L., Lin, Z., & Xu, A. (2016). Fibroblast growth factor 21 protects against atherosclerosis via fine-tuning the multiorgan crosstalk. In *Diabetes and Metabolism Journal* (Vol. 40, Issue 1, pp. 22–31). Korean Diabetes Association. https://doi.org/10.4093/dmj.2016.40.1.22

Johansson, A., Lin, D. S., Mercier, F. E., Yamashita, M., Divangahi, M., & Sieweke, M. H. (2023). Trained immunity and epigenetic memory in long-term self-renewing hematopoietic cells. In *Experimental Hematology* (Vol. 121, pp. 6–11). Elsevier Inc. https://doi.org/10.1016/j.exphem.2023.02.001

Joki, Y., Ohashi, K., Yuasa, D., Shibata, R., Ito, M., Matsuo, K., Kambara, T., Uemura, Y., Hayakawa, S., Hiramatsu-Ito, M., Kanemura, N., Ogawa, H., Daida, H., Murohara, T., & Ouchi, N. (2015). FGF21 attenuates pathological myocardial remodeling following myocardial infarction through the adiponectin-dependent mechanism. *Biochemical and Biophysical Research Communications*, *459*(1), 124–130. https://doi.org/10.1016/j.bbrc.2015.02.081

Juvet, L. K., Andresen, S. M., Schuster, G. U., Dalen, K. T., Tobin, K. A. R., Hollung, K., Haugen, F., Jacinto, S., Ulven, S. M., Bamberg, K., Gustafsson, J. Å., & Nebb, H. I. (2003). On the role of liver X receptors in lipid accumulation in adipocytes. *Molecular Endocrinology*, *17*(2), 172–182. https://doi.org/10.1210/me.2001-0210

Kappus, M. S., Murphy, A. J., Abramowicz, S., Ntonga, V., Welch, C. L., Tall, A. R., & Westerterp, M. (2014). Activation of liver X receptor decreases atherosclerosis in Ldlr mice in the absence of ATP-binding cassette transporters A1 and G1 in myeloid cells. *Arteriosclerosis, Thrombosis, and Vascular Biology*, *34*(2), 279–284. https://doi.org/10.1161/ATVBAHA.113.302781

Karl-Heinz Frömming, & József Szejtli. (1994). *Pharmacokinetics and Toxicology of Cyclodextrins 3.1. Enzymic Degradation of CDs*.

Kaufmann, E., Sanz, J., Dunn, J. L., Khan, N., Mendonça, L. E., Pacis, A., Tzelepis, F., Pernet, E., Dumaine, A., Grenier, J. C., Mailhot-Léonard, F., Ahmed, E., Belle, J., Besla, R., Mazer, B., King, I. L., Nijnik, A., Robbins, C. S., Barreiro, L. B., & Divangahi, M. (2018). BCG Educates Hematopoietic Stem Cells to Generate Protective Innate Immunity against Tuberculosis. *Cell*, *172*(1–2), 176-190.e19. https://doi.org/10.1016/j.cell.2017.12.031

Kawai, T., Autieri, M. V., & Scalia, R. (2021). Adipose tissue inflammation and metabolic dysfunction in obesity. *American Journal of Physiology - Cell Physiology*, *320*(3), C375–C391. https://doi.org/10.1152/ajpcell.00379.2020

Keating, S. T., Groh, L., Thiem, K., Bekkering, S., Li, Y., Matzaraki, V., van der Heijden, C. D. C. C., van Puffelen, J. H., Lachmandas, E., Jansen, T., Oosting, M., de Bree, L. C. J., Koeken, V. A. C. M., Moorlag, S. J. C. F. M., Mourits, V. P., van Diepen, J., Strienstra, R., Novakovic, B., Stunnenberg, H. G., … Riksen, N. P. (2020). Rewiring of glucose metabolism defines trained immunity induced by oxidized low-density lipoprotein. *Journal of Molecular Medicine*, *98*(6), 819–831. https://doi.org/10.1007/s00109-020-01915-w

Kilsdonk, E. P. C., Yancey, P. G., Stoudt, G. W., Bangerter, F. W., Johnson, W. J., Phillips, M. C., & Rothblat, G. H. (1995). Cellular cholesterol efflux mediated by cyclodextrins. *Journal of Biological Chemistry*, *270*(29), 17250–17256. https://doi.org/10.1074/jbc.270.29.17250

Kim, H., Han, J., & Park, J. H. (2020). Cyclodextrin polymer improves atherosclerosis therapy and reduces ototoxicity. *Journal of Controlled Release*, *319*. https://doi.org/10.1016/j.jconrel.2019.12.021

Kim, H. Y., & Lee, W. W. (2025). Trained immunity induced by DAMPs and LAMPs in chronic inflammatory diseases. In *Experimental and Molecular Medicine*. Springer Nature. https://doi.org/10.1038/s12276-025-01542-w

Kim, J., Chung, K., Choi, C., Beloor, J., Ullah, I., Kim, N., Lee, K. Y., Lee, S. K., & Kumar, P. (2016). Silencing CCR2 in Macrophages Alleviates Adipose Tissue Inflammation and the Associated Metabolic Syndrome in Dietary Obese Mice. *Molecular Therapy Nucleic Acids*, *5*, e280. https://doi.org/10.1038/mtna.2015.51

Kiran, S., Kumar, V., Murphy, E. A., Enos, R. T., & Singh, U. P. (2021). High Fat Diet-Induced CD8+ T Cells in Adipose Tissue Mediate Macrophages to Sustain Low-Grade Chronic Inflammation. *Frontiers in Immunology*, *12*. https://doi.org/10.3389/fimmu.2021.680944

Kleinnijenhuis, J., Van Crevel, R., & Netea, M. G. (2014). Trained immunity: Consequences for the heterologous effects of BCG vaccination. *Transactions of the Royal Society of Tropical Medicine and Hygiene*, *109*(1), 29–35. https://doi.org/10.1093/trstmh/tru168

Koelwyn, G. J., Newman, A. A. C., Afonso, M. S., van Solingen, C., Corr, E. M., Brown, E. J., Albers, K. B., Yamaguchi, N., Narke, D., Schlegel, M., Sharma, M., Shanley, L. C., Barrett, T. J., Rahman, K., Mezzano, V., Fisher, E. A., Park, D. S., Newman, J. D., Quail, D. F., … Moore, K. J. (2020). Myocardial infarction accelerates breast cancer via innate immune reprogramming. *Nature Medicine*, *26*(9), 1452–1458. https://doi.org/10.1038/s41591-020-0964-7

Kolb, H. (2022). Obese visceral fat tissue inflammation: from protective to detrimental? In *BMC Medicine* (Vol. 20, Issue 1). BioMed Central Ltd. https://doi.org/10.1186/s12916-022-02672-y

Kostallari, E., Schwabe, R. F., & Guillot, A. (2025). Inflammation and immunity in liver homeostasis and disease: a nexus of hepatocytes, nonparenchymal cells and immune cells. In *Cellular and Molecular Immunology*. Springer Nature. https://doi.org/10.1038/s41423-025-01313-7

Koyama, Y., & Brenner, D. A. (2017). Liver inflammation and fibrosis. In *Journal of Clinical Investigation* (Vol. 127, Issue 1, pp. 55–64). American Society for Clinical Investigation. https://doi.org/10.1172/JCI88881

Kratz, M., Coats, B. R., Hisert, K. B., Hagman, D., Mutskov, V., Peris, E., Schoenfelt, K. Q., Kuzma, J. N., Larson, I., Billing, P. S., Landerholm, R. W., Crouthamel, M., Gozal, D., Hwang, S., Singh, P. K., & Becker, L. (2014). Metabolic dysfunction drives a mechanistically distinct proinflammatory phenotype in adipose tissue macrophages. *Cell Metabolism*, *20*(4), 614–625. https://doi.org/10.1016/j.cmet.2014.08.010

Kulkarni, A., Caporali, P., Dolas, A., Johny, S., Goyal, S., Dragotto, J., Macone, A., Jayaraman, R., & Fiorenza, M. T. (2018). Linear Cyclodextrin Polymer Prodrugs as Novel Therapeutics for Niemann-Pick Type C1 Disorder. *Scientific Reports*, *8*(1). https://doi.org/10.1038/s41598-018-27926-9

Lainez, N. M., Jonak, C. R., Nair, M. G., Ethell, I. M., Wilson, E. H., Carson, M. J., & Coss, D. (2018). Diet-induced obesity elicits macrophage infiltration and reduction in spine density in the hypothalami of male but not female mice. *Frontiers in Immunology*, *9*(SEP). https://doi.org/10.3389/fimmu.2018.01992

Latz, E., Xiao, T. S., & Stutz, A. (2013). Activation and regulation of the inflammasomes. In *Nature Reviews Immunology* (Vol. 13, Issue 6, pp. 397–411). https://doi.org/10.1038/nri3452

Lavillegrand, J. R., Al-Rifai, R., Thietart, S., Guyon, T., Vandestienne, M., Cohen, R., Duval, V., Zhong, X., Yen, D., Ozturk, M., Negishi, Y., Konkel, J., Pinteaux, E., Lenoir, O., Vilar, J., Laurans, L., Esposito, B., Bredon, M., Sokol, H., … Ait-Oufella, H. (2024). Alternating high-fat diet enhances atherosclerosis by neutrophil reprogramming. *Nature*. https://doi.org/10.1038/s41586-024-07693-6

Law, C. W., Chen, Y., Shi, W., & Smyth, G. K. (2014). voom: precision weights unlock linear model analysis tools for RNA-seq read counts. In *Genome Biology* (Vol. 15). http://genomebiology.com/2014/15/2/R29

Lee, C. H., Woo, Y. C., Chow, W. S., Yan Cheung, C. Y., Yi Fong, C. H., Ann Yuen, M. M., Xu, A., Tse, H. F., & Lam, K. S. L. (2017). Role of circulating fibroblast growth factor 21 measurement in primary prevention of coronary heart disease among chinese patients with type 2 diabetes mellitus. *Journal of the American Heart Association*, *6*(6). https://doi.org/10.1161/JAHA.116.005344

Leung, Y. Y., Yao Hui, L. L., & Kraus, V. B. (2015). Colchicine-Update on mechanisms of action and therapeutic uses. In *Seminars in Arthritis and Rheumatism* (Vol. 45, Issue 3, pp. 341–350). W.B. Saunders. https://doi.org/10.1016/j.semarthrit.2015.06.013

Li, X., Ge, H., Weiszmann, J., Hecht, R., Li, Y. sheng, Véniant, M. M., Xu, J., Wu, X., Lindberg, R., & Li, Y. (2009). Inhibition of lipolysis may contribute to the acute regulation of plasma FFA and glucose by FGF21 in ob/ob mice. *FEBS Letters*, *583*(19), 3230–3234. https://doi.org/10.1016/j.febslet.2009.09.012

Li, X., Wang, H., Yu, X., Saha, G., Kalafati, L., Ioannidis, C., Mitroulis, I., Netea, M. G., Chavakis, T., & Hajishengallis, G. (2022). Maladaptive innate immune training of myelopoiesis links inflammatory comorbidities. *Cell*, *185*(10), 1709-1727.e18. https://doi.org/10.1016/j.cell.2022.03.043

Libby, P. (2021). The changing landscape of atherosclerosis. In *Nature* (Vol. 592, Issue 7855). https://doi.org/10.1038/s41586-021-03392-8

Libby, P., & Soehnlein, O. (2025). Inflammation in atherosclerosis: Lessons and therapeutic implications. *Immunity*. https://doi.org/10.1016/j.immuni.2025.09.012

Lin, Z., Pan, X., Wu, F., Ye, D., Zhang, Y., Wang, Y., Jin, L., Lian, Q., Huang, Y., Ding, H., Triggle, C., Wang, K., Li, X., & Xu, A. (2015). Fibroblast growth factor 21 prevents atherosclerosis by suppression of hepatic sterol regulatory element-binding protein-

2 and induction of adiponectin in mice. *Circulation*, *131*(21), 1861–1871. https://doi.org/10.1161/CIRCULATIONAHA.115.015308

Lincoff, A. M., Brown-Frandsen, K., Colhoun, H. M., Deanfield, J., Emerson, S. S., Esbjerg, S., Hardt-Lindberg, S., Hovingh, G. K., Kahn, S. E., Kushner, R. F., Lingvay, I., Oral, T. K., Michelsen, M. M., Plutzky, J., Tornøe, C. W., & Ryan, D. H. (2023). Semaglutide and Cardiovascular Outcomes in Obesity without Diabetes. *New England Journal of Medicine*, *389*(24), 2221–2232. https://doi.org/10.1056/nejmoa2307563

Link, J. C., Chen, X., Arnold, A. P., & Reue, K. (2013). Metabolic impact of sex chromosomes. *Adipocyte*, *2*(2), 74–79. https://doi.org/10.4161/adip.23320

Liu, B., Ramirez, C. M., Miller, A. M., Repa, J. J., Turley, S. D., & Dietschy, J. M. (2010). Cyclodextrin overcomes the transport defect in nearly every organ of NPC1 mice leading to excretion of sequestered cholesterol as bile acid. *Journal of Lipid Research*, *51*(5), 933–944. https://doi.org/10.1194/jlr.M000257

Liu, B., Turley, S. D., Burns, D. K., Miller, A. M., Repa, J. J., & Dietschy, J. M. (2009). *Reversal of defective lysosomal transport in NPC disease ameliorates liver dysfunction and neurodegeneration in the npc1 / mouse*. www.pnas.org/cgi/content/full/

Liu, C., Schönke, M., Zhou, E., Li, Z., Kooijman, S., Boon, M. R., Larsson, M., Wallenius, K., Dekker, N., Barlind, L., Peng, X. R., Wang, Y., & Rensen, P. C. N. (2022). Pharmacological treatment with FGF21 strongly improves plasma cholesterol metabolism to reduce atherosclerosis. *Cardiovascular Research*, *118*(2), 489–502. https://doi.org/10.1093/cvr/cvab076

Liu, S. M., Cogny, A., Kockx, M., Dean, R. T., Gaus, K., Jessup, W., & Kritharides, L. (2003). Cyclodextrins differentially mobilize free and esterified cholesterol from primary human foam cell macrophages. *Journal of Lipid Research*, *44*(6), 1156–1166. https://doi.org/10.1194/jlr.M200464-JLR200

Liu, S. Q., Roberts, D., Kharitonenkov, A., Zhang, B., Hanson, S. M., Li, Y. C., Zhang, L. Q., & Wu, Y. H. (2013). Endocrine protection of ischemic myocardium by FGF21 from the liver and adipose tissue. *Scientific Reports*, *3*. https://doi.org/10.1038/srep02767

Loftsson, T., & Brewster, M. E. (2010). Pharmaceutical applications of cyclodextrins: Basic science and product development. In *Journal of Pharmacy and Pharmacology* (Vol. 62, Issue 11). https://doi.org/10.1111/j.2042-7158.2010.01030.x

Lumeng, C. N., Bodzin, J. L., & Saltiel, A. R. (2007). Obesity induces a phenotypic switch in adipose tissue macrophage polarization. *Journal of Clinical Investigation*, *117*(1), 175–184. https://doi.org/10.1172/JCI29881

Lun A, Smyth G. 2024. *csaw: ChIP-Seq Analysis with Windows.* R package version 1.44.0. Bioconductor. doi:10.18129/B9.bioc.csaw

Magalhaes, M. S., Smith, P., Portman, J. R., Jackson-Jones, L. H., Bain, C. C., Ramachandran, P., Michalidou, Z., Stimson, R. H., Dweck, M. R., Denby, L., Henderson, N. C., Jenkins, S. J., & Bénézech, C. (2021). Role of Tim4 in the regulation of ABCA1+ adipose tissue macrophages and post-prandial cholesterol levels. *Nature Communications*, *12*(1). https://doi.org/10.1038/s41467-021-24684-7

Man, J. J., Beckman, J. A., & Jaffe, I. Z. (2020). Sex as a Biological Variable in Atherosclerosis. *Circulation Research*, *126*(9), 1297–1319. https://doi.org/10.1161/CIRCRESAHA.120.315930

Mann, M., Mehta, A., de Boer, C. G., Kowalczyk, M. S., Lee, K., Haldeman, P., Rogel, N., Knecht, A. R., Farouq, D., Regev, A., & Baltimore, D. (2018). Heterogeneous Responses of Hematopoietic Stem Cells to Inflammatory Stimuli Are Altered with Age. *Cell Reports*, *25*(11), 2992-3005.e5. https://doi.org/10.1016/j.celrep.2018.11.056

Manz, M. G., & Boettcher, S. (2014). Emergency granulopoiesis. In *Nature Reviews Immunology* (Vol. 14, Issue 5, pp. 302–314). Nature Publishing Group. https://doi.org/10.1038/nri3660

Marcovecchio, P. M., Thomas, G. D., Mikulski, Z., Ehinger, E., Müller, K. A. L., Blatchley, A., Wu, R., Miller, Y. I., Nguyen, A. T., Taylor, A. M., Mcnamara, C. A., Ley, K., & Hedrick, C. C. (2017). Scavenger receptor CD36 directs nonclassical monocyte patrolling along the endothelium during early atherogenesis HHS Public Access. *Arterioscler Thromb Vasc Biol*, *37*(11), 2043–2052. https://doi.org/10.1161/ATVBAHA

Martin, S. S., Aday, A. W., Allen, N. B., Almarzooq, Z. I., Anderson, C. A. M., Arora, P., Avery, C. L., Baker-Smith, C. M., Bansal, N., Beaton, A. Z., Commodore-Mensah, Y.,

Currie, M. E., Elkind, M. S. V., Fan, W., Generoso, G., Gibbs, B. B., Heard, D. G., Hiremath, S., Johansen, M. C., … Palaniappan, L. P. (2025). 2025 Heart Disease and Stroke Statistics: A Report of US and Global Data from the American Heart Association. *Circulation*, *151*(8), e41–e660. https://doi.org/10.1161/CIR.0000000000001303

Matencio, A., Navarro-Orcajada, S., González-Ramón, A., García-Carmona, F., & López-Nicolás, J. M. (2020). Recent advances in the treatment of Niemann pick disease type C: A mini-review. *International Journal of Pharmaceutics*, *584*. https://doi.org/10.1016/j.ijpharm.2020.119440

Matsushita, K., Morello, F., Zhang, Z., Masuda, T., Iwanaga, S., Steffensen, K. R., Gustafsson, J. Å., Pratt, R. E., & Dzau, V. J. (2016). Nuclear hormone receptor LXRα inhibits adipocyte differentiation of mesenchymal stem cells with Wnt/beta-catenin signaling. *Laboratory Investigation*, *96*(2), 230–238. https://doi.org/10.1038/labinvest.2015.141

Medrikova, D., Jilkova, Z. M., Bardova, K., Janovska, P., Rossmeisl, M., & Kopecky, J. (2012). Sex differences during the course of diet-induced obesity in mice: Adipose tissue expandability and glycemic control. *International Journal of Obesity*, *36*(2), 262–272. https://doi.org/10.1038/ijo.2011.87

Mendelson, A., & Frenette, P. S. (2014). Hematopoietic stem cell niche maintenance during homeostasis and regeneration. In *Nature Medicine* (Vol. 20, Issue 8, pp. 833–846). Nature Publishing Group. https://doi.org/10.1038/nm.3647

Miller, W. L., & Auchus, R. J. (2011). The molecular biology, biochemistry, and physiology of human steroidogenesis and its disorders. *Endocrine Reviews*, *32*(1). https://doi.org/10.1210/er.2010-0013

Mitchell, C. A., Verovskaya, E. V., Calero-Nieto, F. J., Olson, O. C., Swann, J. W., Wang, X., Hérault, A., Dellorusso, P. V., Zhang, S. Y., Svendsen, A. F., Pietras, E. M., Bakker, S. T., Ho, T. T., Göttgens, B., & Passegué, E. (2023). Stromal niche inflammation mediated by IL-1 signalling is a targetable driver of haematopoietic ageing. *Nature Cell Biology*, *25*(1), 30–41. https://doi.org/10.1038/s41556-022-01053-0

Mitroulis, I., Ruppova, K., Wang, B., Chen, L. S., Grzybek, M., Grinenko, T., Eugster, A., Troullinaki, M., Palladini, A., Kourtzelis, I., Chatzigeorgiou, A., Schlitzer, A., Beyer,

M., Joosten, L. A. B., Isermann, B., Lesche, M., Petzold, A., Simons, K., Henry, I., … Chavakis, T. (2018). Modulation of Myelopoiesis Progenitors Is an Integral Component of Trained Immunity. *Cell*, *172*(1–2). https://doi.org/10.1016/j.cell.2017.11.034

Morrison, S. J., & Scadden, D. T. (2014). The bone marrow niche for haematopoietic stem cells. In *Nature* (Vol. 505, Issue 7483, pp. 327–334). https://doi.org/10.1038/nature12984

Mossadegh-Keller, N., Sarrazin, S., Kandalla, P. K., Espinosa, L., Richard Stanley, E., Nutt, S. L., Moore, J., & Sieweke, M. H. (2013). M-CSF instructs myeloid lineage fate in single haematopoietic stem cells. *Nature*, *497*(7448), 239–243. https://doi.org/10.1038/nature12026

Murphy, A. J., Akhtari, M., Tolani, S., Pagler, T., Bijl, N., Kuo, C. L., Wang, M., Sanson, M., Abramowicz, S., Welch, C., Bochem, A. E., Kuivenhoven, J. A., Yvan-Charvet, L., & Tall, A. R. (2011). ApoE regulates hematopoietic stem cell proliferation, monocytosis, and monocyte accumulation in atherosclerotic lesions in mice. *Journal of Clinical Investigation*, *121*(10), 4138–4149. https://doi.org/10.1172/JCI57559

Nakayama, Y., Fujiu, K., Oshima, T., Matsuda, J., Sugita, J., James Matsubara, T., Liu, Y., Goto, K., Kani, K., Uchida, R., Takeda, N., Morita, H., Xiao, Y., Hayashi, M., Maru, Y., Hasumi, E., Kojima, T., Ishiguro, S., Kijima, Y., … Komuro, I. (2024). Heart failure promotes multimorbidity through innate immune memory. In *Sci. Immunol* (Vol. 9). https://doi.org/10.1038/s41577-024-01054-0

Neaz, S., Alam, M. M., & Imran, A. Bin. (2024). Advancements in cyclodextrin-based controlled drug delivery: Insights into pharmacokinetic and pharmacodynamic profiles. In *Heliyon* (Vol. 10, Issue 21). Elsevier Ltd. https://doi.org/10.1016/j.heliyon.2024.e39917

Netea, M. G., Domínguez-Andrés, J., Barreiro, L. B., Chavakis, T., Divangahi, M., Fuchs, E., Joosten, L. A. B., van der Meer, J. W. M., Mhlanga, M. M., Mulder, W. J. M., Riksen, N. P., Schlitzer, A., Schultze, J. L., Stabell Benn, C., Sun, J. C., Xavier, R. J., & Latz, E. (2020). Defining trained immunity and its role in health and disease. In *Nature Reviews Immunology* (Vol. 20, Issue 6, pp. 375–388). Nature Research. https://doi.org/10.1038/s41577-020-0285-6

Ngai, Y. F., Quong, W. L., Glier, M. B., Glavas, M. M., Babich, S. L., Innis, S. M., Kieffer, T. J., & Gibson, W. T. (2010). Ldlr-/- mice display decreased susceptibility to western-type diet-induced obesity due to increased thermogenesis. *Endocrinology*, *151*(11), 5226–5236. https://doi.org/10.1210/en.2010-0496

Nidorf, S. M., Fiolet, A. T. L., Mosterd, A., Eikelboom, J. W., Schut, A., Opstal, T. S. J., The, S. H. K., Xu, X.-F., Ireland, M. A., Lenderink, T., Latchem, D., Hoogslag, P., Jerzewski, A., Nierop, P., Whelan, A., Hendriks, R., Swart, H., Schaap, J., Kuijper, A. F. M., … Thompson, P. L. (2020). Colchicine in Patients with Chronic Coronary Disease. *New England Journal of Medicine*, *383*(19), 1838–1847. https://doi.org/10.1056/nejmoa2021372

Nishimura, S., Manabe, I., Nagasaki, M., Eto, K., Yamashita, H., Ohsugi, M., Otsu, M., Hara, K., Ueki, K., Sugiura, S., Yoshimura, K., Kadowaki, T., & Nagai, R. (2009). CD8+ effector T cells contribute to macrophage recruitment and adipose tissue inflammation in obesity. *Nature Medicine*, *15*(8), 914–920. https://doi.org/10.1038/nm.1964

Obstfeld, A. E., Sugaru, E., Thearle, M., Francisco, A. M., Gayet, C., Ginsberg, H. N., Ables, E. V., & Ferrante, A. W. (2010). C-C Chemokine Receptor 2 (CCR2) regulates the hepatic recruitment of myeloid cells that promote obesity-induced hepatic steatosis. *Diabetes*, *59*(4), 916–925. https://doi.org/10.2337/db09-1403

Ochando, J., Mulder, W. J. M., Madsen, J. C., Netea, M. G., & Duivenvoorden, R. (2023). Trained immunity — basic concepts and contributions to immunopathology. In *Nature Reviews Nephrology* (Vol. 19, Issue 1, pp. 23–37). Nature Research. https://doi.org/10.1038/s41581-022-00633-5

Ohtani, Y., Irie, T., Uekama, K., Fukunaga, K., & Pitha, J. (1989). Differential effects of α-, β- and γ-cyclodextrins on human erythrocytes. *European Journal of Biochemistry*, *186*(1–2), 17–22. https://doi.org/10.1111/j.1432-1033.1989.tb15171.x

Olson, O. C., Kang, Y. A., & Passegué, E. (2020). Normal hematopoiesis is a balancing act of self-renewal and regeneration. *Cold Spring Harbor Perspectives in Medicine*, *10*(12), 1–23. https://doi.org/10.1101/cshperspect.a035519

Ong, K. L., Campbell, S., Wu, B. J., McClelland, R. L., Kokkinos, J., Szklo, M., Polak, J. F., Allison, M. A., & Rye, K. A. (2019). Relationship of fibroblast growth factor 21 with subclinical atherosclerosis and cardiovascular events: Multi-Ethnic Study of

Atherosclerosis. *Atherosclerosis*, *287*, 46–53. https://doi.org/10.1016/j.atherosclerosis.2019.06.898

Ong, K. L., Hui, N., Januszewski, A. S., Kaakoush, N. O., Xu, A., Fayyad, R., DeMicco, D. A., Jenkins, A. J., Keech, A. C., Waters, D. D., Barter, P. J., & Rye, K. A. (2019). High plasma FGF21 levels predicts major cardiovascular events in patients treated with atorvastatin (from the Treating to New Targets [TNT] Study). *Metabolism: Clinical and Experimental*, *93*, 93–99. https://doi.org/10.1016/j.metabol.2018.11.006

Oppi, S., Lüscher, T. F., & Stein, S. (2019). Mouse Models for Atherosclerosis Research—Which Is My Line? In *Frontiers in Cardiovascular Medicine* (Vol. 6). https://doi.org/10.3389/fcvm.2019.00046

Ouimet, M., Franklin, V., Mak, E., Liao, X., Tabas, I., & Marcel, Y. L. (2011). Autophagy regulates cholesterol efflux from macrophage foam cells via lysosomal acid lipase. *Cell Metabolism*, *13*(6), 655–667. https://doi.org/10.1016/j.cmet.2011.03.023

Paigen, B., Morrow, A., Brandon, C., Mitchell, D., & Holmes, P. (1985). Variation in Susceptibility to Atherosclerosis Among Inbred Strains of Mice. In *Atherosclerosis* (Vol. 57).

Pang, W. W., Price, E. A., Sahoo, D., Beerman, I., Maloney, W. J., Rossi, D. J., Schrier, S. L., & Weissman, I. L. (2011). Human bone marrow hematopoietic stem cells are increased in frequency and myeloid-biased with age. *Proceedings of the National Academy of Sciences of the United States of America*, *108*(50), 20012–20017. https://doi.org/10.1073/pnas.1116110108

Park, Y. M. (2014). CD36, a scavenger receptor implicated in atherosclerosis. In *Experimental and Molecular Medicine* (Vol. 46, Issue 6). Nature Publishing Group. https://doi.org/10.1038/emm.2014.38

Perrin, J. H., Field, F. P., Hansen, D. A., Mufson, R. A., & Torosian, G. (1978). β-cyclodextrin as an aid to peritoneal dialysis. Renal toxicity of β-cyclodextrin in the rat. *Research Communications in Chemical Pathology and Pharmacology*, *19*(2).

Pettersson, U. S., Waldén, T. B., Carlsson, P. O., Jansson, L., & Phillipson, M. (2012). Female Mice are Protected against High-Fat Diet Induced Metabolic Syndrome and Increase the Regulatory T Cell Population in Adipose Tissue. *PLoS ONE*, *7*(9). https://doi.org/10.1371/journal.pone.0046057

Phipson, B., Lee, S., Majewski, I. J., Alexander, W. S., & Smyth, G. K. (2016). Robust hyperparameter estimation protects against hypervariable genes and improves power to detect differential expression. *Annals of Applied Statistics*, *10*(2), 946–963. https://doi.org/10.1214/16-AOAS920

Piedrahita, J. A., Zhang, S. H., Hagaman, J. R., Oliver, P. M., & Maeda, N. (1992). Generation of mice carrying a mutant apolipoprotein E gene inactivated by gene targeting in embryonic stem cells (homologous recombination/atherosclerosis). In *Genetics* (Vol. 89).

Pietras, E. M., Mirantes-Barbeito, C., Fong, S., Loeffler, D., Kovtonyuk, L. V., Zhang, S., Lakshminarasimhan, R., Chin, C. P., Techner, J. M., Will, B., Nerlov, C., Steidl, U., Manz, M. G., Schroeder, T., & Passegué, E. (2016). Chronic interleukin-1 exposure drives haematopoietic stem cells towards precocious myeloid differentiation at the expense of self-renewal. *Nature Cell Biology*, *18*(6), 607–618. https://doi.org/10.1038/ncb3346

Pietras, E. M., Reynaud, D., Kang, Y. A., Carlin, D., Calero-Nieto, F. J., Leavitt, A. D., Stuart, J. A., Göttgens, B., & Passegué, E. (2015). Functionally Distinct Subsets of Lineage-Biased Multipotent Progenitors Control Blood Production in Normal and Regenerative Conditions. *Cell Stem Cell*, *17*(1), 35–46. https://doi.org/10.1016/j.stem.2015.05.003

Plump, A. S., Smith, J. D., Hayek, T., Aalto-Setiilii, K., Walsh, A., Verstuyft, J. G., Rubin, E. M., & Breslow, J. L. (1992). Severe Hypercholesterolemia and Atherosclerosis in Apolipoprotein E-Deficient Mice Created by Homologous Recombination in ES Cells. In *Cell* (Vol. 71).

Prendergast, Á. M., Kuck, A., van Essen, M., Haas, S., Blaszkiewicz, S., & Essers, M. A. G. (2017). IFN α -mediated remodeling of endothelial cells in the bone marrow niche. *Haematologica*, *102*(3), 445–453. https://doi.org/10.3324/haematol.2016.151209

Quintar, A., McArdle, S., Wolf, D., Marki, A., Ehinger, E., Vassallo, M., Miller, J., Mikulski, Z., Ley, K., & Buscher, K. (2017). Endothelial Protective Monocyte Patrolling in Large Arteries Intensified by Western Diet and Atherosclerosis. *Circulation Research*, *120*(11), 1789–1799. https://doi.org/10.1161/CIRCRESAHA.117.310739

R Core Team (2023). R: A language and environment for statistical computing. R Foundation for Statistical Computing, Vienna, Austria. URL https://www.R-project.org/, accessed: 24.11.2025

Raber, J., Wong, D., Buttini, M., Orth, M., Bellosta, S., Pitas, R. E., Mahley, R. W., & Mucke, L. (1998). Isoform-specific effects of human apolipoprotein E on brain function revealed in ApoE knockout mice: Increased susceptibility of females. In *Neurobiology* (Vol. 95). www.pnas.org.

Ralapanawa, U., & Sivakanesan, R. (2021). Epidemiology and the magnitude of coronary artery disease and acute coronary syndrome: A narrative review. In *Journal of Epidemiology and Global Health* (Vol. 11, Issue 2, pp. 169–177). Atlantis Press International. https://doi.org/10.2991/JEGH.K.201217.001

Repa, J. J., Turley, S. D., Lobaccaro, J. M. A., Medina, J., Li, L., Lustig, K., Shan, B., Heyman, R. A., Dietschy, J. M., & Mangelsdorf, D. J. (2000). Regulation of absorption and ABC1-mediated efflux of cholesterol by RXR heterodimers. In *Science* (Vol. 289, Issue 5484). https://doi.org/10.1126/science.289.5484.1524

Reue, K. (2017). Sex differences in obesity: X chromosome dosage as a risk factor for increased food intake, adiposity and co-morbidities. In *Physiology and Behavior* (Vol. 176, pp. 174–182). Elsevier Inc. https://doi.org/10.1016/j.physbeh.2017.02.040

Ridker, P. M., Everett, B. M., Pradhan, A., MacFadyen, J. G., Solomon, D. H., Zaharris, E., Mam, V., Hasan, A., Rosenberg, Y., Iturriaga, E., Gupta, M., Tsigoulis, M., Verma, S., Clearfield, M., Libby, P., Goldhaber, S. Z., Seagle, R., Ofori, C., Saklayen, M., … Glynn, R. J. (2019). Low-Dose Methotrexate for the Prevention of Atherosclerotic Events. *New England Journal of Medicine*, *380*(8), 752–762. https://doi.org/10.1056/nejmoa1809798

Ridker, P. M., Everett, B. M., Thuren, T., MacFadyen, J. G., Chang, W. H., Ballantyne, C., Fonseca, F., Nicolau, J., Koenig, W., Anker, S. D., Kastelein, J. J. P., Cornel, J. H., Pais, P., Pella, D., Genest, J., Cifkova, R., Lorenzatti, A., Forster, T., Kobalava, Z., … Glynn, R. J. (2017). Antiinflammatory Therapy with Canakinumab for Atherosclerotic Disease. *New England Journal of Medicine*, *377*(12), 1119–1131. https://doi.org/10.1056/nejmoa1707914

Ritchie, M. E., Phipson, B., Wu, D., Hu, Y., Law, C. W., Shi, W., & Smyth, G. K. (2015). Limma powers differential expression analyses for RNA-sequencing and microarray studies. *Nucleic Acids Research*, *43*(7), e47. https://doi.org/10.1093/nar/gkv007

Robinson, M. D., McCarthy, D. J., & Smyth, G. K. (2009). edgeR: A Bioconductor package for differential expression analysis of digital gene expression data. *Bioinformatics*, *26*(1), 139–140. https://doi.org/10.1093/bioinformatics/btp616

Robinson, M. D., & Oshlack, A. (2010). *A scaling normalization method for differential expression analysis of RNA-seq data*. http://genomebiology.com/2010/11/3/R25

Rodeheffer, M. S., Birsoy, K., & Friedman, J. M. (2008). Identification of White Adipocyte Progenitor Cells In Vivo. *Cell*, *135*(2), 240–249. https://doi.org/10.1016/j.cell.2008.09.036

Roeters van Lennep, J. E., Öörni, K., Binder, C. J., Kronenberg, F., Mallat, Z., Raggi, P., Benn, M., Afzal, S., Holven, K. B., Kayikcioglu, M., Laufs, U., Liberopoulos, E., Ray, K. K., Nordestgaard, B. G., & Boren, J. (2025). The essential role of sex and gender in atherosclerosis research: A statement from the Editorial Board of Atherosclerosis and Executive Committee of the European Atherosclerosis Society. In *Atherosclerosis* (Vol. 407). Elsevier Ireland Ltd. https://doi.org/10.1016/j.atherosclerosis.2025.120403

Rosenbaum, A. I., Cosner, C. C., Mariani, C. J., Maxfield, F. R., Wiest, O., & Helquist, P. (2010). Thiadiazole carbamates: Potent inhibitors of lysosomal acid lipase and potential niemann-pick type C disease therapeutics. *Journal of Medicinal Chemistry*, *53*(14), 5281–5289. https://doi.org/10.1021/jm100499s

Ross, S. E., Erickson, R. L., Gerin, I., DeRose, P. M., Bajnok, L., Longo, K. A., Misek, D. E., Kuick, R., Hanash, S. M., Atkins, K. B., Andresen, S. M., Nebb, H. I., Madsen, L., Kristiansen, K., & MacDougald, O. A. (2002). Microarray Analyses during Adipogenesis: Understanding the Effects of Wnt Signaling on Adipogenesis and the Roles of Liver X Receptor α in Adipocyte Metabolism. *Molecular and Cellular Biology*, *22*(16), 5989–5999. https://doi.org/10.1128/mcb.22.16.5989-5999.2002

Roy, D., Myers, J. M., & Tedeschi, A. (2022). Protocol for assessing ex vivo lipolysis of murine adipose tissue. *STAR Protocols*, *3*(3). https://doi.org/10.1016/j.xpro.2022.101518

Saederup, N., Chan, L., Lira, S. A., & Charo, I. F. (2008). Fractalkine deficiency markedly reduces macrophage accumulation and atherosclerotic lesion formation in CCR2-/- mice: Evidence for independent chemokine functions in atherogenesis. *Circulation*, *117*(13), 1642–1648. https://doi.org/10.1161/CIRCULATIONAHA.107.743872

Sakkers, T. R., Mokry, M., Civelek, M., Erdmann, J., Pasterkamp, G., Diez Benavente, E., & den Ruijter, H. M. (2023). Sex differences in the genetic and molecular mechanisms of coronary artery disease. In *Atherosclerosis* (Vol. 384). Elsevier Ireland Ltd. https://doi.org/10.1016/j.atherosclerosis.2023.117279

Sangiorgi, G., Roversi, S., Biondi Zoccai, G., Modena, M. G., Servadei, F., Ippoliti, A., & Mauriello, A. (2013). Sex-related differences in carotid plaque features and inflammation. *Journal of Vascular Surgery*, *57*(2), 338–344. https://doi.org/10.1016/j.jvs.2012.07.052

Scantlebery, A. M. L., Ochodnicky, P., Kors, L., Rampanelli, E., Butter, L. M., El Boumashouli, C., Claessen, N., Teske, G. J., van den Bergh Weerman, M. A., Leemans, J. C., Roelofs, J. J. T. H., & Florquin, S. (2019). β-Cyclodextrin counteracts obesity in Western diet-fed mice but elicits a nephrotoxic effect. *Scientific Reports*, *9*(1). https://doi.org/10.1038/s41598-019-53890-z

Schaap, F. G., Kremer, A. E., Lamers, W. H., Jansen, P. L. M., & Gaemers, I. C. (2013). Fibroblast growth factor 21 is induced by endoplasmic reticulum stress. *Biochimie*, *95*(4), 692–699. https://doi.org/10.1016/j.biochi.2012.10.019

Schleh, M. W., Caslin, H. L., Garcia, J. N., Mashayekhi, M., Srivastava, G., Bradley, A. B., & Hasty, A. H. (2023). Metaflammation in obesity and its therapeutic targeting. In *Science Translational Medicine* (Vol. 15, Issue 723). American Association for the Advancement of Science. https://doi.org/10.1126/scitranslmed.adf9382

Schlüter, T., van Elsas, Y., Priem, B., Ziogas, A., & Netea, M. G. (2025). Trained immunity: induction of an inflammatory memory in disease. In *Cell Research*. Springer Nature. https://doi.org/10.1038/s41422-025-01171-y

Schmid, G. (1989). *Cyclodextrin glycosyltransferase production: yield enhancement by overexpression of cloned genes*.

Schwarz, D. H., Engelke, A., & Wenz, G. (2017). Solubilizing steroidal drugs by β-cyclodextrin derivatives. *International Journal of Pharmaceutics*, *531*(2), 559–567. https://doi.org/10.1016/j.ijpharm.2017.07.046

Scolaro, B., Krautter, F., Brown, E. J., Ray, A. G., Kalev-Altman, R., Petitjean, M., Delbare, S., Donahoe, C., Pena, S., Garabedian, M. L., Nikain, C. A., Laskou, M., Tufanli, O., Hannemann, C., Aouadi, M., Weinstock, A., & Fisher, E. A. (2025). Caloric restriction promotes resolution of atherosclerosis in obese mice, while weight regain accelerates its progression. *Journal of Clinical Investigation*, *135*(18). https://doi.org/10.1172/JCI172198

Seufert, A. L., Hickman, J. W., Traxler, S. K., Peterson, R. M., Waugh, T. A., Lashley, S. J., Shulzhenko, N., Napier, R. J., & Napier, B. A. (2022). Enriched dietary saturated fatty acids induce trained immunity via ceramide production that enhances severity of endotoxemia and clearance of infection. *ELife*, *11*. https://doi.org/10.7554/eLife.76744

Sheedy, F. J., Grebe, A., Rayner, K. J., Kalantari, P., Ramkhelawon, B., Carpenter, S. B., Becker, C. E., Ediriweera, H. N., Mullick, A. E., Golenbock, D. T., Stuart, L. M., Latz, E., Fitzgerald, K. A., & Moore, K. J. (2013). CD36 coordinates NLRP3 inflammasome activation by facilitating intracellular nucleation of soluble ligands into particulate ligands in sterile inflammation. *Nature Immunology*, *14*(8), 812–820. https://doi.org/10.1038/ni.2639

Shvetcov, A., Johnson, E. C. B., Winchester, L. M., Walker, K. A., Wilkins, H. M., Thompson, T. G., Rothstein, J. D., Krish, V., Imam, F. B., Burns, J. M., Swerdlow, R. H., Slawson, C., & Finney, C. A. (2025). APOE ε4 carriers share immune-related proteomic changes across neurodegenerative diseases. *Nature Medicine*. https://doi.org/10.1038/s41591-025-03835-z

Sieckmann, K., Winnerling, N., Huebecker, M., Leyendecker, P., Silva Ribeiro, D. J., Gnad, T., Pfeifer, A., Wachten, D., & Hansen, J. N. (2022). AdipoQ—a simple, open-source software to quantify adipocyte morphology and function in tissues and in vitro. *Molecular Biology of the Cell*, *33*(12). https://doi.org/10.1091/mbc.E21-11-0592

Silva Ribeiro, D. J., Yüksel, S., Dolf, A., & Wachten, D. (2024). Isolation and Flow Cytometry Analysis of Macrophages from White Adipose Tissue. In *Methods in Molecular Biology* (Vol. 2713, pp. 149–158). Humana Press Inc. https://doi.org/10.1007/978-1-0716-3437-0_10

Simats, A., Zhang, S., Messerer, D., Chong, F., Beşkardeş, S., Chivukula, A. S., Cao, J., Besson-Girard, S., Montellano, F. A., Morbach, C., Carofiglio, O., Ricci, A., Roth, S.,

Llovera, G., Singh, R., Chen, Y., Filser, S., Plesnila, N., Braun, C., … Liesz, A. (2024). Innate immune memory after brain injury drives inflammatory cardiac dysfunction. *Cell*. https://doi.org/10.1016/j.cell.2024.06.028

Singh, N., Moody, A. R., Zhang, B., Kaminski, I., Kapur, K., Chiu, S., & Tyrrell, P. N. (2017). Age-Specific Sex Differences in Magnetic Resonance Imaging-Depicted Carotid Intraplaque Hemorrhage. *Stroke*, *48*(8), 2129–2135. https://doi.org/10.1161/STROKEAHA.117.017877

Singh, R., Kaushik, S., Wang, Y., Xiang, Y., Novak, I., Komatsu, M., Tanaka, K., Cuervo, A. M., & Czaja, M. J. (2009). Autophagy regulates lipid metabolism. *Nature*, *458*(7242), 1131–1135. https://doi.org/10.1038/nature07976

Solomon, M., DeLay, M., & Reynaud, D. (2020). Phenotypic Analysis of the Mouse Hematopoietic Hierarchy Using Spectral Cytometry: From Stem Cell Subsets to Early Progenitor Compartments. *Cytometry Part A*, *97*(10), 1057–1065. https://doi.org/10.1002/cyto.a.24041

Šošić-Jurjević, B., Lütjohann, D., Renko, K., Filipović, B., Radulović, N., Ajdžanović, V., Trifunović, S., Nestorović, N., Živanović, J., Manojlović Stojanoski, M., Köhrle, J., & Milošević, V. (2019). The isoflavones genistein and daidzein increase hepatic concentration of thyroid hormones and affect cholesterol metabolism in middle-aged male rats. *Journal of Steroid Biochemistry and Molecular Biology*, *190*, 1–10. https://doi.org/10.1016/j.jsbmb.2019.03.009

Stewart, C. R., Stuart, L. M., Wilkinson, K., Van Gils, J. M., Deng, J., Halle, A., Rayner, K. J., Boyer, L., Zhong, R., Frazier, W. A., Lacy-Hulbert, A., Khoury, J. El, Golenbock, D. T., & Moore, K. J. (2010). CD36 ligands promote sterile inflammation through assembly of a Toll-like receptor 4 and 6 heterodimer. *Nature Immunology*, *11*(2), 155–161. https://doi.org/10.1038/ni.1836

Strissel, K. J., DeFuria, J., Shaul, M. E., Bennett, G., Greenberg, A. S., & Obin, M. S. (2010). T-cell recruitment and Th1 polarization in adipose tissue during diet-induced obesity in C57BL/6 mice. *Obesity*, *18*(10), 1918–1925. https://doi.org/10.1038/oby.2010.1

Stroope, C., Nettersheim, F. S., Coon, B., Finney, A. C., Schwartz, M. A., Ley, K., Rom, O., & Yurdagul, A. (2024). Dysregulated cellular metabolism in atherosclerosis:

mediators and therapeutic opportunities. In *Nature Metabolism* (Vol. 6, Issue 4, pp. 617–638). Nature Research. https://doi.org/10.1038/s42255-024-01015-w

Sugiyama, T., Kohara, H., Noda, M., & Nagasawa, T. (2006). Maintenance of the Hematopoietic Stem Cell Pool by CXCL12-CXCR4 Chemokine Signaling in Bone Marrow Stromal Cell Niches. *Immunity*, *25*(6), 977–988. https://doi.org/10.1016/j.immuni.2006.10.016

Sun, S. J., Aguirre-Gamboa, R., de Bree, L. C. J., Sanz, J., Dumaine, A., van der Velden, W. J. F. M., Joosten, L. A. B., Khader, S., Divangahi, M., Netea, M. G., & Barreiro, L. B. (2024). BCG vaccination alters the epigenetic landscape of progenitor cells in human bone marrow to influence innate immune responses. *Immunity*, *57*(9), 2095-2107.e8. https://doi.org/10.1016/j.immuni.2024.07.021

Swann, J. W., Olson, O. C., & Passegué, E. (2024). Made to order: emergency myelopoiesis and demand-adapted innate immune cell production. In *Nature Reviews Immunology*. Nature Research. https://doi.org/10.1038/s41577-024-00998-7

Tabas, I., Williams, K. J., & Borén, J. (2007). Subendothelial lipoprotein retention as the initiating process in atherosclerosis: Update and therapeutic implications. In *Circulation* (Vol. 116, Issue 16, pp. 1832–1844). https://doi.org/10.1161/CIRCULATIONAHA.106.676890

Tacke, F., Alvarez, D., Kaplan, T. J., Jakubzick, C., Spanbroek, R., Llodra, J., Garin, A., Liu, J., Mack, M., Van Rooijen, N., Lira, S. A., Habenicht, A. J., & Randolph, G. J. (2007). Monocyte subsets differentially employ CCR2, CCR5, and CX3CR1 to accumulate within atherosclerotic plaques. *Journal of Clinical Investigation*, *117*(1), 185–194. https://doi.org/10.1172/JCI28549

Tall, A. R., & Fuster, J. J. (2022). Clonal hematopoiesis in cardiovascular disease and therapeutic implications. In *Nature Cardiovascular Research* (Vol. 1, Issue 2, pp. 116–124). Springer. https://doi.org/10.1038/s44161-021-00015-3

Tamura, A., & Yui, N. (2018). Polyrotaxane-based systemic delivery of β-cyclodextrins for potentiating therapeutic efficacy in a mouse model of Niemann-Pick type C disease. *Journal of Controlled Release*, *269*, 148–158. https://doi.org/10.1016/j.jconrel.2017.11.016

Tan, H., Yue, T., Chen, Z., Wu, W., Xu, S., & Weng, J. (2023). Targeting FGF21 in cardiovascular and metabolic diseases: from mechanism to medicine. In *International Journal of Biological Sciences* (Vol. 19, Issue 1, pp. 66–88). Ivyspring International Publisher. https://doi.org/10.7150/ijbs.73936

Tardif, J.-C., Kouz, S., Waters, D. D., Bertrand, O. F., Diaz, R., Maggioni, A. P., Pinto, F. J., Ibrahim, R., Gamra, H., Kiwan, G. S., Berry, C., López-Sendón, J., Ostadal, P., Koenig, W., Angoulvant, D., Grégoire, J. C., Lavoie, M.-A., Dubé, M.-P., Rhainds, D., … Roubille, F. (2019). Efficacy and Safety of Low-Dose Colchicine after Myocardial Infarction. *New England Journal of Medicine*, *381*(26), 2497–2505. https://doi.org/10.1056/nejmoa1912388

Teufel, L. U., Arts, R. J. W., Netea, M. G., Dinarello, C. A., & Joosten, L. A. B. (2022). IL-1 family cytokines as drivers and inhibitors of trained immunity. *Cytokine*, *150*. https://doi.org/10.1016/j.cyto.2021.155773

Tilg, H., Ianiro, G., Gasbarrini, A., & Adolph, T. E. (2025). Adipokines: masterminds of metabolic inflammation. In *Nature Reviews Immunology* (Vol. 25, Issue 4, pp. 250–265). Nature Research. https://doi.org/10.1038/s41577-024-01103-8

Tobb, K., Kocher, M., & Bullock-Palmer, R. P. (2022). Underrepresentation of women in cardiovascular trials- it is time to shatter this glass ceiling. In *American Heart Journal Plus: Cardiology Research and Practice* (Vol. 13). Elsevier Inc. https://doi.org/10.1016/j.ahjo.2022.100109

Tontonoz, P., & Mangelsdorf, D. J. (2003). Liver X receptor signaling pathways in cardiovascular disease. In *Molecular Endocrinology* (Vol. 17, Issue 6, pp. 985–993). https://doi.org/10.1210/me.2003-0061

van Beek, L., van Klinken, J. B., Pronk, A. C. M., van Dam, A. D., Dirven, E., Rensen, P. C. N., Koning, F., Willems van Dijk, K., & van Harmelen, V. (2015). The limited storage capacity of gonadal adipose tissue directs the development of metabolic disorders in male C57Bl/6J mice. *Diabetologia*, *58*(7), 1601–1609. https://doi.org/10.1007/s00125-015-3594-8

Vandoorne, K., Rohde, D., Kim, H. Y., Courties, G., Wojtkiewicz, G., Honold, L., Hoyer, F. F., Frodermann, V., Nayar, R., Herisson, F., Jung, Y., Désogère, P. A., Vinegoni, C., Caravan, P., Weissleder, R., Sosnovik, D. E., Lin, C. P., Swirski, F. K., & Nahrendorf, M. (2018). Imaging the vascular bone marrow niche during inflammatory stress.

Circulation Research, *123*(4), 415–427. https://doi.org/10.1161/CIRCRESAHA.118.313302

Velingkar, A., Vuree, S., Prabhakar, P. K., Kalashikam, R. R., Banerjee, A., & Kondeti, S. (2023). Fibroblast growth factor 21 as a potential master regulator in metabolic disorders. In *American Journal of Physiology - Endocrinology and Metabolism* (Vol. 324, Issue 5, pp. E409–E424). American Physiological Society. https://doi.org/10.1152/ajpendo.00244.2022

Vijayan, V., Wagener, F. A. D. T. G., & Immenschuh, S. (2018). The macrophage heme-heme oxygenase-1 system and its role in inflammation. In *Biochemical Pharmacology* (Vol. 153, pp. 159–167). Elsevier Inc. https://doi.org/10.1016/j.bcp.2018.02.010

Visseren, F., Mach, F., Smulders, Y. M., Carballo, D., Koskinas, K. C., Bäck, M., Benetos, A., Biffi, A., Boavida, J. M., Capodanno, D., Cosyns, B., Crawford, C. A., Davos, C. H., Desormais, I., Di Angelantonio, E., Duran, O. H. F., Halvorsen, S., Richard Hobbs, F. D., Hollander, M., … Mullabayeva, G. (2021). 2021 ESC Guidelines on cardiovascular disease prevention in clinical practice. In *European Heart Journal* (Vol. 42, Issue 34, pp. 3227–3337). Oxford University Press. https://doi.org/10.1093/eurheartj/ehab484

von Ehr, A., Bode, C., & Hilgendorf, I. (2022). Macrophages in Atheromatous Plaque Developmental Stages. In *Frontiers in Cardiovascular Medicine* (Vol. 9). Frontiers Media S.A. https://doi.org/10.3389/fcvm.2022.865367

Vrijenhoek, J. E. P., Den Ruijter, H. M., De Borst, G. J., De Kleijn, D. P. V., De Vries, J. P. P. M., Bots, M. L., Van De Weg, S. M., Vink, A., Moll, F. L., & Pasterkamp, G. (2013). Sex is associated with the presence of atherosclerotic plaque hemorrhage and modifies the relation between plaque hemorrhage and cardiovascular outcome. *Stroke*, *44*(12), 3318–3323. https://doi.org/10.1161/STROKEAHA.113.002633

Wan, X. S., Lu, X. H., Xiao, Y. C., Lin, Y., Zhu, H., Ding, T., Yang, Y., Huang, Y., Zhang, Y., Liu, Y. L., Xu, Z. M., Xiao, J., & Li, X. K. (2014). ATF4- and CHOP-dependent induction of FGF21 through endoplasmic reticulum stress. *BioMed Research International*, *2014*. https://doi.org/10.1155/2014/807874

Wang, B., & Tontonoz, P. (2018). Liver X receptors in lipid signalling and membrane homeostasis. In *Nature Reviews Endocrinology* (Vol. 14, Issue 8, pp. 452–463). Nature Publishing Group. https://doi.org/10.1038/s41574-018-0037-x

Wang, H., Zhang, X., Yu, B., Peng, X., Liu, Y., Wang, A., Zhao, D., Pang, D., Ouyang, H., & Tang, X. (2019). Cyclodextrin Ameliorates the Progression of Atherosclerosis via Increasing High-Density Lipoprotein Cholesterol Plasma Levels and Anti-inflammatory Effects in Rabbits. *Journal of Cardiovascular Pharmacology*, *73*(5). https://doi.org/10.1097/FJC.0000000000000660

Wang, J. S., Sheu, W. H. H., Lee, W. J., Lee, I. Te, Lin, S. Y., Lee, W. L., Liang, K. W., & Lin, S. J. (2017). Associations of fibroblast growth factor 21 with cardiovascular risk and β-cell function in patients who had no history of diabetes. *Clinica Chimica Acta*, *472*, 80–85. https://doi.org/10.1016/j.cca.2017.07.017

Weisberg, S. P., Hunter, D., Huber, R., Lemieux, J., Slaymaker, S., Vaddi, K., Charo, I., Leibel, R. L., & Ferrante, A. W. (2006). CCR2 modulates inflammatory and metabolic effects of high-fat feeding. *Journal of Clinical Investigation*, *116*(1), 115–124. https://doi.org/10.1172/JCI24335

Weisberg, S. P., McCann, D., Desai, M., Rosenbaum, M., Leibel, R. L., & Ferrante, A. W. (2003a). Obesity is associated with macrophage accumulation in adipose tissue. *Journal of Clinical Investigation*, *112*(12), 1796–1808. https://doi.org/10.1172/JCI200319246

Weisberg, S. P., McCann, D., Desai, M., Rosenbaum, M., Leibel, R. L., & Ferrante, A. W. (2003b). Obesity is associated with macrophage accumulation in adipose tissue. *Journal of Clinical Investigation*, *112*(12), 1796–1808. https://doi.org/10.1172/JCI200319246

Weiskopf, K., Schnorr, P. J., Pang, W. W., Chao, M. P., Chhabra, A., Seita, J., Feng, M., & Weissman, I. L. (2016). Myeloid Cell Origins, Differentiation, and Clinical Implications. *Microbiology Spectrum*, *4*(5). https://doi.org/10.1128/microbiolspec.mchd-0031-2016

Wendorff, C., Wendorff, H., Pelisek, J., Tsantilas, P., Zimmermann, A., Zernecke, A., Kuehnl, A., & Eckstein, H. H. (2015). Carotid Plaque Morphology Is Significantly Associated with Sex, Age, and History of Neurological Symptoms. *Stroke*, *46*(11), 3213–3219. https://doi.org/10.1161/STROKEAHA.115.010558

WHO, 2025: The top 10 causes of death, https://www.who.int/news-room/fact-sheets/detail/the-top-10-causes-of-death, date accessed: 24.11.2025

Wiese, C. B., Avetisyan, R., & Reue, K. (2023). The impact of chromosomal sex on cardiometabolic health and disease. In *Trends in Endocrinology and Metabolism* (Vol. 34, Issue 10, pp. 652–665). Elsevier Inc. https://doi.org/10.1016/j.tem.2023.07.003

Willem E. Hellings, Gerard Pasterkamp, Bart A. N. Verhoeven, Dominique P. V. De Kleijn, Jean-Paul P. M. De Vries, Kees A. Seldenrijk, Theo van den Broek, & Frans L. Moll. (2007). Gender-associated differences in plaque phenotype of patients undergoing carotid endarterectomy. In *Journal of Vascular Surgery* (Vol. 45, Issue 2, pp. 296–297). Mosby Inc. https://doi.org/10.1016/j.jvs.2006.09.047

Woods, K., & Guezguez, B. (2021). Dynamic Changes of the Bone Marrow Niche: Mesenchymal Stromal Cells and Their Progeny During Aging and Leukemia. In *Frontiers in Cell and Developmental Biology* (Vol. 9). https://doi.org/10.3389/fcell.2021.714716

Wu, H., & Ballantyne, C. M. (2017). Skeletal muscle inflammation and insulin resistance in obesity. *Journal of Clinical Investigation*, *127*(1), 43–54. https://doi.org/10.1172/JCI88880

Wu, L., Qian, L., Zhang, L., Zhang, J., Zhou, J., Li, Y., Hou, X., Fang, Q., Li, H., & Jia, W. (2020). Fibroblast growth factor 21 is related to atherosclerosis independent of nonalcoholic fatty liver disease and predicts atherosclerotic cardiovascular events. *Journal of the American Heart Association*, *9*(11). https://doi.org/10.1161/JAHA.119.015226

Xu, H., Barnes, G. T., Yang, Q., Tan, G., Yang, D., Chou, C. J., Sole, J., Nichols, A., Ross, J. S., Tartaglia, L. A., & Chen, H. (2003). Chronic inflammation in fat plays a crucial role in the development of obesity-related insulin resistance. *Journal of Clinical Investigation*, *112*(12), 1821–1830. https://doi.org/10.1172/JCI200319451

Xu, J., Lloyd, D. J., Hale, C., Stanislaus, S., Chen, M., Sivits, G., Vonderfecht, S., Hecht, R., Li, Y. S., Lindberg, R. A., Chen, J. L., Jung, D. Y., Zhang, Z., Ko, H. J., Kim, J. K., & Véniant, M. M. (2009). Fibroblast growth factor 21 reverses hepatic steatosis, increases energy expenditure, and improves insulin sensitivity in diet-induced obese mice. *Diabetes*, *58*(1), 250–259. https://doi.org/10.2337/db08-0392

Xu, J., Stanislaus, S., Chinookoswong, N., Lau, Y. Y., Hager, T., Patel, J., Ge, H., Weiszmann, J., Lu, S.-C., Graham, M., Busby, J., Hecht, R., Li, Y.-S., Li, Y., Lindberg, R., & Véniant, M. M. (2009). Acute glucose-lowering and insulin-sensitizing action of

FGF21 in insulin-resistant mouse models-association with liver and adipose tissue effects. *Am J Physiol Endocrinol Metab*, *297*, 1105–1114. https://doi.org/10.1152/ajpendo.00348.2009.-Recombinant

Yamazaki, S., Mabuchi, Y., Kimura, T., Suto, E. G., Hisamatsu, D., Naraoka, Y., Kondo, A., Azuma, Y., Kikuchi, R., Nishikii, H., Morishita, S., Araki, M., Komatsu, N., & Akazawa, C. (2024). Activated mesenchymal stem/stromal cells promote myeloid cell differentiation via CCL2/CCR2 signaling. *Stem Cell Reports*, *19*(3), 414–425. https://doi.org/10.1016/j.stemcr.2024.02.002

Yan, X., Chen, J., Zhang, C., Zhou, S., Zhang, Z., Chen, J., Feng, W., Li, X., & Tan, Y. (2015). FGF21 deletion exacerbates diabetic cardiomyopathy by aggravating cardiac lipid accumulation. *Journal of Cellular and Molecular Medicine*, *19*(7), 1557–1568. https://doi.org/10.1111/jcmm.12530

Yeh, Y. S., Evans, T. D., Iwase, M., Jeong, S. J., Zhang, X., Liu, Z., Park, A., Ghasemian, A., Dianati, B., Javaheri, A., Kratky, D., Kawarasaki, S., Goto, T., Zhang, H., Dutta, P., Schopfer, F. J., Straub, A. C., Cho, J., Lodhi, I. J., & Razani, B. (2025). Identification of lysosomal lipolysis as an essential noncanonical mediator of adipocyte fasting and cold-induced lipolysis. *Journal of Clinical Investigation*, *135*(6). https://doi.org/10.1172/JCI185340

Yong, J., Johnson, J. D., Arvan, P., Han, J., & Kaufman, R. J. (2021). Therapeutic opportunities for pancreatic β-cell ER stress in diabetes mellitus. In *Nature Reviews Endocrinology* (Vol. 17, Issue 8, pp. 455–467). Nature Research. https://doi.org/10.1038/s41574-021-00510-4

Zechner, R., Zimmermann, R., Eichmann, T. O., Kohlwein, S. D., Haemmerle, G., Lass, A., & Madeo, F. (2012). FAT SIGNALS - Lipases and lipolysis in lipid metabolism and signaling. In *Cell Metabolism* (Vol. 15, Issue 3, pp. 279–291). https://doi.org/10.1016/j.cmet.2011.12.018

Zhang, S. H., Reddick, R. L., Piedrahita, J. A., & Maeda, N. (1992). Spontaneous Hypercholesterolemia and Arterial Lesions in Mice Lacking. In *Source: Science, New Series* (Vol. 258, Issue 5081).

Zhang, Y., Cheng, Z., Hong, L., Liu, J., Ma, X., Wang, W., Pan, R., Lu, W., Luo, Q., Gao, S., & Kong, Q. (2023). Apolipoprotein E (ApoE) orchestrates adipose tissue

inflammation and metabolic disorders through NLRP3 inflammasome. *Molecular Biomedicine*, *4*(1). https://doi.org/10.1186/s43556-023-00158-8

Zhao, X., Bartholdy, B., Yamamoto, Y., Evans, E. K., Alberich-Jordà, M., Staber, P. B., Benoukraf, T., Zhang, P., Zhang, J., Trinh, B. Q., Crispino, J. D., Hoang, T., Bassal, M. A., & Tenen, D. G. (2022). PU.1-c-Jun interaction is crucial for PU.1 function in myeloid development. *Communications Biology*, *5*(1). https://doi.org/10.1038/s42003-022-03888-7

Zhou, H., Goldman, M., Wu, J., Woestenborghs, R., Hassell, A. E., Lee, P., Baruch, A., Pesco-Koplowitz, L., Borum, J., & Wheat, L. J. (1998). A pharmacokinetic study of intravenous itraconazole followed by oral administration of itraconazole capsules in patients with advanced human immunodeficiency virus infection. *Journal of Clinical Pharmacology*, *38*(7), 593–602. https://doi.org/10.1002/j.1552-4604.1998.tb04465.x

Zimmer, S., Grebe, A., Bakke, S. S., Bode, N., Halvorsen, B., Ulas, T., Skjelland, M., De Nardo, D., Labzin, L. I., Kerksiek, A., Hempel, C., Heneka, M. T., Hawxhurst, V., Fitzgerald, M. L., Trebicka, J., Björkhem, I., Gustafsson, J. Å., Westerterp, M., Tall, A. R., … Latz, E. (2016). Cyclodextrin promotes atherosclerosis regression via macrophage reprogramming. *Science Translational Medicine*, *8*(333). https://doi.org/10.1126/scitranslmed.aad6100

Zimmermann, R., Strauss, J. G., Haemmerle, G., Schoiswohl, G., Birner-Gruenberger, R., Riederer, M., Lass, A., Neuberger, G., Eisenhaber, F., Hermetter, A., & Zechner, R. (2004). Fat Mobilization in Adipose Tissue Is Promoted by Adipose Triglyceride Lipase. In *Source: Science, New Series* (Vol. 306, Issue 5700).

Zou, Y., Wang, D., Sun, W., Wu, Q., Liu, S., Ren, Z., Li, Y., Zhao, T., Li, Z., Li, X., Cao, W., Han, J., Guo, X., & Ren, G. (2024). Fibroblast growth factor 21 mitigates lupus nephritis progression via the FGF21/Irgm 1/NLRP3 inflammasome pathway. *International Immunopharmacology*, *131*. https://doi.org/10.1016/j.intimp.2024.111875

9. Statement on own contribution

The work was carried out at the Institute of Innate Immunity under the supervision of Prof. Dr. Eicke Latz and the mentoring of Prof. Dr. Dagmar Wachten. The work was designed in collaboration with PD Dr. Peter Düwell, researcher in the Latz lab, Dr. Anette Christ, former Postdoc in the Latz lab, Univ. Prof. Dr. med. Sebastian Zimmer, physician and researcher at the University Hospital Bonn, and Prof. Dr. Dagmar Wachten, Institute director of the Institute of Innate Immunity, University of Bonn.

The following experiments (including animal experiment and organ retrieval) were carried out by me with the support of Romina Kaiser, Maximilian Rothe, Dr. Dennis de Graaf, and Theresa Wagner: *Ldlr*$^{-/-}$ and WT diet induction model. Routine caretaking of mice was done by the staff members of the HET and the iFET. FACS-sorting was performed by David Kühne from the Flow Cytometry Core Facility (FCCF) of the University of Bonn. Downstream assays were done by me (preparation of cells for ATAC-seq, multiplex cytokine assays, flow cytometry, ELISA), Romina Kaiser (RNA isolation, ELISA), Dr. Matthias Ziehm (Olink), and the Next Generation Sequencing Core Facility of the University of Bonn (ATAC- and RNA-seq). Preparation of cells for ATAC-seq was done after training by Maike Kreutzenbeck. Multiplex assays using Ayoxxa Biosystems were done after training by Kai Zimmer. Flow cytometry using the BD FACS Canto™ II was done after training by Praveen Mathor from the FCCF. Data analysis of the *Ldlr*$^{-/-}$ model was done by me (weight calculations, flow cytometry data, and statistical analsis of these data sets), Kai Zimmer and Titus Schlüter (multiplex cytokine data), Dr. Lena Standke (RNA-seq analysis), Dr. Jamie Gearing (Haemopedia analysis of RNA-seq data), and Dr. Svetozar Nesic from the Core Facility Bioinformatics of the University of Bonn (ATAC-seq data). Data analysis of the WT model was done by me (weight calculations, flow cytometry, and statistical analsis of these data sets) and Dr. Jamie Gearing (cytokine data of ELISA and Olink).

The following experiments were carried out in collaboration with the Zimmer lab: *Apoe*$^{-/-}$ models. The animal experiments were conducted by members of the Zimmer lab (Marta Stei, Dr. Sandra Adler, and technicians). Organ retrieval was done by me, with support of

Romina Kaiser, Maximilian Rothe, Dr. Dennis de Graaf, Theresa Wagner, and members of the Zimmer lab. Downstream assays were performed by the lab of Univ. Prof. Dr. Sebastian Zimmer, in particular Saskia Claeys (atherosclerotic plaques), the lab of Prof. Dr. Dr. rer. nat. Dieter Lütjohann, particularly Anja Kerksiek (cholesterol), the lab of Prof. Christoph Thiele, particularly Dr. Jelena Zurkovic (lipidomics), Romina Kaiser (qPCR, Wes™, HTRF, ELISA), Shahd Nagieb (ELISA), and me (weight calculations, flow cytometry, ELISA, multiplex cytokine assays). Flow cytometry was done after training by Dr. Dalila Juliana Silva Ribeiro (Attune NxT Flow Cytometer) and Andreas Dolf from the FCCF (ID7000 Spectral Analyser 5L). Multiplex cytokine assays using the Luminex™ FLEXMAP 3D™ were done after training by Praveen Mathoor from the FCCF. Histological stainings of the gWAT and preparation of slides for subsequent imaging were done by the Histology Platform of the ImmunoSensation Cluster. Automated imaging of the slides was done by Romina Kaiser and Maximilian Rothe. Lipidomics and cholesterol data was pre-processed by the members of the lab that generated the data. Plaque data was kindly shared by the lab of Univ. Prof. Dr. Sebastian Zimmer. Cholesterol data was kindly shared by the lab of Dr. Dr. rer. nat. Dieter Lütjohann. Data was analysed by me (flow cytometry, lipidomics, histological images of the gWAT, ELISA, HTRF, qPCR, and Wes™), PD Dr. Peter Düwell (atherosclerotic plaques, cholesterol), and Dr. Jamie Gearing (multiplex cytokine data). Analysis of spectral flow cytometry data was with the help of Titus Schlüter. Analysis of histological images of the gWAT was done after training by Dr. Katharina Sieckmann. Wes™ analysis was done after training by Matilde Vasconcelos. Statistical analyses were done by me using GraphPad Prism.

The following experiments were carried out by me with support of Romina Kaiser: *ex vivo* lipolysis assay, *in vitro* adipogenesis assay, and gWAT explant culture. The adipogenesis assay and analysis was done after training by Dr. Katharina Sieckmann. Explant culture was supported by Maximilian Rothe, and was done after training by Seniz Yüksel. Imaging was done by me after training by Dr. Gabor Horvath from the Microscopy Core Facility of the University of Bonn. Data analysis and statistical evaluation using GraphPad Prism were done by me.

Interpretation of the data was done by me, with support of my supervisor Prof. Eicke Latz, and my thesis advisory committee consisting of PD Dr. Peter Düwell, Prof. Dr. Dagmar Wachten and Univ. Prof. Dr. med. Sebastian Zimmer.

In preparing this work, I used ChatGPT 5.1 Plus to improve the readability and language of the manuscript, to search for relevant literature, and to get a brief overview into new topics. I furthermore used it to solve problems with software tools like Fiji, Adobe Illustrator, Mendeley and Word. I also applied it to learn about statistical analyses to have a comprehensive understanding of the in-build statistical tests of GraphPad Prism. After using this tool, I reviewed and edited the relevant passages and take full responsibility for the content of the published dissertation.

I confirm that I have written this thesis independently and have not used any sources or aids other than those specified by me.

I hereby confirm that my thesis complies with the Statement by the Executive Committee of the Deutsche Forschungsgemeinschaft (DFG, German Research Foundation) on the Influence of Generative Models of Text and Image Creation on Science and the Humanities and on the DFG's Funding Activities.

Appendix

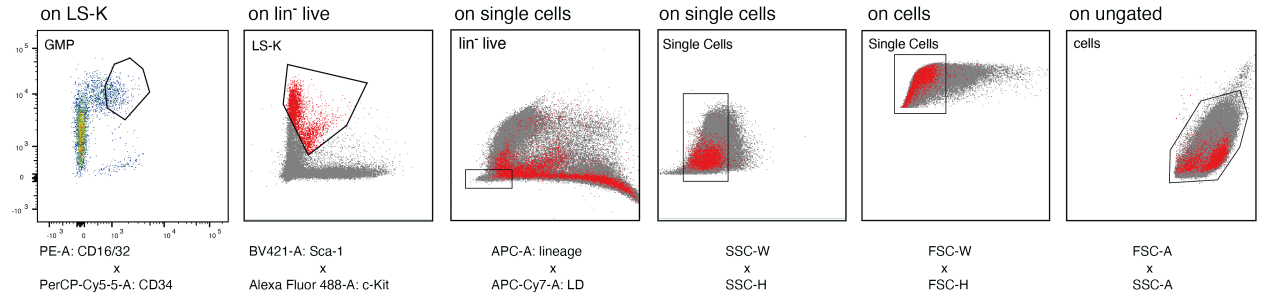

Supplementary Fig. S1: Backgating of the GMP gate in the *Ldlr*$^{-/-}$ model. The antibody panel used for sorting had suboptimal fluorophore and antibody combinations, which caused difficulties in compensation (e.g. banana-shaped APC/lineage population). Backgating was done to identify the distribution of GMP within the upstream gating strategy. The LS^{-}K gate was deliberately expanded to avoid the exclusion of CD34^{+} CD16/32^{+} cells.

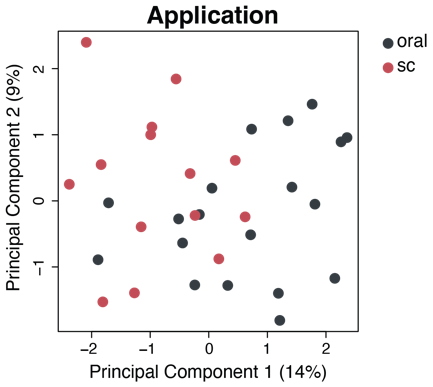

Supplementary Fig. S2: GMP sorted from *Ldlr*$^{-/-}$ mice cluster mainly by application route. The PCA plot shows the of the first two dimensions (PC1 and PC2) of the top 50 DE genes. Samples are colored by application route of HPβCD (oral vs s.c.).

Supplementary Fig. S3: List of 533 genes used for the gene set enrichment analysis (GSEA) of sorted GMP. The list contains 533 LXR target genes that have been published before to investigate the effects of HPβCD (Zimmer et al., 2016).

Gene	Accession No.
1110032E23Rik	NM_133187.2
1200011M11Rik	NM_024262.1
1500035H01Rik	NM_023813.3
1600002D24Rik	XM_001473403.1
1600014C10Rik	NM_028166.3

1600014C23Rik	XM_128667.1
1700010C24Rik	NM_027401.2
1700011E24Rik	XM_128789.5
1700012B15Rik	NM_028796
1700017N19Rik	XM_487140
1700019M22Rik	NM_027076.2
1700025G04Rik	NM_197990.2
1700027L20Rik	XM_906114.3
1700112H15Rik	XM_149010.2
1810019J16Rik	NM_001083916.1
2010107E04Rik	NM_027360.2
2210010L05Rik	NM_133829.1
2310005N03Rik	NM_025511.2
2310005P05Rik	NM_026189.2
2310011J03Rik	NM_025521.3
2310028O11Rik	XM_901483.3
2310033K02Rik	NM_001080708.1
2310035K24Rik	NM_027129.2
2310040G24Rik	XM_001480154.1
2310043N10Rik	NR_003513.2
2310045A20Rik	NM_172710.3
2610204M08Rik	NM_198411.2
2610209M04Rik	NM_025665.1
2610307O08Rik	XM_921606.2
2700038C09Rik	NM_025598.1
2810046L04Rik	NM_173382
2810439F02Rik	AK080904
2810474O19Rik	NM_026054.2
3110003A17Rik	NM_028440.1
3110023E09Rik	AK014071
3830408P04Rik	NM_023647
4921513D23Rik	NM_001081154
4930522O17Rik	XM_898933.3
4930543E12Rik	XM_922816
4930546C10Rik	XM_484744
4932425I24Rik	NM_001081025.1
4932443I19Rik	XM_980156.1
4933402G07Rik	AK016617
5031425E22Rik	XM_149592.1
5033441K04Rik	NM_001003948.1
5430405G24Rik	XM_152907.3
5430435G22Rik	NM_145509.2
5730525O22Rik	AK017789
5830415L20Rik	NM_001042501.1
6330442E10Rik	NM_178745.3
6330503K22Rik	NM_182995.1

6430548M08Rik	NM_172286
6530418L21Rik	NM_175398.3
8430432M10Rik	NM_176831.2
9430041J06Rik	NM_001081045
9830002I17Rik	XM_126365.3
A430090L17Rik	NM_177004
A530088I07Rik	AK080244
AB124611	NM_206536.1
Abca1	NM_013454.3
Abca17	NM_001031621.1
Abcg1	NM_009593
Abr	NM_198894.1
Acls3	NM_028817.2
Acly	NM_134037.2
Acp2	NM_007387.1
Acsl4	NM_001033600.1
Actn1	NM_134156.1
Adap2	NM_172133.1
Adcy7	NM_007406.1
Adk	NM_134079.1
Ado	NM_001005419.1
Adrbk1	NM_130863.1
Adss	NM_007422.2
Aebp2	AK045838
Agpat4	NM_026644.1
AI427809	NM_001033454.1
AI836003	NM_177716.2
Ak2	NM_016895.3
Akna	NM_001045514.1
Akr1a4	NM_021473.2
Alad	NM_008525.3
Aldh4a1	NM_175438.3
Aldh9a1	NM_019993.3
Ankrd55	NM_029898.2
Aoah	NM_012054.2
Arf2	NM_007477.4
Arhgef10l	NM_172415.2
Arid1a	NM_033566.1
Arl4d	NM_031160.1
Arl6ip6	NM_022989.2
Art3	NM_181728.1
Asph	NM_133723.2
Atp13a3	XM_001480958.1
Atp1a1	NM_144900.1
Atp2a2	NM_009722.2
Atp5g3	NM_175015.2

Atp5l	NM_013795.4
Atp8b2	NM_001081182.1
Atp8b4	XM_141343
Axl	NM_009465.3
B3galnt1	NM_020026.2
B3gat1	NM_029792.1
B4galt5	NM_019835.2
Bard1	NM_007525.2
Bbc3	NM_133234.1
BC006965	NM_146031
BC017158	NM_145590.1
Bcar3	NM_013867.1
Bcat1	NM_007532.3
Bckdhb	NM_199195.1
Bcl2ll	NM_009743.4
Bcl7b	NM_009745.1
Bex6	NM_001033539.2
Birc6	AK086619
Bms1	NM_194339.1
Bola3	NM_175277.2
Brms1l	NM_134155.2
Btg2	NM_007570.2
C130026I21Rik	NM_175219.3
C230095G01Rik	NM_178768.3
C5ar1	NM_007577.3
C730024G19Rik	XM_921354.2
Casc1	NM_177222.3
Cc2d1b	NM_177045.2
Ccdc109b	NM_025779.2
Ccdc45	NM_177088.2
Ccnd3	NM_007632.2
Cct5	NM_007637.2
Cd19	NM_009844.2
Cd28	NM_007642.2
Cd5l	NM_009690.1
Cd63	NM_007653.1
Cd9	NM_007657.2
Cd97	NM_011925.1
Cdc2l5	NM_001081058.1
Cdca1	NM_023284.1
Cdca3	NM_013538.4
Cdk5rap2	NM_145990.3
Cdk6	NM_009873.2
Cdkn2aipnl	NM_029976.2
Cebpd	NM_007679.4
Cenpn	NM_028131.3

Cetn1	NM_007593.5
Chd2	NM_001081345.1
Chd9	NM_177224.1
Chmp4b	NM_029362.3
Chsy1	NM_001081163.1
Cic	NM_027882.2
Cirbp	NM_007705.2
Clca5	NM_178697.4
Clec2d	NM_053109.2
Clec4d	NM_010819.3
Cln6	NM_001033175.1
Clstn3	NM_153508.3
Cltc	NM_001003908
Cmah	NM_007717.1
Cngb3	NM_013927.2
Cnot2	NM_028082.1
Cnpy3	NM_028065.2
Cntnap5a	NM_001077425.1
Col17a1	NM_007732.1
Col22a1	XM_907370.3
Col4a3bp	NM_023420.1
Commd4	NM_025417.1
Coro6	NM_139128.1
Cpeb2	NM_175937.2
Cps1	NM_001080809.1
Cpsf6	NM_001013391.1
Crat	NM_007760.3
Creb3l2	NM_178661.3
Creg1	NM_011804.2
Cryga	NM_007774.3
Ctsd	NM_009983.2
Ctss	NM_021281.1
Cux1	NM_009986.3
Cxcl4	NM_019932.2
Cyp26b1	NM_175475.2
Cyth4	NM_028195.3
D1Ertd471e	NM_001164528
D4Ertd196e	XM_975887.1
D6Wsu176e	NM_138587.4
D930001I22Rik	NM_173397
Dcbld2	NM_028523.3
Ddx50	NM_053183.1
Dhx35	NM_145742.1
Diap2	NM_017398.2
Dip2c	NM_001081426.1
Dirc2	NM_153550.3

Dlx1as	NR_002854.1
Dpp10	NM_199021.2
Dpp3	NM_133803.1
Dppa3	NM_139218.1
Dr1	NM_026106.4
Dtd1	NM_025314.1
Dtnb	AK083752
Dusp14	NM_019819.3
Dusp6	NM_026268.2
E030010A14Rik	NM_183160.3
Edem1	NM_138677.2
Efna1	NM_010107.3
Egr3	NM_018781
Eif2ak4	AK077199
Eif4a2	NM_013506
Elovl5	NM_134255.2
Emg1	NM_013536.1
Emp1	NM_010128.4
Endod1	NM_028013.2
Entpd1	NM_009848
Epb7.2	NM_013515.1
Eps8	NM_007945.2
Erh	NM_007951.1
Erlin2	NM_153592.1
Ermpl1	NM_001081213.1
Esr1	NM_007956.4
Etv6	NM_007961.3
Exoc2	NM_025588.2
Eya3	NM_010166.2
Fam129b	NM_146119.1
Fam176b	NM_172145.3
Fasn	NM_007988.3
Fbxo32	NM_026346.1
Fcer1g	NM_010185.2
Fcgr1	NM_010186.4
Fer113	XM_001480162.1
Fgd2	NM_013710.3
Fhl3	AF114382
Fkbp3	NM_013902.4
Fli1	NM_008026.4
Fmnl1	NM_019679.2
Fndc3b	NM_173182.1
Fndc7	NM_177091.2
Foxc1	NM_008592.2
Frrs1	NM_009146.1
Fut8	NM_016893.4

Gabpb2	NM_029885.1
Gad2	NM_008078.1
Galnt4	NM_015737.3
Galnt9	NM_198306.1
Gapdh	NM_008084.2
Gas7	NM_008088.1
Gda	AK044078
Gdi2	NM_008112.4
Gene	Accession no
Ggnbp1	NM_027544.1
Gh	NM_008117.2
Gltp	NM_019821.2
Gm528	XM_986482.1
Gm572	NM_001085505.1
Gm71	NM_001033236.2
Gm8286	NM_001033411.1
Gng10	NM_025277.3
Gpr68	NM_175493.2
Gpx1	NM_008160.5
Grcc10	NM_013535.1
Grin2b	NM_008171.3
Grk5	NM_018869.2
Grm4	NM_001013385.1
Gsx1	NM_008178.2
Gtf2e1	NM_028812.3
Gtpatch4	NM_025663.2
Gucy2g	NM_001081076.1
H2-Q1	NM_010390.2
H2afx	NM_010436.2
Hal	NM_010401.3
Hells	NM_008234.3
Hif1a	NM_010431.1
Hip1	NM_146001
Hivep2	NM_010437.2
Hnt	NM_172290.3
Hoxa1	NM_010449.3
Hsd11b1	NM_008288.1
Htr6	NM_021358.1
Icam2	NM_010494.1
Ifnab	NM_008336.2
Ifnar2	NM_010509.1
Igsf3	NM_207205.1
Ikbke	NM_019777.3
Il17rd	NM_134437.1
Il20ra	NM_172786.1
Il6	NM_031168.1

Il6ra	NM_010559.2
Insr	AK052187
Iqch	XM_981814.1
Irf2	NM_008391.3
Irf8	NM_008320.3
Itgb1	NM_010578.1
Itpkc	NM_181593.2
Itpr2	NM_010856.1
Jph1	NM_020604.1
Junb	NM_008416.1
Klf9	NM_010638.4
Klhdc4	NM_145605.1
Kpna2	NM_010655.3
Laptm4a	NM_008640.2
Lass2	NM_029789.1
Lass6	NM_172856.3
Leprel2	NM_013354.4
Lox	NM_010728.1
Lpcat3	NM_145130.1
Lpin1	NM_015763
Lpl	NM_008509.2
Lrp1	NM_008512.2
Lrrc28	NM_175124.4
Lrrc33	NM_146069.4
Lrrk1	NM_146191.3
Ltbp1	AK054512
Luzp1	NM_024452.2
Ly86	NM_010745.1
Lyzl4	NM_026915.2
Maf	NM_001025577.2
Mafk	NM_010757.2
March7	NM_020575.2
March8	NM_027920.4
Maz	XM_133827.2
Mdfic	NM_175088.3
Mdm1	NM_148922.2
Med8	NM_020000.2
Mef2d	NM_133665.3
Mgat5	NM_145128.3
Mgst3	NM_025569.1
Mllt6	NM_139311.2
Mmp9	NM_013599.2
Mnd1	NM_029797.1
Mnt	NM_010813.2
Morn4	NM_198108.2
Mppe1	NM_172630.1

Mrpl1	NM_053158.1
Mrpl2	NM_025302.3
Mrpl33	NM_025796.2
Mtap7	NM_008635
Mtx2	NM_016804.2
Muc1	NM_013605.1
Mylc2b	NM_023402.1
Mylip	NM_153789.3
Myo16	NM_001081397.1
Myo3b	XM_194023.1
N6amt1	NM_026366.1
Ncf4	NM_008677.1
Nfatc4	NM_023699.2
Nfe2l2	NM_010902.3
Nfia	NM_177176.2
Nfkb2	NM_019408.1
Nfyb	NM_010914.2
Ngrn	NM_031375.3
Nnat	AK077465
Nob1	NM_026277.1
Nomo1	NM_153057.3
Notch2	NM_010928.1
Npffr1	XM_905368.1
Npm3-ps1	NR_002702.1
Nrbf2	NM_001036293.2
Nsl1	NM_198654.2
Nuak1	NM_001004363.1
Nubpl	NM_029760.1
Nup160	NM_021512.2
Ogg1	NM_010957.3
Olf588	NM_147111.1
Olfr726	NM_146316
Olfr951	NM_001011812.1
Opn5	NM_181753.2
Osbpl9	NM_173350.1
Osgin1	NM_027950.1
OTTMUSG00000009 97	NM_001037932.1
Oxa11	NM_026963.3
Pacrgl	NM_025755.3
Papd4	NM_133905.1
Pdgfb	NM_011057.2
Pfkfb2	NM_008825.3
Pgsl	NM_133757.2
Phlpp	XM_129968.4
Phospho1	NM_153104.2

Phtf2	NM_172992.2
Pi4kb	NM_175356.1
Pik3ap1	NM_031376.2
Pim1	NM_008842.3
Plce1	NM_019588.2
Plekho2	NM_153119.2
Pltp	NM_011125.2
Pmp22	NM_008885.2
Pon1	NM_011134.2
Ppp1r9b	NM_172261.2
Ppp3r1	NM_024459.2
Prkag2	NM_145401.1
Prkar1a	NM_021880.2
Prkcbp1	NM_027230.3
Prkcd	NM_011103.2
Prl4a1	NM_011165.3
Prnpip1	NM_080469.2
Prr13	NM_025385.2
Prrc1	NM_028447.2
Prss2	NM_009430.1
Prx	NM_198048.1
Psap	NM_011179.2
Psma6	NM_011968.2
Ptafr	XM_357441.1
Ptchd3	XM_109751.6
Ptgs1	NM_008969.3
Ptp4a2	NM_008974.2
Ptpro	NM_011216.2
Ptprs	NM_011218.1
Ralgds	NM_009058.1
Rapgef2	NM_001099624.1
Rara	NM_009024.2
Rasgef1b	NM_181318.4
Rassf8	NM_027760.2
Rbpj	NM_009035.4
Reep3	NM_178606.4
Rffl	NM_001007465.1
Rgl1	NM_016846.3
Rheb	NM_053075.2
Rhoc	NM_007484.1
Ripk5	NM_172516.4
Rnfl86	NM_025786.2
Ror1	NM_013845.4
Rpl31	NM_053257.1
Rps19bp1	NM_175109.3
Rps20	NM_026147

Rps27a	NM_001033865.1
S100a6	NM_011313.2
S100a7a	NM_199422.1
Sag	NM_009118.2
Sall4	NM_175303.3
Scd1	NM_009127.3
Scd2	NM_009128.1
Scd3	NM_024450.2
Scg5	NM_009162.3
Scnn1a	NM_011324.1
Scotin	NM_025858.1
Sdc1	NM_011519.2
Sec22b	NM_011342.2
Selk	NM_019979.1
Sepn1	NM_029100.2
Sergef	NM_013789.1
Sesn1	NM_001013370.1
Setdb1	NM_018877.2
Sfl	NM_011750.1
Sfpi1	NM_011355.1
Sgk1	NM_011361.1
Sh3bgrl3	NM_080559.1
Sh3yl1	NM_013709.4
Slc13a4	NM_172892.1
Slc15a3	NM_023044.1
Slc15a4	NM_133895.1
Slc1a4	NM_018861.2
Slc30a6	NM_144798.4
Slc4a4	NM_018760.1
Slc5a3	NM_017391.2
Slc6a14	NM_020049.3
Slc7a1	NM_007513.3
Slc7a14	NM_172861.2
Slpr1	NM_007901.4
Smap2	NM_133716.2
Smg7	NM_001005507.1
Snx27	NM_029721.1
Snx29	NM_028964.3
Socs3	NM_007707.2
Spink10	NM_177829.3
Spp1	NM_009263.1
Spry4	NM_011898.2
Srebf1	NM_011480.1
Ssbp4	NM_133772.1
Ssfa2	NM_080558
Sspn	NM_010656.2

St6gal1	NM_145933.3
St6galnac6	NM_001025311.1
Stard3nl	NM_024270.2
Stx7	NM_016797.4
Stx8	NM_018768.2
Syne2	NM_001005510.2
Synpr	NM_028052.3
Tacc1	NM_199323.2
Taf5	NM_177342.3
Tatdn1	NM_175151.2
Tatdn2	NM_001033463.1
Tdrd7	NM_146142.1
Terf2ip	NM_020584.1
Tex14	NM_031386.1
Tgfbr2	AK090393
Timm13	NM_013895.2
Tiprl	NM_145513.3
Tle4	NM_011600.2
Tlr2	NM_011905.2
Tlr4	NM_021297.1
Tmc1	NM_028953.2
Tmc6	NM_145439.1
Tmem119	NM_146162.1
Tmem120a	NM_172541.2
Tmem120b	NM_001039723.2
Tmem16b	NM_153589.1
Tmem17	NM_153596.1
Tmem23	NM_144792.2
Tmem41b	NM_153525.5
Tmem69	NM_177670.3
Tmem86a	NM_026436.3
Tn7sf3	NM_026281.2
Tnfaip2	NM_009396.1
Tnfaip3	NM_009397.2
Tnrc4	NM_172434.2
Traf3ip2	NM_134000.3
Trcg1	NM_001014398.1
Tsen2	NM_199033.1
Tspan14	NM_145928.1
Ttc9	NM_001033149.2
Ttpal	NM_029512.2
Txndc11	NM_134105.2
Txnip	NM_023719.1
Ubash3b	NM_176860.5
Ube2i	NM_011665.3
Uchl4	NM_033607.1

Uck2	NM_030724.3
Unc5b	NM_029770.2
Uqcrc2	NM_025899.2
Usp6nl	NM_181399.3
Usp7	NM_001003918.2
Vac14	NM_146216.2
Vav3	NM_020505.2
Veph1	NM_145820.2
Wdfy3	NM_172882
Wdr36	NM_144863.3
Wipf2	NM_197940.1
Wnt5a	NM_009524.2
Wsb1	NM_001042565.2
Zc3h11a	NM_144530.5
Zc3h12a	NM_153159.1
Zc3h14	NM_029334.1
Zc3h6	NM_178404.2
Zeb2	NM_015753.3
Zfand3	NM_148926.2
Zfp364	NM_026406.2
Zfp644	NM_026856.2
Zmat5	NM_026015.2
Zubr1	XM_001479450.1
Zzz3	NM_198416.2

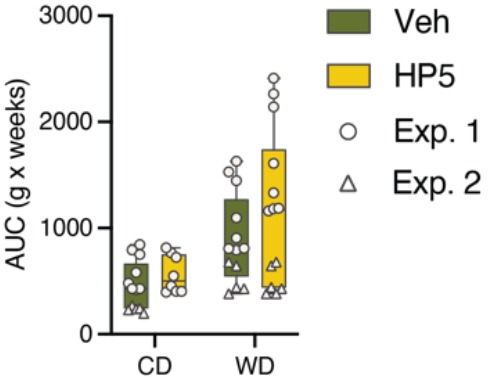

Supplementary Fig. S4: BW changes (AUC) of WT mice fed a WD for 6 weeks. Data is shown of two independent experiments, with the second experiment lacking the CD-HP5 group.

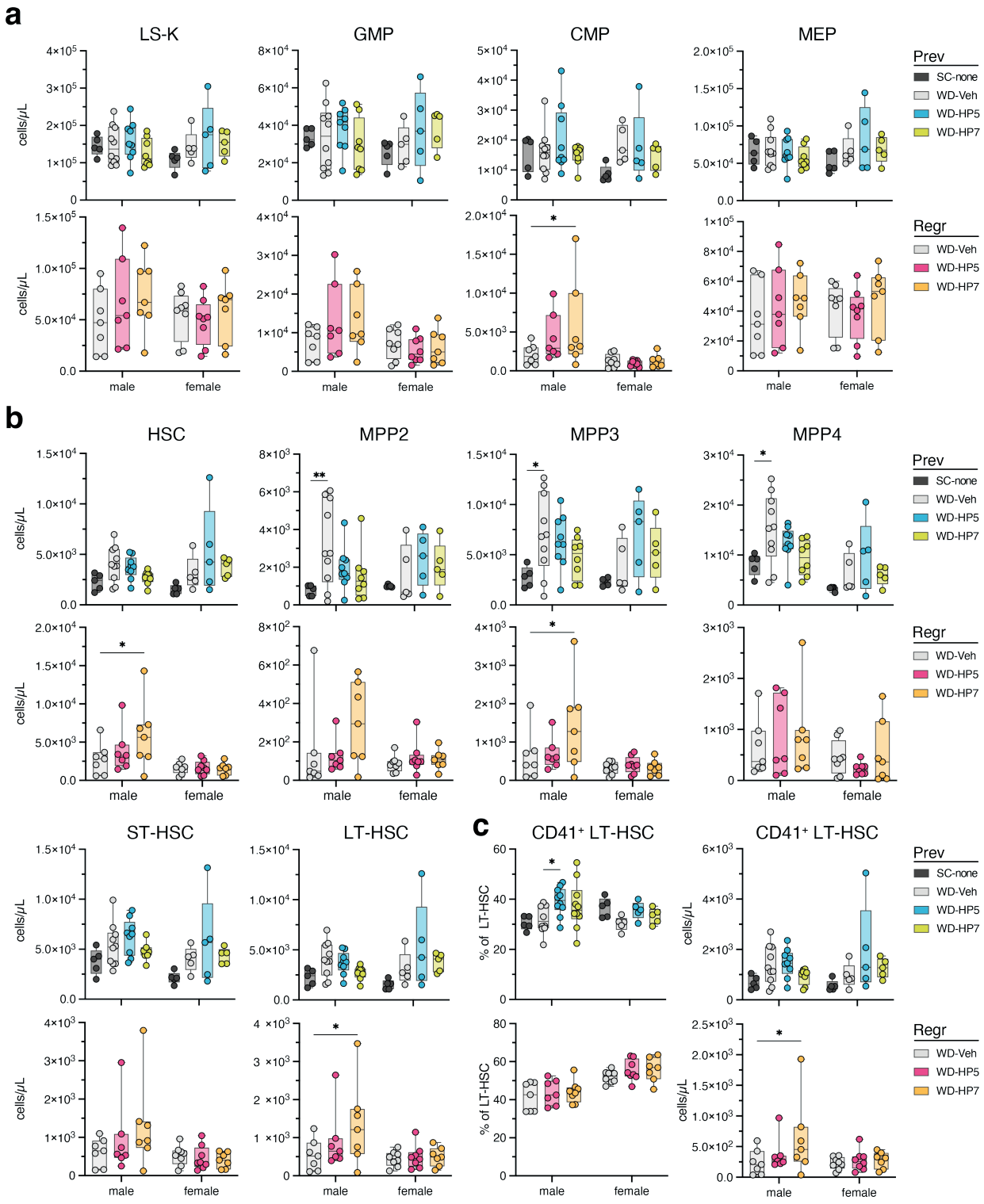

Supplementary Fig. S5: Effects of HPβCD-HP5 and HPβCD-HP7 on bone marrow hematopoietic cells in WD-fed *Apoe*$^{-/-}$ mice. a) Counts of LS^{-}K cells and subpopulations b) Counts of HSC and subpopulations. c) Frequencies of CD41^{+} and CD61^{+} LT-HSC. Statistical analysis was performed using two-way ANOVA followed by Dunnett's multiple comparisons test. Displayed *p*-values are adjusted for multiple testing. *n* (males) = 7-10, *n* (females) = 5-8 mice per group.

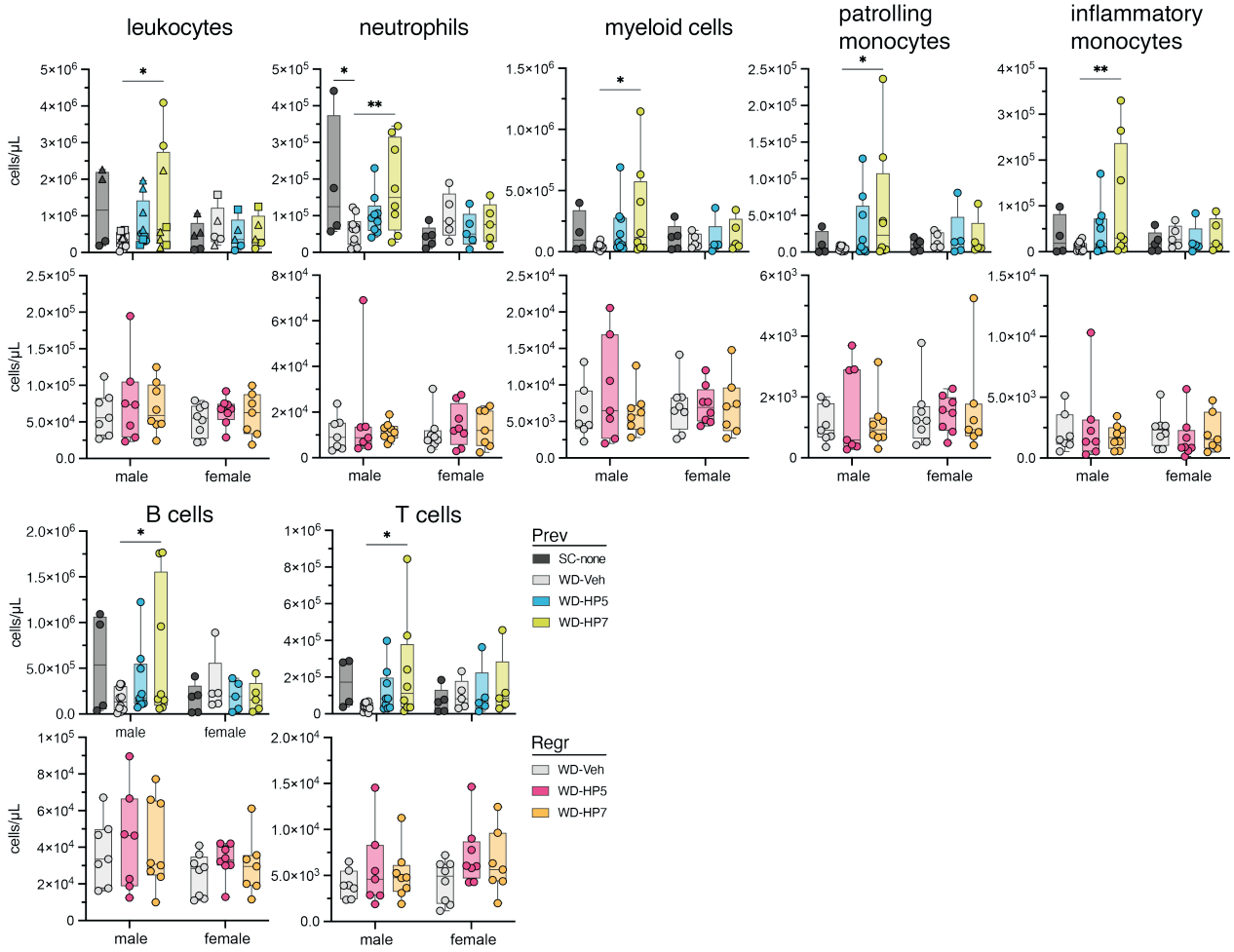

Supplementary Fig. S6: Effects of HPβCD-HP5 and HPβCD-HP7 on circulating immune cells in the blood. a) Cell counts of myeloid and lymphoid cells in the circulation, analyzed by flow cytometry. Statistical analysis was performed using two-way ANOVA followed by Dunnett's multiple comparisons test. Displayed *p*-values are adjusted for multiple testing. *n* (males) = 7-10, *n* (females) = 5-8 mice per group.

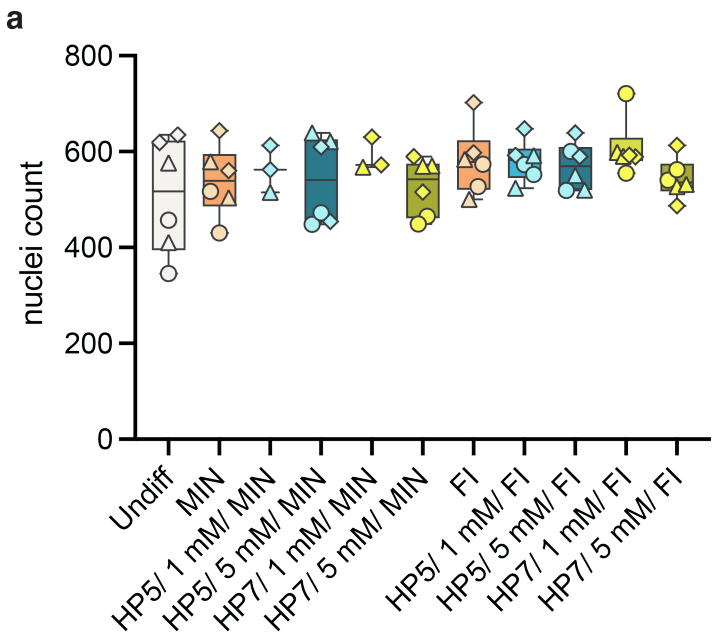

Supplement Fig. S7: Effects of HPβCD-HP5 and HPβCD-HP7 on *ex vivo* adipogenesis of SVF cells. Isolated SVF (Lin^-) from gWAT of WT mice were cultured and adipogenesis was induced in pre-adipocyte cells. Cells were fixed on the day of induction (d0), as well as on day 3, 6 and 8. Cells were stained with DAPI, LD540 and Ki-67. Images were analyzed using the AdipoQ plugin in Fiji. a) DAPI counts from day 8. Statistical analysis was performed using two-way ANOVA followed by Dunnett's multiple comparisons test. Displayed *p*-values are adjusted for multiple testing. *n*=3-6 mice per condition; similar shapes of the data points indicate different mice from the same experiment.